Experimental analysis of the influence of key process parameters on synthesis gas fermentation in continuous operation with *Clostridium ljungdahlii*

Zur Erlangung des akademischen Grades eines
DOKTORS DER INGENIEURWISSENSCHAFTEN (DR.-ING.)

von der KIT-Fakultät für Chemieingenieurwesen und Verfahrenstechnik
des Karlsruher Instituts für Technologie (KIT)
genehmigte

DISSERTATION

von
M. Sc. Lukas Perret
aus Essen

Tag der mündlichen Prüfung: 11. Dezember 2024
Erstgutachter: Prof. Dr.-Ing. Jörg Sauer
Zweitgutachter: Prof. Dr.-Ing. Thomas Meurer

Declaration

I declare that this thesis represents my own work and that I have written this thesis independently by myself, without the use of other documents or sources beyond those stated in the references.

Munich, 5th of May 2024

Lukas Perret

Acknowledgements

The present study dealing with the experimental analysis of key parameters on synthesis gas fermentation was carried out as part of my work as a research assistant at the Institute of Catalysis Research and Technology at the Karlsruhe Institute of Technology during the period 2020 - 2023. Due to the interdisciplinary focus of this experimental research topic, employees from a wide range of disciplines have successfully contributed.

First of all, I would like to thank my supervisor and head of the Institute of Catalysis Research and Technology, Prof. Sauer, for the opportunity to do my PhD and for supervising my work. In particular, the possibility to discuss scientific issues at any time and to receive expert advice and helpful suggestions was unique. Many thanks for the great support in publishing the research data and the opportunity to present the results at international conferences.

I would also like to thank Prof. Meurer for taking on the second evaluation.

Furthermore, I would like to thank Dr. Boukis for his very kind acceptance into his work group, the supervision of my work, the advice and organizational help with research projects, conferences and publications and the support with modifications to the test rig.

I would especially like to express my gratitude towards Elena Hauer for her support in preparing and conducting the experiments, especially for taking over sample analyses on weekends. I would also like to thank Karl Weiss for the mechanical work and a total of three major modifications to the test rig. With each modification, the test rig has become more stable in operation and more user-friendly. Elena and Karl: thank you so much for the very friendly and quick integration into our work group and the very personal support during my time at the institute. I would also like to thank Stefan Henecka for the mechanical work on the test rig, the numerous tips on mechanical and instrumentation issues and the rapid implementation of new ideas.

Many thanks to Veronika Holderied and Armin Lautenbach for their excellent support and for taking over the sample analysis. I especially appreciated their feedback concerning unexpected results and their expert advice on how to interpret the measured values.

I would also like to thank Xenia Dominke, Katharina Hanisch, Emely Fuderer, Davis Limanjaya Nugroho and Jorge Navas, who successfully contributed to the synthesis gas fermentation project as part of their Master's thesis and/or as student assistants.

Furthermore, I would like to thank Dr. Anke Neumann, Dr. Karla Herrera Delgado, Dr. Bruno Lacerda de Oliveira Campos and Dr. Thomas A. Zevaco for the great cooperation and the joint publication on the comparison of heterogeneous catalysis and synthesis gas fermentation. I would also like to thank Dr. Thomas A. Zevaco for taking professional photographs of the test rig.

Many thanks to Roland Fritz for his excellent IT support, for his quick and uncomplicated help with urgent questions and for planning and implementing the wireless internet network in the laboratory, which made it possible to fully interconnect the measurement and control technology. I would also like to thank Volker Meinzer and Holger Kahrau's electrical engineering workshop for their implementation and advice on electrical engineering issues and Ricardo Valencia for his tireless efforts in Siemens programming.

I would also like to thank Monika Zimmer, Michaela Schmidt, Kerstin Barnack, Martin Bergemann, Stefan Kapp and Bernhard Hemmer for their support in all matters concerning personnel, organization and infrastructure.

In addition, I would like to thank the IKFT doctoral students and especially Moritz Herfet, Athanasios Vadarlis, Julian Dutzi, Victor Zaghini Francesconi and Marius Drexler for very helpful scientific discussions and valuable inspiration.

Finally, I would like to express my special thanks to my family for their great support before, during and after my doctoral thesis, especially for coaching, guidance and advice, which contributed significantly to the success of this work.

Preamble

This is a publication-based dissertation and therefore part of the content has been previously published in three peer-reviewed articles:

1.) L. Perret, B. Campos, K. Herrera Delgado, T. A. Zevaco, A. Neumann, J. Sauer. CO_x *Fixation to Elementary Building Blocks: Anaerobic Syngas Fermentation vs. Chemical Catalysis*. Chem. Ing. Tech. 2022, 94 (11), 1667–1687. DOI: 10.1002/cite.202200153

2.) L. Perret, N. Boukis, J. Sauer. *Influence of Increased Cell Densities on Product Ratio and Productivity in Syngas Fermentation*. Ind. Eng. Chem. Res. 2023, 62 (35), 13799–13810. DOI: 10.1021/acs.iecr.3c01911

3.) L. Perret, N. Boukis, J. Sauer. *Synthesis Gas Fermentation at High Cell Density: How pH and Hydrogen Partial Pressure Affect Productivity and Product Ratio in Continuous Fermentation*. Bioresour. Technol. 2023, 391, 1-9. DOI: 10.1016/j.biortech.2023.129894

Hence, parts of the following work are identical to the published articles, with minor modifications, such as formatting, citation style or even modification of the figures, tables, and layout.

Selected parts of the content of publication number (1) from the list above were used for Chapter 2, Chapter 3 and Chapter 7.

The content of publication number (2) has been included in Chapter 1, Chapter 4, Section 5.1, Section 5.2.1, Section 6.1 and Chapter 7.

Publication number (3) was used for Chapter 1, Chapter 4, Section 5.2.2-5.2.4, Section 6.1.1, Section 6.2-6.4 and Chapter 7.

List of Publications

Peer-reviewed original research papers

L. Perret, B. Campos, K. Herrera Delgado, T. A. Zevaco, A. Neumann, J. Sauer. CO_x *Fixation to Elementary Building Blocks: Anaerobic Syngas Fermentation vs. Chemical Catalysis*. Chem. Ing. Tech. 2022, 94 (11), 1667–1687. DOI: 10.1002/cite.202200153

L. Perret, N. Boukis, J. Sauer. *Influence of Increased Cell Densities on Product Ratio and Productivity in Syngas Fermentation*. Ind. Eng. Chem. Res. 2023, 62 (35), 13799–13810. DOI: 10.1021/acs.iecr.3c01911

L. Perret, N. Boukis, J. Sauer. *Synthesis Gas Fermentation at High Cell Density: How pH and Hydrogen Partial Pressure Affect Productivity and Product Ratio in Continuous Fermentation*. Bioresour. Technol. 2023, 391, 1-9. DOI: 10.1016/j.biortech.2023.129894

Data repository

L. Perret, N. Boukis, J. Sauer, 2023. *Raw measurement data on the influence of increased cell densities on product ratio and productivity in syngas fermentation with Clostridium ljungdahlii*. Mendeley Data, V1, DOI: 10.17632/8gtc54zykn.1

L. Perret, N. Boukis, J. Sauer, 2023. *Raw measurement data on the influence of pH and H2 partial pressure on syngas fermentation with Clostridium ljungdahlii*. Mendeley Data, V2, DOI: 10.17632/nnx6brc9hj.2

Conference talks

L. Perret, X. Dominke, I. K. Stoll, N. Boukis, J. Sauer. *Effizienzsteigerung der Synthesegasfermentation mit Clostridium ljungdahlii durch den Einsatz einer Zellrückhaltung im CSTR*. ETG-Kongress: Von Komponenten bis zum Gesamtsystem für die Energiewende, Wuppertal (online), DE, May 2021

L. Perret, A. Robazza, A. Neumann. *Closing the carbon cycle with syngas fermentation*. Workshop des Topic 5 „Ressourcen- und Energieeffizienz“ (Subtopic 1 und 2) des Helmholtzprogramms MTET, Eggenstein-Leopoldshafen, DE, October 2021

L. Perret, N. Boukis, J. Sauer. *Synthesis gas fermentation - Biocatalytic CO_x-conversion to elementary building blocks*. 26th International Congress of Chemical and Process Engineering (CHISA), Prag, CZE, August 2022

L. Perret, N. Boukis, J. Sauer. *Methods of reaction and reactor engineering to adjust product ratios and increase efficiency of syngas fermentation with Clostridium ljungdahlii*. (Bio)Process Engineering - a Key to Sustainable Development: A joint event of ProcessNet and DECHEMA-BioTechNet Jahrestagungen 2022 together with 13th ESBES Symposium, Aachen, DE, September 2022. DOI: 10.1002/cite.202255034

L. Perret, N. Boukis, J. Sauer, *Optimization and efficiency increase of syngas fermentation through control of elementary process variables*. 14th European Congress of Chemical Engineering and 7th European Congress of Applied Biotechnology (ECCE 14 & ECAB 7), Berlin, DE, September 2023

Poster presentations

L. Perret, X. Dominke, I. K. Stoll, N. Boukis, J. Sauer. *Efficiency enhancement of synthesis gas fermentation by the use of cell retention in a CSTR*. 29th European Biomass Conference & Exhibition (EUBCE), Marseille (online), FR, April 2021

L. Perret, N. Boukis, J. Sauer. *Key process parameters to influence space-time yield and product ratio of syngas fermentation*. 27^{th} International Symposium for Chemical Reaction Engineering (ISCRE 27), Québec City, CAN, June 2023

Abstract

Synthesis gas fermentation could play a key role in a future circular carbon economy due to the possibility of first converting CO, CO_2 and H_2 into C_2 compounds such as ethanol and acetic acid with the help of microorganisms and then producing higher-value products such as proteins and lipids by coupling further reaction stages. The synthesis gas could be provided by gasification of biomass, by (co)-electrolysis, by capturing CO_2 from the air or by using waste gases from industry. Acetogenic microorganisms, such as the model organism *Clostridium ljungdahlii*, use the reductive acetyl-CoA pathway, also known as Wood-Ljungdahl pathway (WLP), for carbon fixation. Here, the molecule acetyl-CoA, a central building block of biotechnology for the formation of biomass, acetates and alcohols, is synthesized by the fixation of CO and/or CO_2 and sequential reactions. However, the low volumetric productivity due to low gas-liquid mass transfer and low biomass concentrations in the reactor is a critical and major limitation of syngas fermentation on the way to commercialization. While the biomass-specific productivity of the biocatalyst is comparable to the mass-specific productivity of a traditional chemical catalyst, e. g. for heterogeneous methanol synthesis, the space-time yield is up to three orders of magnitude lower.

Therefore, the aim of the present study was to investigate an external cycle for the retention of biomass in order to increase the cell density in the reactor. In addition, research focused on investigating and identifying key influencing parameters in order to further optimize and increase the efficiency of the process and, in the long term, enable this technology to be used economically on an industrial scale.

For this purpose, a test rig for the fermentation of synthesis gas consisting of CO, CO_2 and H_2 with *C. ljungdahlii* as biocatalyst was operated in a fully continuous experimental setup. It was possible to increase the cell density in the reactor by recirculating the biocatalyst by switching on an external circuit to retain biomass. The construction of the plant together with the external circuit for retaining biomass is designed for operation under increased process pressure of up to 10 bar. After each parameter change, it is waited until a steady-state operating point is reached before the next parameter change is made. The continuous operation mode helps to avoid or

reduce product inhibition or limitations of nutrient medium components, which often occur in batch operation.

By using an external circuit to retain biomass with a hollow fiber membrane operated in cross-flow, the cell density in the reactor could be increased by more than 160 %, and the C_2-space-time yield has also increased significantly by 46 %. The operation of a biomass retention system therefore contributes significantly to an increase in efficiency. In addition, investigating the influence of total biomass retention has shown that ethanol formation is favored and a product shift towards ethanol is achieved. The measured space-time yield of ethanol with 8.71 $\mathrm{mmol\,L^{-1}\,h^{-1}}$ is the highest measured so far in continuous operation with an unmodified strain of *C. ljungdahlii*. It is assumed that the use of total biomass retention leads to reduced or stagnating cell growth. Since the growth of biomass requires a high consumption of NADPH and ferredoxin, reduced or even stagnating growth reduces the need of uptake of these reduction potentials, resulting in a surplus of reduction potential. This surplus can be reduced by an increased reduction of acetic acid to ethanol, and therefore, the product shift towards ethanol could be the result of stagnating cell growth at high cell densities and operation of total biomass retention.

In addition, a linear relationship was found between the biomass-specific partial pressure of CO in the off-gas and the hydrogen uptake and product ratio. The higher the biomass-specific partial pressure of CO in the off-gas, the lower the hydrogen uptake and product ratio of ethanol to acetic acid.

Furthermore, lowering the pH from 5.9 to 5.7 leads to increased hydrogen uptake and to a shift in the product ratio towards ethanol. A further decrease in pH, on the other hand, reduces hydrogen uptake and ethanol productivity, while the space-time yield of the C_2 products remains almost constant.

In addition, an increase in the hydrogen partial pressure to 1.52 bar results in an increase in hydrogen uptake and ethanol space-time yield, with the product ratio shifting towards ethanol. An ethanol space-time yield of 10 $\mathrm{mmol\,L^{-1}\,h^{-1}}$ was achieved, but this was not stable over the long-term. Furthermore, the measurement data show that above a hydrogen partial pressure of 1.52 bar, which corresponds to a theoretical equilibrium concentration of $c^*_{\mathrm{l,H_2}} = 1.2\,\mathrm{mmol\,L^{-1}}$, the hydrogen uptake decreases significantly, indicating an inhibition of an enzymatic reaction.

The results of the present study have therefore not only contributed to a significant increase in volumetric productivity through detailed investigation of the influence of a biomass retention system, but also to a much better understanding of the influence of key process parameters such as H_2 partial pressure on the fermentation process with *C. ljungdahlii*. Important parameters

influencing productivity and product ratio, such as biomass-specific partial pressure of CO in the off-gas or theoretical equilibrium concentration of H_2 in the fermentation broth, were identified and correlations were developed. By taking measurements in steady state of continuous operation with up to 3000 hours of stable operation, a valuable database for future kinetic modeling has been built up.

Zusammenfassung

Die Synthesegasfermentation ermöglicht eine mikrobielle Umwandlung von CO, CO_2 und H_2 zu C_2-Verbindungen wie z. B. Ethanol und Essigsäure. Durch Kopplung weiterer Reaktionsstufen können schließlich höherwertige Produkte wie Proteine und Lipide hergestellt werden. Die Synthesegasfermentation könnte daher eine Schlüsselposition bei einer zukünftigen Kohlenstoff-Kreislaufwirtschaft einnehmen.

Das Synthesegas könnte dabei sowohl durch Vergasung von Biomasse, durch (Co)-Elektrolyse, durch Abscheidung von CO_2 aus der Luft oder auch durch Nutzung von Abgasen der Industrie bereitgestellt werden. Der im Synthesegas enthaltene Kohlenstoff wird mit Hilfe von acetogenen Mikroorganismen, wie zum Beispiel *Clostridium ljungdahlii*, über den Wood-Ljungdahl-Reaktionsmechanismus fixiert. Hierbei wird über Bindung von CO und/oder CO_2 und sequentielle Reaktionen das Molekül Acetyl-CoA gebildet, ein zentraler Baustein der Biotechnologie für die Bildung von Biomasse, Acetaten und Alkoholen. Allerdings ist die volumetrische Produktivität aufgrund von niedrigem Gas-Flüssig-Stofftransport und geringer Biomassekonzentration im Reaktor klein und stellt damit einen zentralen und schwerwiegenden Nachteil der Synthesegasfermentation auf dem Weg zur Kommerzialisierung dar. Während die biomassespezifische Produktivität des Biokatalysators mit der massenbezogenen Produktivität eines herkömmlichen chemischen Katalysators vergleichbar ist (z.B. für die heterogene Methanolsynthese), liegt die Raum-Zeit-Ausbeute um bis zu drei Größenordnungen niedriger.

Das Ziel der vorliegenden Arbeit bestand daher zum einen in der Untersuchung eines externen Kreislaufs zum Rückhalt von Biomasse zur Steigerung der Zelldichte im Reaktor und zum anderen in der Untersuchung und Erfassung zentraler Einflussparameter, damit eine weitere Optimierung und Effizienzsteigerung des Prozesses und langfristig eine wirtschaftliche industrielle Nutzung dieser Technologie möglich werden.

Hierfür wurde eine Versuchsanlage zur Fermentation von Synthesegas bestehend aus CO, CO_2 und H_2 mit *C. ljungdahlii* als Biokatalysator in vollkontinuierlicher Versuchsführung betrieben. Es bestand die Möglichkeit, durch Zuschaltung eines externen Kreislaufs zum Rückhalt von Biomasse die Zelldichte im Reaktor durch Rückführung des Biokatalysators

zu erhöhen. Die Konstruktion der Anlage zusammen mit dem externen Kreislauf zum Rückhalt von Biomasse wurde für Prozessdrücke von bis zu 10 bar ausgelegt. Nach jeder Parameteränderung wurde gewartet, bis sich ein stationärer Betriebspunkt eingestellt hat, erst dann erfolgte die nächste Parameteränderung. Durch die vollkontinuierliche Versuchsführung wurden Produktinhibierung oder Limitierungen von Nährmediumsbestandteilen, wie sie im Satz-Betrieb häufig zum Ende der Versuchszeit auftreten, vermieden bzw. reduziert.

Durch Einsatz eines externen Kreislaufes zum Rückhalt von Biomasse mit einer im Kreuzstrom betriebenen Hohlfiltermembran konnte die Zelldichte im Reaktor um mehr als 160 % gesteigert werden, auch die C_2-Raum-Zeit-Ausbeute ist um 46 % signifikant gestiegen. Der Betrieb eines Biomasserückhaltesystems steigerte daher erheblich die Effizienz. Darüber hinaus haben die Untersuchungen gezeigt, dass ein vollständiger Biomasserückhalt die Ethanolbildung begünstigt und eine Produktverschiebung in Richtung von Ethanol erzielt. Die gemessene Raum-Zeit-Ausbeute von Ethanol mit 8,71 $\mathrm{mmol\,L^{-1}\,h^{-1}}$ ist bisher die höchste, die mit einem nicht-modifizierten Stamm von *C. ljungdahlii* im Dauerbetrieb gemessen wurde. Es wird vermutet, dass der Einsatz eines totalen Biomasserückhaltes zu reduziertem oder stagnierendem Zellwachstum führt. Da allerdings der Aufbau von Biomasse mit einem hohen Verbrauch an NADPH und Ferredoxin verbunden ist, wird folglich durch reduziertes bzw. stagnierendes Wachstum der Verbrauch dieser Reduktionspotentiale reduziert, es entsteht somit ein Überschuss an Reduktionspotential. Dieser Überschuss kann durch vermehrte Reduktion von Essigsäure zu Ethanol abgebaut werden. Diese Produktverschiebung hin zu Ethanol könnte die Folge von stagnierendem Zellwachstum bei hohen Zelldichten während des Betriebes mit vollständigem Biomasserückhalt sein.

Darüber hinaus wurde ein linearer Zusammenhang zwischen biomassespezifischem Partialdruck von CO im Abgas und Wasserstoffaufnahme und Produktverhältnis festgestellt: Je höher der biomassespezifische Partialdruck von CO im Abgas ist, desto niedriger sind Wasserstoffaufnahme und Produktverhältnis von Ethanol zu Essigsäure.

Weiterhin führte eine Absenkung des pH-Wertes von 5,9 auf 5,7 zu einer erhöhten Wasserstoffaufnahme und einer Verschiebung des Produktverhältnisses in Richtung von Ethanol. Eine weitere Absenkung des pH-Wertes hingegen verringerte Wasserstoffaufnahme und Ethanolproduktivität, die Raum-Zeit-Ausbeute der C_2-Produkte blieb dabei nahezu unverändert.

Eine Erhöhung des Wasserstoffpartialdrucks auf 1,52 bar bewirkte eine Steigerung von Wasserstoffaufnahme und Ethanol-Raum-Zeit-Ausbeute, das Produktverhältnis verschob sich in Richtung von Ethanol. Eine Ethanol-Raum-Zeit-Ausbeute von 10 $\mathrm{mmol\,L^{-1}\,h^{-1}}$ wurde erzielt, allerdings war diese nicht langzeitstabil. Weiterhin haben die Messdaten gezeigt,

dass oberhalb eines Wasserstoffpartialdrucks von 1,52 bar, dies entspricht einer theoretischen Gleichgewichtskonzentration von $c^*_{l,H_2} = 1,2\,\mathrm{mmol\,L^{-1}}$, die Wasserstoffaufnahme deutlich abnimmt, was auf eine Hemmung einer enzymatischen Reaktion hinweisen könnte.

Die Ergebnisse der vorliegenden Arbeit haben daher nicht nur zu einer erheblichen Steigerung der volumetrischen Produktivität durch detaillierte Untersuchung des Einflusses eines Biomasserückhaltesystems beigetragen, sondern auch zu einem wesentlich besseren Verständnis des Einflusses zentraler Prozessparameter wie z. B. vom H_2-Partialdruck auf den Fermentationsprozess mit *C. ljungdahlii*. Wichtige Einflussgrößen auf Produktivität und Produktverhältnis, wie z. B. der biomassespezifische Partialdruck von CO im Abgas oder die theoretische Gleichgewichtskonzentration von H_2 in der Fermentationsbrühe, wurden erfasst und es wurden Korrelationen entwickelt. Durch Messung in stationären Versuchszuständen bei kontiniuierlicher Versuchsführung und Langzeitversuchen mit teils über 3000 Stunden stabilem Betrieb wurde eine wertvolle Datenbasis für zukünftige kinetische Modellierungen geschaffen.

Contents

Declaration I

Acknowledgements II

Preamble IV

List of Publications V

Abstract VII

Zusammenfassung X

List of Abbreviations XVI

List of Symbols XVIII

1 Introduction 1

2 Synthesis gas fermentation - principles and challenges 4

2.1 Syngas fermentation with acetogenic microorganisms 4

2.2 Reaction mechanism 6

2.3 Process development 8

2.3.1 Hardware 8

2.3.2 Metabolic engineering and modeling 9

2.3.3 Operating conditions 10

3 Anaerobic syngas fermentation vs. chemical catalysis 12

3.1 Tolerance of the catalyst to syngas impurities 13

3.2 Process parameters 15

3.2.1 Temperature and pressure 15

3.2.2 Gas conversion and product ratio 17

3.2.3 Productivity . . . 18
3.2.4 Intermediates and by-products . . . 20
3.3 Downstream . . . 20

4 Materials and Methods 23
4.1 Microorganism, cultivation and nutrient medium . . . 23
4.2 System of continuous fermentation . . . 25
4.2.1 Experimental setup . . . 25
4.2.2 Foam separation system . . . 28
4.2.3 Process parameters . . . 29
4.2.4 Analytical methods . . . 31
4.3 Measurement campaigns . . . 32

5 Results 35
5.1 Influence of a total biomass retention system . . . 35
5.1.1 Cell density, product ratio, productivity . . . 35
5.1.2 Deactivation of cell retention - reversibility . . . 39
5.1.3 Potential accumulation of carbon in the fermentation broth . . . 40
5.2 Parameter study at increased cell densities . . . 41
5.2.1 Influence of an increased substrate gas flow . . . 41
5.2.2 Influence of an increased dilution rate . . . 45
5.2.3 Influence of a pressure increase at a volume-constant hydrogen input . 48
5.2.4 Influence of a gradually reduced pH value . . . 55

6 Discussion 60
6.1 Influence of high cell densities by using biomass retention . . . 61
6.1.1 Limitation of substrate gas and nutrients . . . 61
6.1.2 Biomass-specific partial pressure of CO in the off-gas . . . 63
6.1.3 Growth stagnation . . . 66
6.2 Influence of a pressure increase at a constant volumetric hydrogen input . . . 70
6.2.1 Increase in hydrogen uptake at moderate increased H_2 partial pressure 70
6.2.2 Inhibition of hydrogen uptake at high H_2 partial pressure . . . 72
6.2.3 No inhibitory effect by CO_2 . . . 73
6.3 Limit of long-term stable ethanol concentrations . . . 73
6.4 Influence of a gradually reduced pH value . . . 74

7 Conclusion 77

A Appendix **80**
A.1 Detailed process flow diagram 81
A.2 Development of a foam separation system 82
A.3 Calculation of the reactor wall thickness depending temperature and pressure 84
A.4 Measurement data of the long-term experiments 86
A.5 Measurement data of potential carbon accumulation 90
A.6 History of evolution of the test rig for the fermentation of synthesis gas 91
A.7 Maximum hours of operation of the agitator coupling with friction bearings . 94
A.8 List of chemicals 95

List of Tables **97**

List of Figures **99**

Bibliography **102**

List of Abbreviations

AcOH	acetic acid
AdhE	bifunctional acetaldehyde/alcohol deydrogenase
AOR	aldehyde ferredoxin oxidoreductase
Cat	catalyst
CBM	constraint-based model
CDW	cell dry weight
CoA	coenzyme A
CODH	CO-dehydrogenase
CoFeS	corrinoid/iron sulfur protein
CR	cell retention
$\overline{\mathrm{CR}}$	without cell retention
CSTR	continuous stirred-tank reactor
CZA	$Cu/ZnO/Al_2O_3$
Ech	energy-converting hydrogenase
EtOH	ethanol
Fb	fermentation broth
Fd	ferredoxin
FSS	foam separation system
GC	gas chromatograph
GRT	gas retention time
HC	heterogeneous catalysis
HF	hollow fiber

HPLC	high performance liquid chromatography
Hyd	electron-bifurcating hydrogenases
IC	inorganic carbon
KOH	potassium hydroxide
LHV	lower heating value
ME	macromolecular synthesis
MeOH	methanol
MES	2-(N-morpholino) ethanesulfonic acid
NADP	nicotinamide adenine dinucleotide phosphate
Nfn	electron-bifurcating transhydrogenase
NIR	near-infrared spectroscopy
NM	nutrient medium
OD	optical density
PES	polyethersulfone
Rnf	*Rhodobacter* nitrogen fixation
RWGSR	reverse water-gas shift reaction
rpm	revolutions per minute
rSMM	reduced stoichiometric metabolic model
SF	syngas fermentation
STR	stirred-tank reactor
TC	total carbon
THF	tetrahydrofolate
TOC	total organic carbon
vol.	volume
WGSR	water-gas shift reaction
WLP	Wood-Ljungdahl pathway

List of Symbols

Latin symbols

C_i	carbon content of component i	$\mathrm{mg\,L^{-1}}$
c_i	concentration of product i	$\mathrm{mmol\,L^{-1}}$
$c^*_\mathrm{l,i}$	theoretical equilibrium concentration of component i in the liquid	$\mathrm{mmol\,L^{-1}}$
c_1, c_2	allowance	mm
D	dilution rate	$\mathrm{h^{-1}}$
D_o	outer diameter	m
e_B	specific energy to synthesize biomass	$\mathrm{kJ\,g^{-1}_{CDW}}$
f_CDW	conversion factor	$\mathrm{g\,L^{-1}}$
H_i	Henry's Law constant of component i	$\mathrm{mol\,m^{-3}\,bar^{-1}}$
K	strength parameter	$\mathrm{N\,m^{-2}}$
$k_\mathrm{L}a$	gas-liquid mass transfer coefficient	$\mathrm{s^{-1}}$
M	molar mass	$\mathrm{g\,mol^{-1}}$
m	mass	g
n	amount of substance	mmol
$\dot{n}$	molar flow rate	$\mathrm{mmol\,min^{-1}}$
P	power	W
p	pressure	bar
p_B	specific power for the biomass synthesis	$\mathrm{J\,g^{-1}_{CDW}\,h^{-1}}$
p_i	partial pressure of component i	mbar
p_M	specific power for the maintenance metabolism	$\mathrm{J\,g^{-1}_{CDW}\,h^{-1}}$

q_{G}	biomass-specific gas uptake rate	$\mathrm{mmol\,g^{-1}\,h^{-1}}$
q_{P}	biomass-specific productivity	$\mathrm{mmol\,g^{-1}\,h^{-1}}$
R	gas constant	$\mathrm{J\,mol^{-1}\,K^{-1}}$
R^2	coefficient of determination	$-$
r	gas uptake rate	$\mathrm{mmol\,L^{-1}\,h^{-1}}$
$r^*_{\mathrm{H_2}}$	gas uptake ratio of hydrogen to carbon	$-$
S	selectivity	$-$
S_{f}	safety factor	$-$
STY	space-time yield	$\mathrm{mmol\,L^{-1}\,h^{-1}}$
s	wall thickness	mm
T	temperature	$^{\circ}\mathrm{C}$
TOF	turnover frequency	$\mathrm{h^{-1}}$
t	time	h
u	velocity	$\mathrm{m\,s^{-1}}$
V	volume	$\mathrm{m^3}$
$\dot{V}$	volume flow	$\mathrm{mL\,min^{-1}}$
v	weld factor	$-$
X_{i}	conversion of i	$-$
x_{i}	mole fraction in the liquid phase	$-$
y_{i}	mole fraction in the gaseous phase	$-$

Greek symbols

β_{i}	mass concentration of product i	$\mathrm{g\,L^{-1}}$
ΔC	deviation of carbon content	$\%$
$\Delta G^{\circ\prime}$	free energy change	$\mathrm{kJ\,mol^{-1}}$
ΔH_{LHV}	lower heating value	$\mathrm{kJ\,mol^{-1}}$
μ	growth rate	$\mathrm{h^{-1}}$
τ	liquid retention time	h

Sub- and Superscripts

E	educt
G	gas
l	liquid
m	molar
n	standard reference
o	outer
ox	oxidized
off	off-gas
P	product
R	reactor
red	reduced
W	working part

1 Introduction

The possibility of using synthesis gas fermentation to convert hydrogen and carbonaceous gases such as CO and CO_2 into chemicals, fuels and other valuable products could be of great importance to a future circular economy [1, 2]. The advantages of syngas fermentation over heterogeneous catalysis are low process pressures and process temperatures, self-regeneration of the biocatalyst, and complete gas conversion without the need for a recirculation loop. H_2, CO and CO_2 can be obtained e. g. by (co-)electrolysis [3, 4], gasification of biomass [5], from industrial waste gases [6] or air capture [7] and could be converted to C_2 - C_8 compounds by acetogenic bacteria [8–11]. Anaerobic acetogenic bacteria convert CO_2 to acetyl-CoA via the Wood-Ljungdahl pathway and they produce acetic acid and ethanol in a first process step [12]. Both H_2 and CO serve as reducing agents [13, 14].

A major bottleneck for the commercialization of syngas fermentation is the low space-time yield, which is up to three orders of magnitude lower than of heterogeneous catalysis. Due to low product concentrations, product separation as well as purification are associated with high costs. Therefore, an increase of the cell density, which means an increase of the density of the biocatalyst in the reactor, represents an essential key variable in order to increase the space-time yield as part of the process development. By using a biomass retention system, the outflow of the biocatalyst in the product stream during continuous operation can be avoided and thus an increase in cell density can be achieved. Centrifugation, filtration, or solid/liquid separators can be used to retain biomass [15]. Higher cell densities and an increase of space-time yield through the use of a biomass retention system have already been demonstrated in numerous studies on acetogenic microorganisms, see DE MEDEIROS ET AL. [16], KANTZOW ET AL. [17], RICHTER ET AL. [18], GADDY ET AL. [15], PHILLIPS ET AL. [19], ABUBACKAR ET AL. [20], MAYER ET AL. [21] and MOLITOR ET AL. [22]. However, detailed studies on the influence of cell retention on syngas fermentation and the reaction engineering principles are missing.

Furthermore, the process parameters pressure and pH are key process parameters in terms of influencing productivity and product ratio of ethanol to acetic acid. YOUNESI ET AL. [23] found that they were able to increase overall productivity and ethanol space-time yield by increasing process pressure. ABUBACKAR ET AL. [20] use a two-stage reactor setup to achieve

high growth at optimal pH in stage 1 and increased ethanol formation at reduced pH in stage 2. However, detailed studies on the influence of increased partial pressure of H_2 and reduced pH on syngas fermentation at high cell densities and continuous operation are missing.

To determine the reaction engineering principles of monoculture with *Clostridium ljungdahlii* and to understand the influence of the key process parameters on the reaction, experiments in continuous mode are a prerequisite and of essential importance. Studies in batch mode are not very useful, since product inhibition or medium limitations can occur during the course of the experiment. Therefore, the following study answers essential research questions on efficiency increase and reaction engineering principles in continuous operation in more detail:

1.) When using a biomass retention system to increase the cell density, does cell retention affect the product ratio?

2.) Is the space-time yield proportional to the cell density?

3.) Does total cell retention lead to an accumulation of carbon in the reactor?

4.) When using a biomass retention system, is it possible to increase the hydrogen uptake rate by increasing the process pressure at a constant volumetric hydrogen input, thus further increasing ethanol formation? The constant-volume hydrogen feed implies an increase in the hydrogen partial pressure in order to improve the gas-liquid mass transfer of H_2.

5.) With the use of a biomass retention system and already high space-time yields of ethanol, can the product ratio be shifted even further in the direction of ethanol by lowering the pH?

In order to answer these scientific questions, the fundamentals of synthesis gas fermentation and the state of the art are first summarized in Chapter 2. In Chapter 3, a comparison is made between chemical heterogeneous catalysis and synthesis gas fermentation in order to highlight both the challenges and the opportunities of synthesis gas fermentation. The driver for the experimental investigations carried out as part of this thesis is to achieve an improvement in the two fundamental weaknesses of synthesis gas fermentation, a low volumetric productivity due to low cell densities and a lack of knowledge of reaction engineering principles in continuous operation mode. The experimental investigations are carried out on a test rig in continuous operation mode, the setup, the execution procedure and the data analysis are described in Chapter 4. In Chapter 5, the measurement results on the influence of increased cell densities and varied parameters such as substrate gas flow, dilution rate, hydrogen partial pressure and pH

are presented. These results are analyzed and discussed in Chapter 6 followed by a conclusion in Chapter 7.

With the novel experimental setup used for this study, it is possible to carry out fermentation experiments in fully continuous operating mode with pH control, a biomass retention system to increase cell density, and with pressure-stable designs to increase process pressure. With this setup, it is possible to fill the current knowledge gap on the influence of biomass retention as well as dilution rate, substrate gas flow, pH and H_2 partial pressure at high cell densities. These data would also provide an important basis for future studies on the co-cultivation of *C. ljungdahlii* and caproate-producing bacteria, which could be used to convert acetic acid and ethanol to higher added-value products.

2 Synthesis gas fermentation - principles and challenges

2.1 Syngas fermentation with acetogenic microorganisms

Fermentation processes take place in aqueous solutions. A redox reaction delivers the energy for the bacteria to grow, that means to synthesize more bacteria. In opposite to traditional fermentation processes that are based on starch feedstocks [24, 25], synthesis gas fermentation uses gaseous C_1-substrates. The fermentation reaction is catalyzed by a chemolithoautotrophic microorganism, and the products could be fuels, chemicals, fats, and proteins [26]. Knallgas bacteria, carboxydotrophs, methanotrophs and methanogens could be used as chemolithoautotrophic platforms for gas fermentation [26–32]. Beyond that, anaerobic acetogens represent another possibility for gas fermentation. They are well investigated and already successfully in use at industrial pilot scale and commercial plants for anaerobic syngas fermentation [13, 26, 33]. Therefore, they are discussed in more detail here.

Acetogens are found in 23 genera, and they are distributed all over the world with many possible habitats, among which: different types of sediment, soil, sewage, or manure [34]. Table 2.1 contains a list of well investigated mesophilic and thermophilic acetogenic microorganisms. They can use either CO or CO_2 and H_2 or all three gases as substrate gas and convert these to acetic acid, ethanol, 2,3-butanediol and other alcohols and organic acids as products. Metabolic engineering enables the conversion of substrate gas to higher added-value compounds like butanol and isoprene. Optimal growth for mesophilic acetogenic microorganisms is between $25 - 40\,^{\circ}\mathrm{C}$ and up to $65\,^{\circ}\mathrm{C}$ for thermophilics [35]. Further details on both optimal and possible temperature operating ranges of acetogenic bacteria can be found elsewhere [9, 29, 36].

Table 2.1: Acetogenic microorganisms: a selection of key organisms of different genus.

Microorganism	Substrate gas	Products	Products of metabolic engineered strains	References
Acetobacterium woodii	CO_2/H_2, CO	Acetic acid, ethanol	Acetone, 1-butanol	[37–42]
Clostridium aceticum	CO_2/H_2, CO	Acetic acid, ethanol, 2-oxobutyrate	Acetone	[34, 36, 43–45]
Clostridium autoethanogenum	Syngas, CO_2/H_2, CO	Acetic acid, ethanol, 2,3-butanediol, lactic acid	Butanol, acetone, isopropanol, fatty acid ethyl ester, fatty acid butyl ester, 3-Hydroxypropionate, 2-butanol, MEK, meso-2,3-butanediol, butanoic acid butyl ester, mevalonate, isoprene, franesene, ethylene glycol, poly-3-hydroxybutyrate	[36, 37, 46–56]
Clostridium carboxidivorans	CO_2/H_2, CO	Butanol, butyrate, acetic acid, ethanol, lactate, 2,3-butanediol, hexanol, hexanoic acid, caproate	Propanal, propan-1-ol	[9, 36, 53, 57, 58]
Clostridium ljungdahlii	Syngas, CO_2/H_2, CO/H_2,CO	Acetic acid, ethanol, 2,3-butanediol, 2-oxobutyrate, formic acid	Butanol, butyrate, isoprene, lactate, acetone, mevalonate, isopropanol, hexanol	[9, 37, 43, 49, 54, 59–65]
Blautia productus	CO_2/H_2, CO	Acetic acid	1-butanol	[37, 66–68]
Moorella thermoacetica	CO_2/H_2, CO	Acetic acid	Acetone	[68, 69]

2.2 Reaction mechanism

Anaerobic acetogens are able to produce acetate or ethanol through the fixation of CO_2 via the so-called Wood-Ljungdahl pathway (WLP) see Figure 2.1. The free energy of the production of acetate and ethanol from either H_2/CO_2 or CO is given in Equations 2.1-2.4, where $\Delta G^{\circ\prime}$ is the free energy change calculated under standard conditions (1 M concentrations of substrates and products, partial pressure of gases 1 bar, pH 7):

$$4\,H_2 + 2\,CO_2 \longrightarrow CH_3COOH + 2\,H_2O \qquad \Delta G^{\circ\prime} = -95\,\mathrm{kJ\,mol^{-1}} \tag{2.1}$$

$$4\,CO + 2\,H_2O \longrightarrow CH_3COOH + 2\,CO_2 \qquad \Delta G^{\circ\prime} = -175\,\mathrm{kJ\,mol^{-1}} \tag{2.2}$$

$$6\,H_2 + 2\,CO_2 \longrightarrow CH_3CH_2OH + 3\,H_2O \qquad \Delta G^{\circ\prime} = -105\,\mathrm{kJ\,mol^{-1}} \tag{2.3}$$

$$6\,CO + 3\,H_2O \longrightarrow CH_3CH_2OH + 4\,CO_2 \qquad \Delta G^{\circ\prime} = -224\,\mathrm{kJ\,mol^{-1}} \tag{2.4}$$

Due to the mechanistic constraints the energy of these reactions can only partially be harvested by the bacteria. This is a result of the reactions and interactions of the WLP, the enzymes bifurcating hydrogenase (Hyd) and electron-bifurcating transhydrogenase (Nfn) and either the energy-converting hydrogenase complex (Ech) or the *Rhodobacter* nitrogen fixation complex (Rnf) [13, 14].

In the methyl-branch (upper branch) of the WLP, CO_2 is reduced to formate. In an ATP dependent reaction formate is activated and bond to tetrahydrofolate (THF). In two reducing steps, it is further reduced to a THF-bound methyl group. This methyl group is transferred via a corrinoidiron-sulfur protein to the central CO-dehydrogenase/acetyl-CoA-synthase enzyme complex (CODH/AcCoA-S). This enzyme also binds and reduces one CO_2 to CO with reduced ferredoxin (Fd^{red}) as electron donor in the carbonyl branch. Finally, the methyl-CoA and the bond CO are fused to yield one acetyl-CoA [34, 71, 72]. Acetyl-CoA is converted by the phosphotransacetylase and acetate kinase to yield one acetate and the ATP needed for the activation of formate. Hydrogen enters the reaction through Hyd delivering Fd^{red}. Nfn supplies NADPH [13]. Depending on the microorganism, either the membrane bound Ech or the Rnf complex reoxidizes Fd^{red} whilst transferring H^+ (or Na^+) across the membrane. An overview of the presence of Ech or Rnf and H^+ or Na^+ as protons is given by ROSENBAUM and MÜLLER [14]. For every 3 to 4 (3.66 in *C. ljungdahlii*) protons reentering the cell through the ATP-ase one ATP is generated. The NADH produced in this final step by the Rnf complex is reoxidized in the methyl branch. The ATP gain per one mole of acetate synthesized depends on the nature of the reducing equivalents (2[H]) used in those three reducing reactions in the methyl branch of the WLP. For *M. thermoacetica* this results in the formation of 0.5 ATP [13],

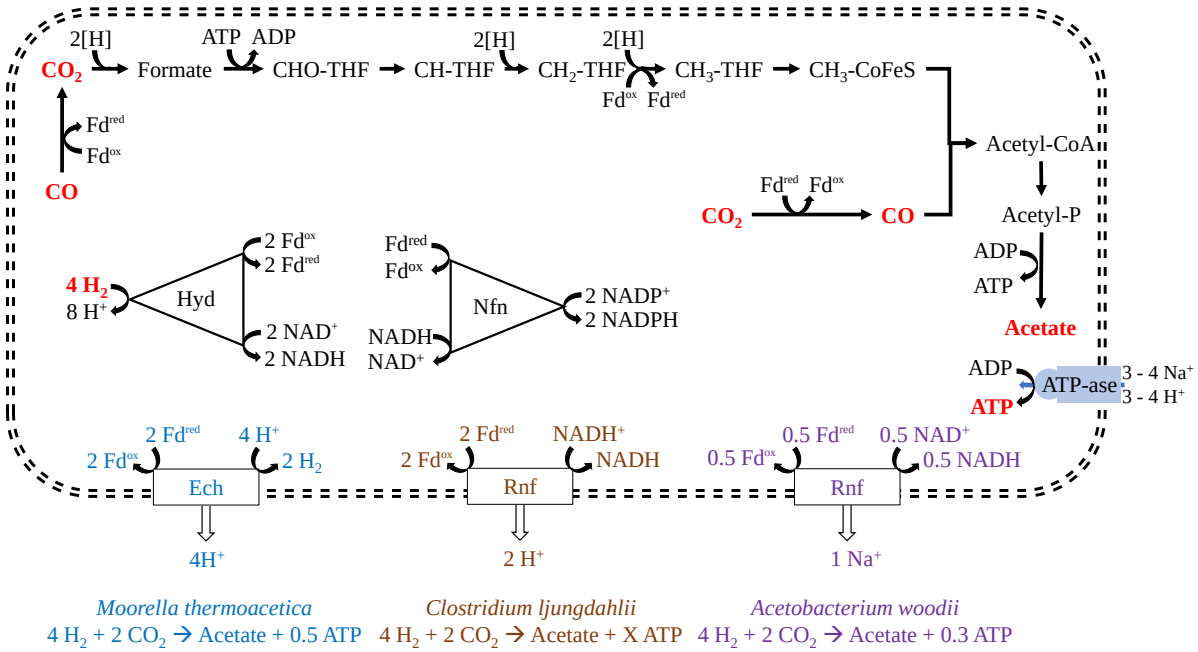

Figure 2.1: Overview of the Wood-Ljungdahl pathway and a model for chemiosmotic energy conservation in Ech and Rnf acetogens. THF: Tetrahydrofolate; CoFeS: corrinoid/iron sulfur protein; CoA: coenzyme A; $\mathrm{Fd^{red}}$: reduced ferredoxin; $\mathrm{Fd^{ox}}$: oxidized ferredoxin; [H]: reducing equivalent ($= 1e^- + 1H^+$); Hyd: bifurcating hydrogenase; Nfn: electron-bifurcating transhydrogenase; Ech: energy-converting hydrogenase; Rnf: Rhodobacter nitrogen fixation. The $\mathrm{Na^+}$-dependent Rnf in *Acetobacterium woodii* is boosted by the addition of NaCl to the culture medium [70]. Adapted from SCHUCHMANN and MÜLLER [13] and ROSENBAUM and MÜLLER [14].

whereas for *C. ljungdahlii* from –0.14 [73] up to 0.63 [13] ATP per mole acetate have been proposed. CO can also be used directly in the carbonyl branch and saves one $\mathrm{Fd^{red}}$ leading to higher ATP yield [74].

The second main product of syngas fermentation is ethanol. It can be either produced from acetyl-CoA via acetaldehyde or via reduction of non-activated acetate by an aldehyde oxidoreductase (AOR) and the reduction of the formed acetaldehyde to ethanol via an alcohol dehydrogenase reaction with $\mathrm{Fd^{red}}$ as electron donor. It is assumed that all commercially used acetogens produce ethanol via this AOR pathway as it is more energy efficient (first formation of ATP by acetate production, then formation of acetaldehyde and ethanol) [75]. Products other than acetate and ethanol are thermodynamically very difficult, since for mechanistic and thermodynamic reasons only less than 1 ATP can be formed per organic acid produced [76].

2.3 Process development

Due to WLP as reaction mechanism space-time yield in syngas fermentation is limited by the availability of the substrate. This could be optimized by the reactor design and pressure. The "concentration" of the catalyst, the biomass, could be enhanced by cell retention and optimization of media and fermentation conditions. To synthesize other products like butanol or acetone the cell internal flux of acetyl-CoA and the balance of redox equivalents could be influenced by metabolic engineering. Therefore, the main research topics can be classified in three categories: hardware, metabolic engineering and modeling as well as operating conditions, see Figure 2.2.

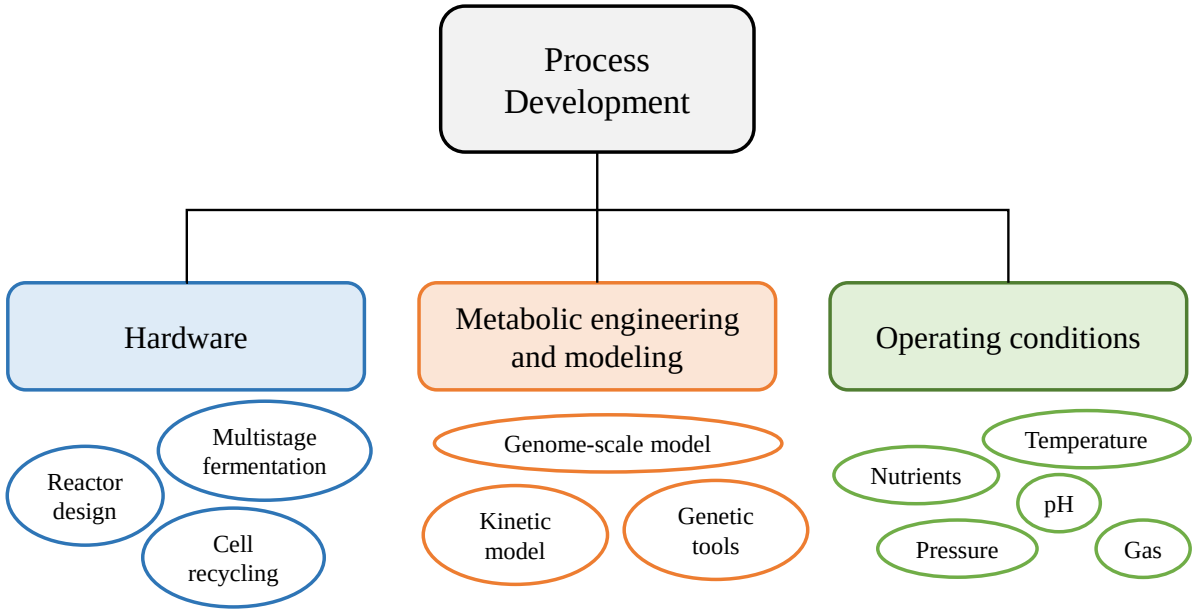

Figure 2.2: Components of process development for acetogenic syngas fermentation.

2.3.1 Hardware

The reactor design has strong influence on the mass transfer rate and, therefore, it has to be optimized in order to overcome a low gas-liquid mass transfer, since H_2 and CO have a low solubility in water [77]. Reactor types for syngas fermentation processes could be agitated reactor systems, like stirred vessels, and non-agitated ones, such as bubble columns, gas lift reactors, loop reactors, trickle bed reactors, membrane and biofilm reactors [78–80]. Stirred vessels, e. g., continuously stirred-tank reactors (CSTR), enable high gas-liquid mass transfer

rates by mechanical agitation. However, the specific energy input for agitation is typically around $1\,\mathrm{kW\,m^{-3}}$ [81], which is too high for the commercialization of syngas fermentation processes at industrial scale, as it should not surpass $0.3\,\mathrm{kW\,m^{-3}}$ [82]. Trickle bed reactors have a thin liquid film contacting the gas phase and, therefore, a low liquid resistance to mass transfer [83]. Membrane reactors could reach a maximum $k_\mathrm{L}a$ of $1096\,\mathrm{h^{-1}}$ at laboratory scale, which is three times higher than that of industrially used bubble columns [84]. However, due to the high membrane costs, they are less suitable for the production of bulk chemicals like ethanol [84]. Another possibility to achieve high mass transfer rates but with low operational and maintenance costs are bubble and gas-lift reactors. LanzaTech developed a modified, improved loop reactor by adding a secondary loop to a forced-circulation loop reactor [85]. Furthermore, a serial adding of reactors in a row, called multistage fermentation, could enable optimized conditions in each reactor system [9] leading to enhanced growth and productivity [15, 18, 20, 86]. However, for large industrial-scale reactors, it must be considered that significant gas concentration gradients can occur along the reactor height. PUIMAN ET AL. [87] have found in an Euler-Lagrangian CFD simulation that in an industrial-scale external-loop gas-lift reactor, the dissolved gas concentrations can oscillate by up to an order of magnitude in a period of 5-30 seconds. Further improvements and patents of reactor engineering are summarized in TAKORS ET AL. [88].

The low productivity of fermentation processes is, among others, caused by low cell densities. Cell recycling via separation and retention could be implemented through the use of centrifuges, membranous filtration techniques (e. g., hollow fibers, ceramic filter systems) or other solid/liquid separator systems [15]. DE MEDEIROS ET AL. [16] has observed a 3.6 times higher cell density and an increased ethanol productivity of 30 % with cell retention. Further investigations on the influence of cell retention can be found elsewhere [17–21, 89–92].

2.3.2 Metabolic engineering and modeling

Metabolic engineering and modeling have the goal of expanding product spectrum, increasing productivity and better understanding the microbial process steps. Adaptive laboratory evolution, DNA transfer and knock-down of target genes are among others very successful tools to expand product spectrum and increase productivity [36, 59, 93]. Overexpressing of THF-dependent enzymes in WLP has led to an increase in volumetric acetate productivity [94]. Furthermore, production of butanol as well as acetone and isopropanol under autotrophic growth on syngas has been successfully demonstrated as a result of genetically modified

Clostridia [37, 95]. More information on genetic tools for manipulating microorganisms can be found in LIEW ET AL. [95] and FACKLER ET AL. [26].

For metabolic engineering, a particularly deep understanding of the metabolic network is necessary. There are two different modeling approaches: a constraint-based model (CBM) and a kinetic model. CBMs are able to predict flux distribution, growth rate, knockouts and theoretical yields [96]. NAGARAJAN ET AL. [62] developed the first genome-scale model for the acetogen *Clostridium ljungdahlii*, which included 637 genes, 785 reactions and 698 metabolites. This model gives insight into the genetic and energetic metabolic constraints. MARCELLIN ET AL. [48] compared heterotrophic growth on fructose with autotrophic growth on syngas, in order to investigate the Rnf and Nfn complex. LIU ET AL. [97] developed the first macromolecular synthesis model (ME-model) of a gram-positive bacterium and used it to investigate the influence of protein allocation and media composition on metabolic pathway and energy conservation. With a reduced stoichiometric metabolic model (rSMM), HERMANN ET AL. [74] found out that the consumption of CO led to a higher energy availability than the use of H_2 as electron source. FOSTER ET AL. [98] investigated the influence of cell fusion on growth phenotype and panel of metabolites with a co-culture of *Clostridium acetobutylicum* and *Clostridium ljungdahlii*. For further information on genome-scale models, see VEES ET AL. [92] and FACKLER ET AL. [26].

However, since a relationship between the prediction of flux distribution, growth rate and theoretical yields cannot be built in a constraint-based model, a kinetic model approach should be used in this case. With a kinetic model, metabolic states and rate-limiting steps can be predicted. DE MEDEIROS ET AL. [16] optimized CO conversion and ethanol productivity by using a differential equation system with kinetic parameters as well as with experimental data from operating conditions. By combining a genome-scale model with thermodynamics via implementing a Gibbs free energy constraint, GREENE ET AL. [99] accurately predicted intracellular metabolite concentrations and engineering strategies for improved ethanol production.

2.3.3 Operating conditions

The gas-liquid mass transfer is known to be a bottleneck in syngas fermentation. Due to Henry's law, an increase in gas pressure leads to higher gas solubility and increased gas-liquid mass transfer. KANTZOW and WEUSTER-BOTZ [100] found that an increased hydrogen partial pressure from 0.4 bar to 2.1 bar led to both significant reduction in acetate and significant increase in formate concentration. BERTSCH and MÜLLER [101] stated that the hydrogen

partial pressure has strong dependence on the energy-conserving enzyme Ech. YOUNESI ET AL. [23] have seen that a slight increase in syngas pressure of up to 1.8 bar promotes ethanol productivity, while acetate concentration stays almost constant. HURST and LEWIS [102] observed that acetate concentration decreases when CO partial pressure is above 1 bar. High pressures up to 6 bar and 8 bar in a continuous operating mode were investigated for the first time by GADDY ET AL. [15] and STOLL [103], respectively. For both investigations, the highest ethanol concentrations of 25 $\mathrm{g\,L^{-1}}$ and 4.8 $\mathrm{g\,L^{-1}}$ occur at 6 bar. The highest overall efficiency of C_2-compounds as well as highest cell density can be detected at 2 bar [103].

Another important operating parameter is the gas composition. Different COx/H_2 ratios have a significant influence on the fermentation performance. If CO is supplied together with H_2, ethanol concentration will be enhanced [104]. However, JACK ET AL. [105] observed an increase in acetate to ethanol ratio when the amount of hydrogen in the headspace is raised in a range of 0.5 – 2 (initial hydrogen to carbon monoxide headspace concentration ratio). High H_2 ratios together with low amounts of CO_2 direct the cell metabolism towards ethanol synthesis [106]. Furthermore, CO and H_2 can both serve as electron donors [104, 107], while CO is preferred due to a higher available Gibbs free energy [105]. Besides the gas composition, the gas rate also has strong influence on the fermentation process. Substrate inhibition can occur if too much gas is transferred into the liquid phase [15, 105, 107–111]. Syngas impurities also influence the fermentation process [106, 112–114], see Chapter 3.1.

Experimental results have shown that lowering the pH shifts the products from acidogenic phase (growth and mainly acetate formation occurs) to solventogenic phase (growth rate is lower and more reduced products like ethanol are built) [18, 19, 58, 108].

A moderate lowering of temperature to 32 °C with *Clostridium ragsdalei* leads to higher ethanol concentration [115, 116]. Lowering the temperature to 25 °C with *Clostridium carboxidivorans* (optimal growth temperature 37 – 40 °C) favors alcohol production and carbon chain elongation [117–119].

Furthermore, nutrients like salts, trace elements, vitamins and reducing agents have high impact on microbial growth and product formation. Reviews on the influence of medium composition and medium costs as well as further experimental studies can be found elsewhere [9, 36, 108, 115, 118, 120–129].

3 Anaerobic syngas fermentation vs. chemical catalysis

Heterogeneous catalysis and anaerobic syngas fermentation represent two different approaches for the conversion of synthesis gas into chemicals and fuels. In order to identify both the advantages and existing challenges of synthesis gas fermentation in comparison to the established chemical catalysis, in this chapter, chemical and biological catalysis for the conversion of syngas into chemicals are compared, taking into account the process parameters and the syngas nature used as feed gas. A brief overview of the main characteristics from both approaches is presented in Table 3.1. For chemical catalysis heterogeneous methanol (MeOH) synthesis is chosen, while for biological catalysis ethanol (EtOH) and acetic acid (AcOH) by syngas fermentation are considered.

Table 3.1: Characteristics of pure chemical catalysts versus biochemical catalysts for the production of synthetic carbon-neutral and oxygenated hydrocarbons (Part I).

	Heterogeneous catalyst	Biocatalyst
Catalyst	Solid metal-based; simple inorganic molecules as reactants	Living cells; simple inorganic molecules as reactants
Synthesis / Cultivation	Multi step syntheses; metal loss via leaching issues; high temperature needed	Cultivation under mild conditions; narrow optimal window
Reaction media	Solid-Gas / Solution-Gas / Solution-Solid	Water and solutions
Operating conditions	High temperature and pressure	Mild temperature and pressure, close to ambient conditions
Selectivity	Fair-to-high	High

Table 3.1: Characteristics of pure chemical catalysts versus biochemical catalysts for the production of synthetic carbon-neutral and oxygenated hydrocarbons (Part II)

	Heterogeneous catalyst	Biocatalyst
Space-Time-Yield	Generally high	Low-to-fair
Waste	Potentially dangerous for the environment; cost intensive regeneration and disposal	Low environmental footprint; easy disposal

3.1 Tolerance of the catalyst to syngas impurities

Depending on the feedstock and the process route for the synthesis gas production, the type of impurities present may vary, e. g., particulate matter, condensable hydrocarbons, sulfur compounds, nitrogen compounds like nitric oxides, alkali metals, reactive oxygen species as well as hydrogen chloride [5, 26, 36, 93, 106, 130–132]. In comparison to wood or wheat straw, synthesis gas based on the gasification of coal has the highest impurity content for sulfur, ash, ammonia and hydrogen cyanide [130]. Gasification of biomass leads to higher concentration of alkali than the gasification of coal [115]. Natural gas may contain 1-5000 ppmv sulfur, which would be a problem for nickel and copper-based catalysts [116]. Composition and purity of the synthesis gas are fundamental in processes such as the heterogeneous catalyzed methanol synthesis, especially regarding to operation and investment costs [133]. Specific purity requirements for methanol synthesis in terms of particulates, tars, sulfur, nitrogen and alkali halides are summarized by WOOLCOCK and BROWN [134]. Information on purification technology of synthesis gas can be found elsewhere [106, 116, 117, 130, 132, 135].

In the following section, the effects of relevant syngas impurities on chemical (focus on CZA-based catalysts $Cu/ZnO/Al_2O_3$) and biological catalysis (focus on acetogenic microorganisms) are compared, see Table 3.2. Both syngas fermentation and MeOH synthesis rely on metal-containing catalysts such as transition metal-based catalysts or metalloenzymes to convert C_1-gases to products. In the case of syngas fermentation, metalloenzymes are responsible for the conversion. However, the risk of biocatalyst poisoning is lower than that of chemical catalyst poisoning, as the microorganisms acting as the biocatalyst are continuously regenerated [26]. In contrast to the biocatalyst used for syngas fermentation, the chemical catalyst cannot

Table 3.2: Most common syngas impurities and their influence on process performance in comparison for fermentation and heterogeneous MeOH synthesis differentiated according to negative impact (-), positive impact (+) and no impact/neutral (o).

Impurity component	Fermentation	MeOH synthesis	References
Sulfur compounds	+	-	[77, 126, 137, 138]
Tar	o / -	o	[36, 112, 138, 139]
HCN	o / -	o	[140–142]
HCl	o	-	[108, 140, 143]
Particulates	-	-	[36]
O_2	+ / o / -	-	[36, 138, 144–147]
NOx	o / -		[112, 113, 139, 148]
NH_3 / NH_4^+	+ / -	-	[112, 113, 137, 138]

regenerate by itself. Deactivation due to poisoning and sintering takes place over time and therefore a catalyst's lifetime is commonly limited to 2 – 6 years for industrial use [136].

A key difference between fermentation and chemical catalysis is the tolerance to sulfur compounds in the substrate gas. Sulfur is an important nutrient to stimulate growth of microorganisms, as reported by MOHAMMADI ET AL. [108] PHILLIPS ET AL. [77]. In contrast, CZA-based catalysts are strongly deactivated by H_2S, which blocks part of the Cu active sites, hence reducing the surface area and therefore leading to a significant decrease of carbon conversion. The extent of the activity loss is proportional to the sulfur molar concentration accumulated on the catalyst [130, 131, 137]. An impurity level of H_2S should be lower than 0.1 ppm in order to avoid catalyst poisoning [106].

On the other hand, the chemical catalyst has a much higher tolerance to HCN than the microorganisms. There is no catalyst deactivation even at HCN concentrations of up to 101.5 ppmv [140], while HCN is very toxic for microorganisms as it binds to the key enzyme CODH [36]. HCN concentrations lower than 1 ppm are required for industrial syngas fermentation [141], but a laboratory study concluded that the microorganisms are able to adapt to HCN concentrations lower than 2.7 ppm [142].

For syngas fermentation, the removal of polycyclic aromatics is necessary, although adaptation to tar after prolonged exposure is possible [36, 112, 139]. For CZA-based catalysts, hydrocarbons seem to act as inert spectators with no effect on catalytic activity, selectivity and process stability during methanol synthesis [138].

Studies on the influence of oxygen on syngas fermentation do not come to a clear conclusion: while O_2 is particularly critical during inoculation [36], tolerance in certain conditions [144] and even detoxification and enhancement of ethanol formation is possible [145]. For CZA-based catalysts, O_2 deactivates Cu and Zn active sites by oxidation. This is reversed by syngas reducing agents (H_2, CO), but O_2 concentration should not surpass 300 ppm, otherwise this oxidation-reduction cycle is fast enough to accelerate irreversible sintering [146, 147].

Ammonia directly leads to a significant decrease of the productivity in case of methanol synthesis. However, after ammonia removal full generation of catalyst takes place [138]. The formation of the by-product trimethylamine is triggered when ammonia is present in syngas. For syngas fermentation, one study concludes that ammonia reduces cell growth and inhibits hydrogenase [112], while increased cell growth and ethanol formation are observed in another study [113].

Another syngas contaminant, HCl, accelerates sintering of CZA-based catalysts due to the formation of low-melting CuCl [140]. There is literature that even mentions concentration limits for HCl as low as 1 ppb [143]. In contrast, microorganisms are less susceptible to poisoning by chlorine [108].

Microorganisms are sensitive to NO, as hydrogenase activity is inhibited [139]. A concentration for nitric oxide lower than 40 ppm could be tolerated by the biocatalyst without a loss in enzyme activity and growth [148]. So far, no studies on the influence of NO on CZA-based catalysts are known.

3.2 Process parameters

3.2.1 Temperature and pressure

Anaerobic syngas fermentation and methanol synthesis show significant differences in operating conditions for pressure and temperature, see Figure 3.1. While syngas fermentation with acetogens is operated at low temperature and pressure, MeOH synthesis requires high temperature and pressure conditions. Due to enzyme activities, acetogens have a narrow operating temperature window. Cultivation, growth and productivity is possible between 15 – 65 °C [35, 149]. An increase in temperature above that limit would not lead to an enhanced productivity, but instead irreversibly destroy the microorganisms. Fermentation typically takes place at atmospheric pressure conditions with the highest process pressure of 8 bar at continuous operating mode being reported by STOLL [103]. In contrast to fermentation, the

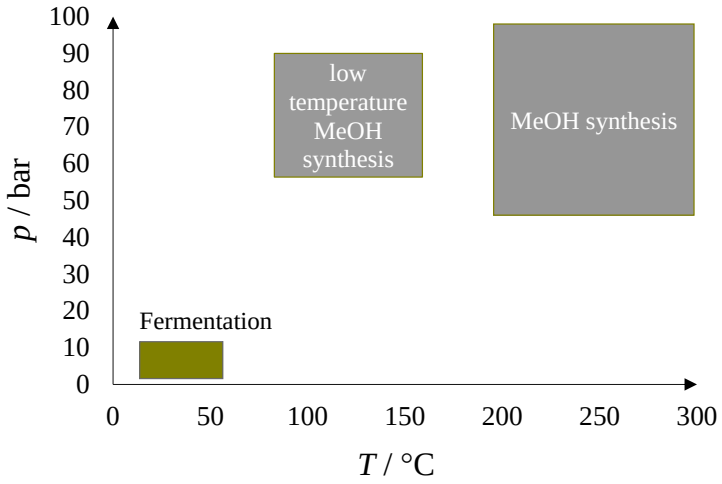

Figure 3.1: Operating windows for anaerobic syngas fermentation and MeOH synthesis. Data taken from [15, 35, 103, 149–154].

heterogeneous catalysis for MeOH synthesis needs higher temperatures of 200 – 300 °C [150]. Typical process pressures range between 50 – 100 bar [150]. Methanol synthesis can be also operated at lower temperatures (80 – 150 °C) by using alternative catalysts (Ru, Mn, Fe, Co) in a liquid phase [151–153], although this process is currently not commercially available. A TOF of 458 h^{-1} with a Ru(tdppcy)(TMM) catalyst at 90 bar H_2, 30 bar CO_2 and 120 °C was reported by SCHIEWECK ET AL. [154]. A further reduction of temperature and pressure with current catalysts materials would directly lead to a significantly reduced reaction rate and a productivity close to zero. As a result, activity of microorganisms used for anaerobic syngas fermentation is significant higher compared to heterogeneous catalysts at low temperature and pressure conditions.

The much milder conditions of syngas fermentation present an interesting advantage in comparison to heterogeneous catalysis. The required high pressures of the latter, significant investment costs are related to the compressors, while considerable operating costs are related to their power input [147, 155]. Besides, the wall thickness of the equipment must be thicker to handle high pressures, at least doubling the price in relation to operating at atmospheric pressure, see Section A.3 in the appendix. Finally, to achieve the required high temperatures in the catalytic process, it is necessary to build preheating and cooling units, as well as to implement strategies to control the reactor temperature, which also have an impact on the investment and operating costs. However, heat of reaction can be used directly for generating steam and heating the distillation columns for downstream product recovery. Temperature

control of syngas fermentation is also necessary, but at a lower level and therefore the heat of reaction cannot be directly used for heat integration.

3.2.2 Gas conversion and product ratio

Figure 3.2 shows the theoretical thermodynamic equilibrium for CO_2 conversion to MeOH and EtOH at two different pressures. The following reaction equations are considered for the formation of methanol and ethanol:

$$CO_2 + 3\,H_2 \rightleftarrows CH_3OH + H_2O \tag{3.1}$$

$$2\,CO_2 + 6\,H_2 \rightleftarrows CH_3CH_2OH + 3\,H_2O \tag{3.2}$$

At typical syngas fermentation conditions (e. g., p = 5 bar, T < 65 °C), CO_2 conversion of more than 95 % is possible. In this temperature range, there is no significant influence of the pressure on the equilibrium conversion. However, at typical catalytic methanol synthesis conditions (e. g., p = 50 bar, T > 200 °C), CO_2 conversion is lower and ranges between 30 – 40 %. Even at low temperatures (< 100 °C) regardless of the pressure, CO_2 conversion during MeOH synthesis is lower than during EtOH synthesis.

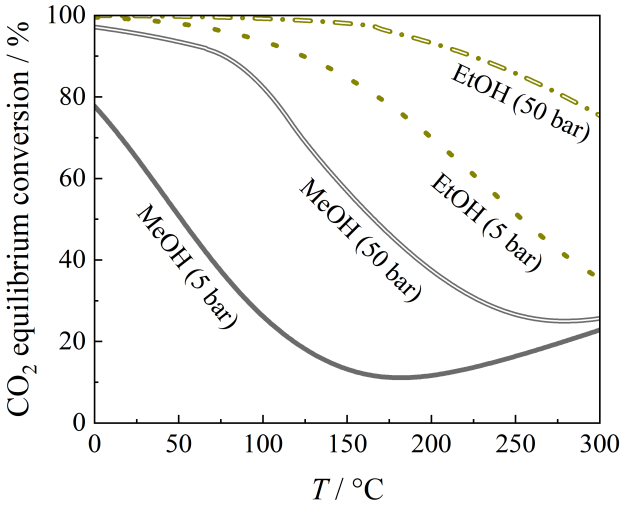

Figure 3.2: Theoretical CO_2 equilibrium conversion of methanol synthesis (see Equation 3.1) and ethanol synthesis (see Equation 3.2) at stoichiometric conditions (H_2/CO_2 : 3/1), different temperatures and two different pressures (5 bar, 50 bar). The WGSR is considered in both cases. Data generated with Aspen Plus V10 with UNIF-DMD as property methods.

Furthermore, Figure 3.2 shows according to Le Chatelier's principle a strong influence of pressure and temperature on CO_2 conversion: the lower the temperature and the higher the pressure, the higher the conversion rate. However, CO_2 conversion during methanol synthesis at 5 bar increases for temperatures higher than 175 °C. This is due to the endothermic reverse water-gas shift reaction (RWGSR), which is more present at high temperatures, converting CO_2 to CO resulting in an increased CO_2 equilibrium conversion. In addition, Figure 3.2 makes clear that CO_2 conversion during EtOH synthesis is higher at any operating condition compared to MeOH synthesis.

During methanol synthesis, gas composition also influences COx equilibrium conversion as COx equilibrium conversion is lower for CO_2-rich syngas compositions in comparison to CO/H_2-rich gas. In case of syngas fermentation, this means, that if gas-to-liquid mass transfer is high enough, then complete gas conversion and simultaneous usage of CO and CO_2 are possible. Many experimental studies revealed CO or CO_2 conversion of more than 90 % [15, 89, 103, 106, 156]. Furthermore, anaerobic syngas fermentation is flexible in terms of COx/H_2 ratio [81, 157]. However, the COx/H_2 ratio of substrate gas can be used to influence product ratio of fermentation, see Section 2.3.3.

3.2.3 Productivity

Figure 3.3a shows the (bio)mass-specific productivity q_P in $\mathrm{g_i}$ of product i per hour and mass of the cell-dry weight of the biomass $\mathrm{g_{CDW}}$ or mass of the heterogeneous catalyst $\mathrm{g_{Cat}}$. The data shown in Figure 3.3a are taken from experiments at continuous operating mode. C_2 compounds (acetic acid and ethanol) via syngas fermentation (SF) and methanol and DME via heterogeneous catalysis (HC) are presented. The mass-specific productivity of methanol is between $0.02-2\,\mathrm{g_{MeOH}\,g_{Cat}^{-1}\,h^{-1}}$ with $0.08\,\mathrm{g_{MeOH}\,g_{Cat}^{-1}\,h^{-1}}$ as the lowest quartile for MeOH formation reported by SLOTBOOM ET AL. [160] and $0.45\,\mathrm{g_{MeOH}\,g_{Cat}^{-1}\,h^{-1}}$ as the highest quartile reported by LACERDA DE OLIVEIRA CAMPOS ET AL. [159]. A narrow range of mass-specific productivities compared to heterogeneous catalysis can be observed for syngas fermentation ($0.2-0.7\,\mathrm{g_{C_2}\,g_{CDW}^{-1}\,h^{-1}}$). The quartiles are comparable to that of LACERDA DE OLIVEIRA CAMPOS ET AL. [159] and almost an order of magnitude higher compared to SLOTBOOM ET AL. [160], thus indicating that the mass-specific productivities of syngas fermentation are of the same order of magnitude and even of one order higher compared to heterogeneous catalysis.

Apart from the mass-specific productivity, the volumetric productivity is of particular importance for operation and profitability of a process. Figure 3.3b shows the volumetric productivity

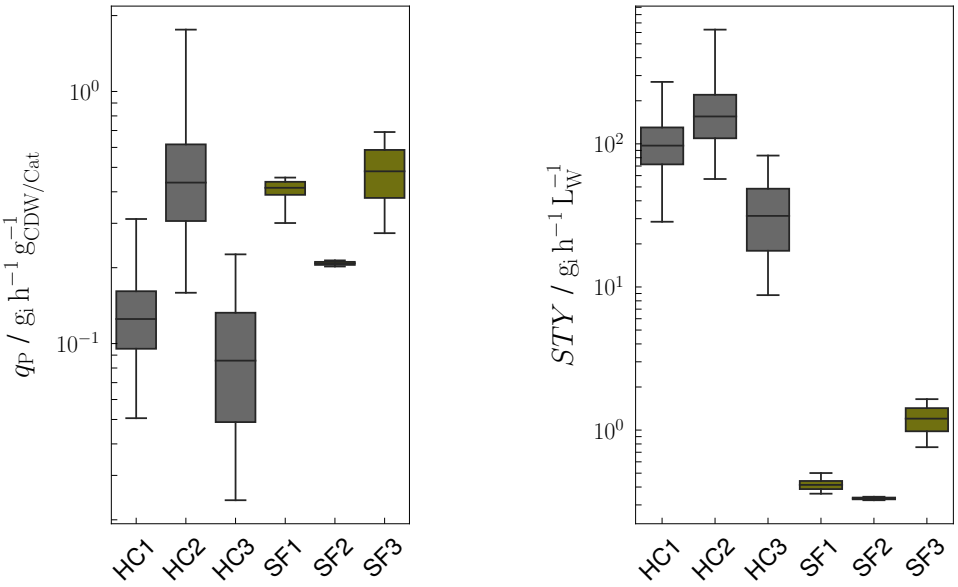

(a) Mass-specific productivity **(b)** Space-time yield

Figure 3.3: A comparative perspective of productivities between heterogeneous catalysis (HC) and syngas fermentation (SF) for (bio)mass-specific productivity q_P and space-time yield STY on a log scale. The boxes show the quartiles of the productivity values, the whiskers extend to show the rest of the distribution. HC1 (syngas): $\sum$MeOH + DME, WILD ET AL. [158]; HC2 (syngas): MeOH, LACERDA DE OLIVEIRA CAMPOS ET AL. [159]; HC3 (CO_2, H_2): MeOH, SLOTBOOM ET AL. [160]; SF1 (syngas): $\sum$AcOH + EtOH, STOLL [103], SF2 (syngas): $\sum$AcOH + EtOH, ACHARYA ET AL. [161]; SF3 (CO_2, H_2): AcOH, KANTZOW ET AL. [17].

also known as space-time yield STY in g_i of product i per hour and working volume in L_W^{-1}. In the case of fermentation, the working volume corresponds to the fermentation broth (Fb); in the case of heterogeneous methanol catalysis, the working volume is the volume required for the catalyst in the reactor; in general, it corresponds to the reactor volume, as the reactor is completely filled with catalyst. The data in Figure 3.3b are taken from the same source as in Figure 3.3a and the mass-specific productivities have been converted to volumetric productivities. Volumetric productivities of methanol synthesis range from $9-650\,g_{MeOH}\,L_{Cat}^{-1}\,h^{-1}$, while for acetic acid and ethanol formation via fermentation volumetric productivities are lower and range from $0.3-1.7\,g_{C_2}\,L_{Fb}^{-1}\,h^{-1}$. This difference between fermentation and catalysis is in the range of two to three orders of magnitude and points out a significant disadvantage of syngas fermentation: due to low cell densities of the biomass in the fermenter, volumetric productivity is low. Therefore, there is still need for research to increase the cell density in the reactor, see also Section 2.3.1 for cell recycling.

3.2.4 Intermediates and by-products

The number of intermediates and by-products is low for both fermentation and catalysis. An overview of the reaction mechanisms is described in PERRET ET AL. [162]. For fermentation, formate is an intermediate product in the methyl branch of WLP. Besides formate, acetyl-CoA is another important intermediate, as biomass, acetate and ethanol could be built by further conversion of acetyl-CoA. In some cases, acetate is also treated as an intermediate, as acetate could be converted to ethanol via AOR [163]. Formate is an important intermediate for methanol synthesis as well, as it is converted to methanol via CO_2 hydrogenation. However, formate accumulates and is an inhibitor of direct CO hydrogenation. The occurrence of water as a by-product of catalytic methanol synthesis depends, among other things, on the substrate gas. When working with CO_2-rich syngas, water is formed via both methanol synthesis and RWGSR, leading to reduced productivities [137, 157]. Further by-products occur at hot reactor zones [164]. Compared to methanol synthesis, there are no by-products worth mentioning during fermentation. The high product selectivity of syngas fermentation leads to fewer and less toxic by-products [165].

3.3 Downstream

For product recovery of MeOH, EtOH and AcOH, different separation techniques are necessary. Figure 3.4 and Figure 3.5 portray the product recovery process for fermentation and MeOH synthesis. In the methanol synthesis, distillation costs for methanol recovery can represent up to 10 % of the plant's investment costs [166]. Costs of separation processes for syngas fermentation can account for over 60 % of the production costs [167].

In a LanzaTech process for ethanol production via syngas fermentation, a distillation-based separation system is used for product and co-product recovery. However, distillation for low titer products represents an energy-intensive and therefore cost-intensive separation technique. 2.0 – 2.5 t of steam per ton of ethanol are necessary for product separation [168]. Biomass, other organics and waste liquids from the fermenter are separated by ultrafiltration and are finally treated on-site in an anaerobic digestion unit [168]. The successful usage of microbial biomass waste as animal feed due to its similar amino acid profile to that of fishmeal was investigated by CHEN ET AL. Electro-membrane processes as well as liquid-liquid extraction represents promising separation techniques to remove organic acids like acetic acid at reduced separation costs [36, 170, 171]. Further information on separation techniques can be found in LI ET AL. [167].

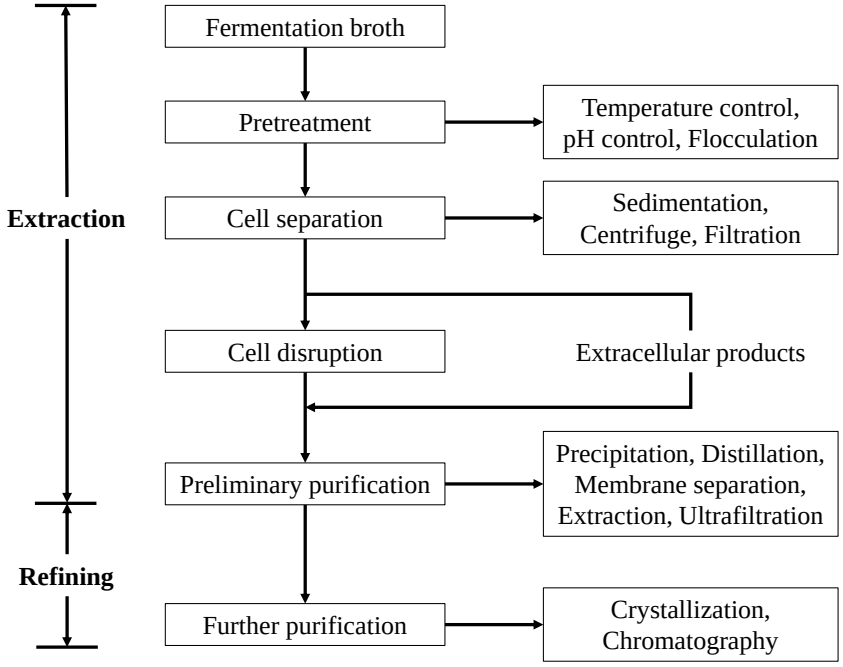

Figure 3.4: Process scheme of product separation for fermentation broth recovery. Figure copyright: The Korean Society for Microbiology and Biotechnology [167].

Since distillation columns are cost intensive due to the necessary phase change, it is less advisable to already separate after the production step for C_2-compounds when using syngas fermentation (as shown in Figure 3.4). Rather there is the possibility of using co-cultures or serially adding further fermentation stages without the need for intermediate treatment and separation in order to synthesize high-value products such as fats, lipids and long-chain alcohols and carboxylic acids [36]. HU ET AL. [172], OSWALD ET AL. [127], LAGOA-COSTA ET AL. [173], TRAN and SIMPSON [165] and MOLITOR ET AL. [22] are using different microorganisms in their multistage fermentation systems to convert syngas in several steps to lipids, malic acids, polyhydroxybutyrate (PHB) and single-cell proteins. By using these further process steps for chain elongation, product separation can be processed using less energy-intensive extraction, crystallization and precipitation compared to distillation columns.

For methanol purification, a unit distillation system is used to remove undesirable by-products and the water generated during methanol synthesis. For fuel grade methanol process a single distillation column is sufficient to meet commercial specifications [136]. However, for chemical grade methanol several extraction and distillation steps are necessary [174]. When using CO_2-rich synthesis gas, the amount of water to be separated from the crude methanol is three times higher than with syngas [175], but the amount of by-products is 2 - 12 times lower

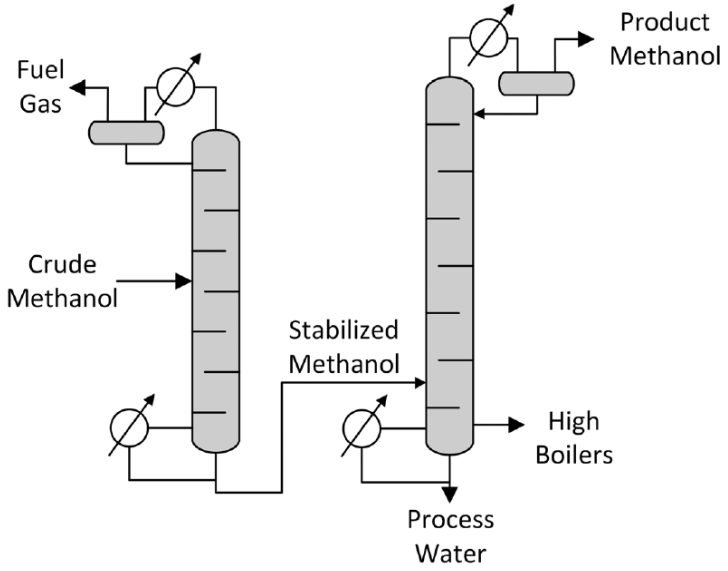

Figure 3.5: Two-column methanol distillation for product recovery with permission from the Royal Society of Chemistry [136].

[136]. For example, the amount of ketones in crude methanol after methanol synthesis with CO_2-rich synthesis gas is less than 1 ppm, thus reducing the complexity of the distillation process [175].

4 Materials and Methods

This chapter deals with the procedure for preparing and conducting the experimental studies. Section 4.1 presents the cultivation process of the biocatalyst with all the necessary components. This is followed in Section 4.2 by a description of the operational management for the continuous fermentation of synthesis gas. Section 4.3 contains a description and overview of the experiments carried out as part of this doctoral thesis on the continuous fermentation of synthesis gas.

4.1 Microorganism, cultivation and nutrient medium

The anaerobic, acetogenic bacterium *Clostridium ljungdahlii* (DSM 13528), a wildtype strain, is used as the biocatalyst. Double distilled water with a maximum conductivity of 0.08 $\mu\mathrm{S\,cm^{-1}}$ is used to prepare the solutions of culture medium, vitamins, trace elements, L-cysteine and fructose. A detailed list of all chemicals used for cultivation and process operation of syngas fermentation can be found in the appendix in Table A.3. The required volume of culture medium for pre-cultivation and process is prepared according to the composition in Table 4.1, with resazurin serving as an oxygen indicator. In the presence of oxygen in the nutrient medium, resazurin causes a blue-purple colouration. After successful anaerobization, the color changes to transparent to light yellow. If oxygen enters the nutrient medium after anaerobization, the colour of the nutrient medium changes again. The pH of the culture medium is adjusted to the desired value adding potassium hydroxide (KOH) pellets. In case of preculture, the pH is set to 5.9; for the culture medium, the pH is adjusted to the target value in the reactor with a surcharge of 0.1 to take into account the decrease after the addition of L-cysteine. The culture medium is first anaerobized by intensive sparkling with nitrogen. In a further step it is anaerobized with a gas mixture of 80 vol.% N_2 and 20 vol.% CO_2 and then sterilized at 121 °C for 20 min with the bottle closed. Subsequently, for pre-cultivation, 1 $\mathrm{g\,L^{-1}}$ L-cysteine is sterilely injected into the culture medium, while for the culture medium supplied in continuous operating mode 0.3 $\mathrm{g\,L^{-1}}$ is sterilely injected.

Table 4.1: Composition of the culture medium for pre-cultivation and process. The composition is adapted from STOLL ET AL. [176].

Component i	β_i / $\mathrm{g\,L^{-1}}$
MES	20
yeast extract	0.5
NaCl	2
NH_4Cl	0.33
KCl	0.25
KH_2PO_4	0.25
$MgSO_4 \cdot 7\,H_2O$	0.5
$CaCl_2 \cdot 2\,H_2O$	0.1
resazurin	0.001
solution of vitamins	$10\,\mathrm{ml\,L^{-1}}$
solution of trace elements	$10\,\mathrm{ml\,L^{-1}}$

The composition of the vitamin and trace element solution is listed in Table 4.2 and Table 4.3, respectively. The vitamin and trace element solutions are prepared in large quantities in advance and frozen. They are defrosted and used as required. These solutions are not sterilized or anaerobized. When preparing the trace element solution, the pH value is adjusted to 6.5 by adding potassium hydroxide pellets to dissolve nitrilotriacetic acid.

L-cysteine and fructose solutions with a concentration of $100\,\mathrm{g\,L^{-1}}$ and $250\,\mathrm{g\,L^{-1}}$ respectively are both produced in the anaerobic tent. Therefore, a subsequent anaerobization, as with the culture medium, is not necessary. Finally, the L-cysteine and fructose solutions are autoclaved at $121\,^{\circ}\mathrm{C}$ for 20 min.

The preparation of glycerol stocks for long-term storage of the strain *Clostridium ljungdahlii* is carried out according to STOLL [103]. For this purpose, 5 ml of a culture growing heterotrophically in the exponentially growing phase (optical density $\mathrm{OD}_{600} < 2$ and $\mathrm{pH} > 4.7$) consisting of culture medium (see Table 4.1), $1\,\mathrm{g\,L^{-1}}$ L-cysteine and $10\,\mathrm{g\,L^{-1}}$ fructose are removed from a preculture bottle. After centrifugation at $3000\,\mathrm{x\,g}$ and $4\,^{\circ}\mathrm{C}$ for 5 min, the pellet is separated from the supernatant and transferred to a 1 ml solution consisting of half a glycerol solution (50 % water, 50 % glycerol) and the other half from the culture medium together with $1\,\mathrm{g\,L^{-1}}$ L-cysteine and $10\,\mathrm{g\,L^{-1}}$ fructose and then stored at -80 °C.

Table 4.2: Composition of the vitamin solution.

Component i	β_i / g L^{-1}
biotin	0.002
folic acid	0.002
pyridoxine	0.01
thiamine-HCl	0.005
riboflavin	0.005
nicotinic acid	0.005
Ca-pantothenate	0.005
cyanocobalamin	0.005
4-aminobenzoic acid	0.005
lipoic acid	0.005

Table 4.3: Composition of the trace element solution.

Component i	β_i / g L^{-1}
$C_6H_9NO_6$	2
$MnSO_4 \cdot H_2O$	1
$FeSO_4 \cdot 7\,H_2O$	0.567
$CoCl_2 \cdot 6\,H_2O$	0.2
$ZnSO_4 \cdot 7\,H_2O$	0.2
$CuCl_2 \cdot 2\,H_2O$	0.02
$NiCl_2 \cdot 6\,H_2O$	0.02
$Na_2MoO_4 \cdot 2\,H_2O$	0.02
$Na_2SeO_3 \cdot 5\,H_2O$	0.02
$Na_2WO_4 \cdot 2\,H_2O$	0.022

Pre-cultivation is performed strictly anaerobically in three steps at 37 °C adapted from STOLL [103]. For this purpose, a serum bottle with a total of 50 ml culture medium and a concentration of L-cysteine and fructose with 1 g L^{-1} and 10 g L^{-1} respectively is inoculated with a glycerol stock and kept for 51 hours at 37 °C. After analyzing optical density and pH, 5 ml is removed from this serum bottle and used to inoculate the next serum bottle with 50 ml culture medium and a concentration of L-cysteine and fructose of 1 g L^{-1} and 5 g L^{-1} respectively and kept at 37 °C for 48 hours. Again, after analyzing optical density and pH, 2.5 ml of this serum bottle is removed and used to inoculate a bottle with 250 ml culture medium and a concentration of L-cysteine and fructose with 1 g L^{-1} and 5 g L^{-1} respectively and stored for 64 hours at 37 °C. In a final step, after analyzing optical density and pH, a volume of 220 ml is used to inoculate the reactor (10 % inoculum).

4.2 System of continuous fermentation

4.2.1 Experimental setup

A scheme of the experimental setup for continuous fermentation is shown in Figure 4.1, a detailed process flow diagram is shown in Figure A.1 in the appendix. The test rig is controlled via a process control system (Simatic S7) and WinCC as the user interface.

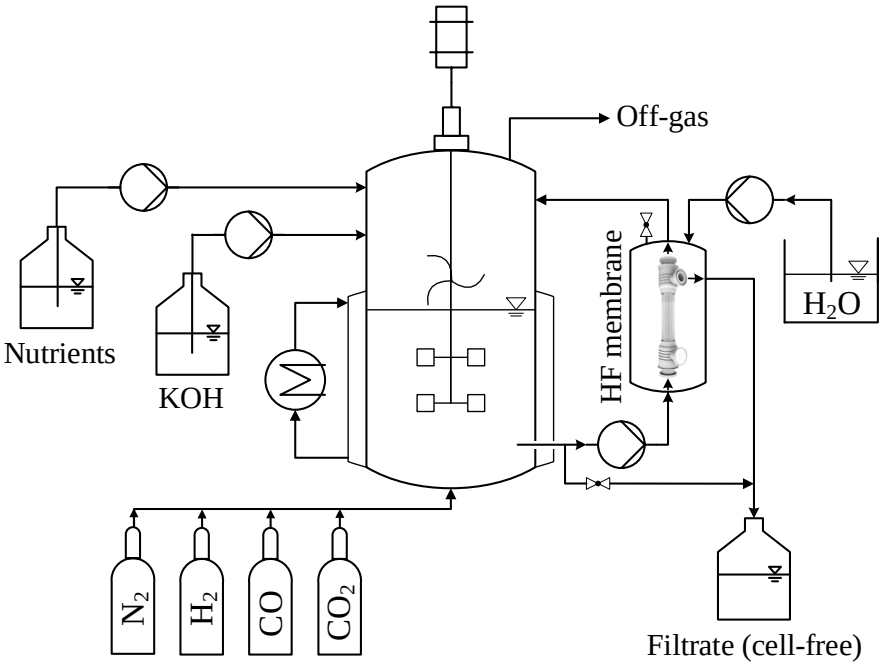

Figure 4.1: Experimental setup for a continuous fermentation including cross-flow filtration with a hollow fiber (HF) membrane (reference: repligen.com) in an external cycle for biomass retention. The hollow fiber membrane is placed in a pressure-stable vessel flooded with water. The pressure in the vessel can be increased by adding water via a pump and thus adapted to the process pressure in the reactor. A detailed process flow diagram is shown in Figure A.1 in the appendix.

The experimental unit includes a stainless steel CSTR (4 liter, inner diameter 126 mm) with double jacket and thermostat for temperature control (Julabo Dyneo, Germany), a gas mixing station (mass flow controller, Bronkhorst, Netherlands) to adjust gas flow rate and gas composition of the four gases N_2 (purity 99.9999 %), H_2 (purity 99.9999 %), CO (purity 99.97 %) and CO_2 (purity 99.995 %), a syringe pump unit (Nemesys M, CETONI, Germany) to deliver the nutrient medium, a HPLC pump (BISCHOFF, Germany) to deliver the base and a peristaltic pump (Albin Pump, France) for the external circuit of cross-flow filtration with a hollow fiber membrane (REPLIGEN, Netherlands, PES membrane, pore size 0.2 μm, specific surface 470 cm^2) for biomass retention during continuous operation. Bacteria are not able to leave the system, since the cross filtration module is too fine to cross. This circuit is also sterilized before the start of the experiment and is not opened again during the experiment. The hollow fiber membrane is placed in a pressure-stable vessel flooded with water. The pressure in the vessel can be increased by adding water via a pump and thus adapted to the process pressure in the reactor. This device allows the hollow fiber membrane for cross-flow filtration

(a) Pressure-stable vessel **(b)** Hollow fiber membrane with periphery

Figure 4.2: Hollow fiber membrane with stainless steel tube connections, vessel head with connections and pressure sensors in the right (b), and pressure-stable vessel in the left (a). For operation, the hollow fiber membrane with fittings is submerged in the vessel flooded with water and tightly sealed via the vessel head.

to be operated at higher pressures, since by bringing the pressure in the vessel into line with the process pressure in the reactor, the hollow fiber membrane does not experience any significant differential pressure (maximum allowed differential pressure of the membrane: 2 bar). For the detailed design of the pressure-stable construction for the hollow fiber membrane, see Figure 4.2.

The gas inlet is at the bottom of the reactor via two gas frits (bbi-biotech, Germany, pore size 20 μm) and distributed via two six-bladed disk impellers (Buddeberg, Germany) mounted on the stirrer shaft. The stirrer shaft is 330 mm long, the agitator blades are positioned at the lower end (0 mm) and at a height of 69 mm. The stirrer shaft is driven by a synchronous servomotor (SEW Eurodrive, Germany) and the transmission to the stirrer shaft is via a magnetic coupling (Büchi, Switzerland). In addition, fixed stainless steel baffles, adapted from OSWALD [177], are installed in the reactor. An impeller (C3 Prozess- und Analysentechnik, Germany, outer diameter 94 mm) for mechanical foam destruction is located on the stirrer shaft above the filling level at a height of 153 mm. Chemical additives for foam destruction are not used since they are expected to influence the gas-liquid mass transfer [178].

A high-pressure/high-temperature pH electrode (Walchem, USA) is located in the reactor connected to the HPLC pump to dose the base. Via a magnetic valve (RCT, Germany),

fermentation broth can either be drained directly from the reactor or via the filtrate outlet at the hollow filter membrane; this allows the experimental plant to be operated even without the external circuit for biomass retention. A level probe (Vega, Germany) in a communicating vessel (dead volume 270 ml, without aeration) is used to detect the level in the reactor and is linked to the magnetic valve to keep the level of the fermentation broth constant.

The reactor with periphery is sterilized with 0.5 % peracetic acid and superheated steam (120 - 130 °C) just before the beginning of the experiment. Sterile filters (pore size 0.2 μm, Swagelok, Germany) in the gas supply pipe, in the feed supply pipe and in the exhaust gas prevent external contamination during operation of the experiment. Before each experiment, a sample of the preculture used for inoculation and of the fermentation broth in the reactor is taken, aerobically spread on agar plates and after 48 hours at 37 °C analyzed for contamination.

4.2.2 Foam separation system

In order to avoid feeding antifoam agents into the reactor and at the same time not exceed a critical amount of foam formation for safe operation, a system for the reduction and separation of foam (foam separation system, FSS) was developed that can be used successfully at process pressures of up to 10 bar. At higher pressures, the wall thickness of the components would have to be adjusted accordingly. The pressure-stable system for the reduction and separation of foam is shown in Figure 4.3, the development steps of this system are described in the appendix in Section A.2. The system consists of three different components:

1.) Impeller on the agitator shaft in the reactor

2.) Stainless steel mesh at the gas outlet of the reactor

3.) Foam separator with antifoam agent in the off-gas pipe.

The impeller is positioned at an axial height of 153 mm measured from the lower end of the agitator shaft and is between the liquid level and the reactor head on the agitator shaft in the gas phase. The impeller rotates with the agitator shaft and is used to push down and break up rising foam. Nevertheless, if foam rises and enters the exhaust pipe, it must pass through a stainless steel mesh. This stainless steel mesh is used to break up the foam mechanically. The remaining foam, which then continues to rise through the exhaust pipe, is fed directly into a bath of antifoam agent. When the foam hits this liquid, the foam collapses and remains in the foam separator vessel as a liquid. The exhaust gas can escape via the second opening at the top of the separator vessel and is directed to the off-gas analysis system. This three-part system for preventing and separating foam ensures that rising foam via the exhaust gas line does not block

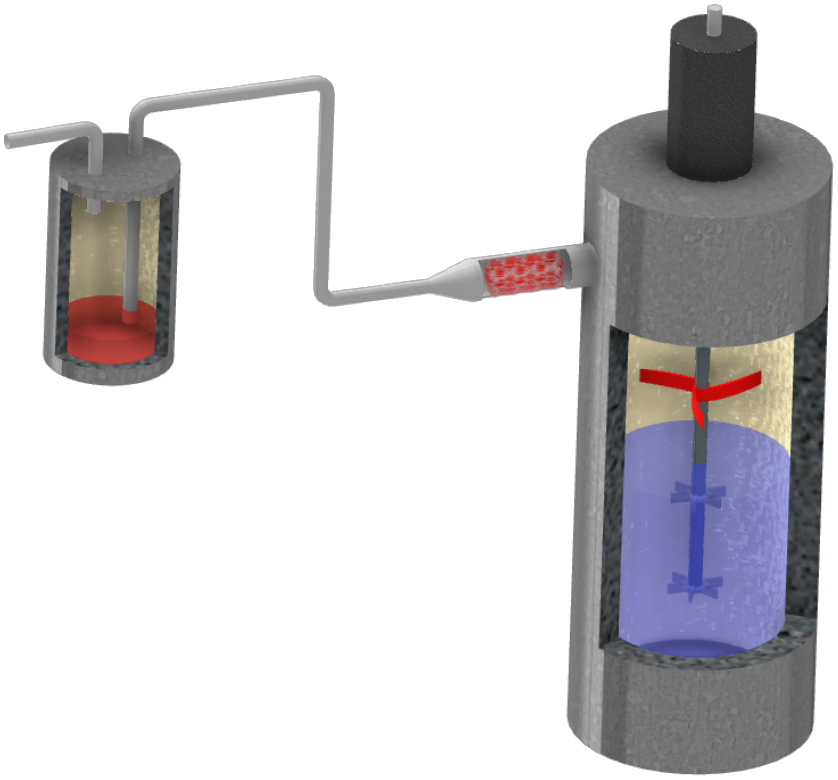

Figure 4.3: Three-part pressure-stable system for the prevention and separation of rising foam. In the reactor, an impeller (colored red) is placed on the agitator shaft above the liquid level, the second component is a stainless steel mesh (colored red) placed in the exhaust line to break up the foam structure and the third component is a pressure-stable foam separator with antifoam agent (colored red) at the bottom of the vessel.

the sterile filter for off-gas analysis and thus cause an increase in pressure. This system has proven to be very successful under experimental conditions. Problems with rising foam in the level probe or exhaust gas pipe did not occur even during long-term experimental runs of over 3000 hours.

4.2.3 Process parameters

The measured data presented in this work were generated during long-term experimental runs in continuous operation. The typical operating range for the process parameters at the test rig is given in Table 4.4. Each time a parameter is changed, it is waited until a steady state is reached

Table 4.4: Typical operating range for the process parameters at the test rig.

Parameter	Typical range of operation
pH	5.1 ... 6.0
T	37 °C
p	1 ... 5 bar
$\dot{V}_{\mathrm{NM}}$	1 ... 3 $\mathrm{ml\,min^{-1}}$
$\dot{V}_{\mathrm{G}}$	40 ... 300 $\mathrm{ml\,min^{-1}}$
Gas composition	Adjustable
Cell density	1 ... 15 $\mathrm{g\,L^{-1}}$
Stirrer speed	400 ... 800 rpm

before the next parameter change is made. Areas with steady-state behavior are those areas in which gas uptake rates and productivities neither increase nor decrease continuously, but remain constant and fluctuate around an average value. The standard deviation in these areas is less than 10 %. For the evaluation, data points from steady-state areas are averaged.

The following parameters apply to all experiments: the temperature in the reactor is 37 °C, and the reaction volume in the 4-liter reactor is 2.2 liters excluding the volumes of the circuits for level detection (269 ml) and biomass retention (126 ml). For the continuous, fully automated adjustment of the pH value, 4 molar potassium hydroxide solution is used. The specific energy input P/V_{l} into the CSTR through the stirrer (600 rpm) is 1.36 $\mathrm{kW/m^3}$. The volume flow of the peristaltic pump in the external circuit for biomass retention is 10 $\mathrm{L/h}$, the average residence time of the liquid phase in the external circuit is 45 seconds. In the external circuit for biomass retention, there is no external supply of substrate gas. For the composition of the substrate gas, it was ensured that hydrogen was present in excess for the stoichiometrically complete conversion of CO and CO_2 to ethanol. As part of the investigations carried out, further process parameters such as pressure, pH, dilution rate, gas composition and gas volume flow have been changed in order to determine the influence of these parameter changes. Detailed information on these parameter settings can be found in the corresponding process parameter tables in Chapter 5.

4.2.4 Analytical methods

The gases N_2, H_2, CO and CO_2 fed to the reactor are each controlled by their own mass flow controller, and thus both the mass flow $\dot{m}_{\mathrm{G}}$ and the density ρ_{G} of the supplied gas are given. The composition of the exhaust gas is analyzed via a 2-channel micro gas chromatograph (INFICON, USA) every 15 minutes, the measurement time is three minutes, the carrier gases are argon (purity 99.9999 %) and helium (purity 99.9999 %). The micro gas chromatograph is recalibrated for each gas setting. It is assumed that the gas is ideal and thus the volume fraction corresponds to the mole fraction. Since gaseous nitrogen is not utilized by the bacteria, the mole fraction of nitrogen in the feed gas $y_{\mathrm{N_2}}$ and exhaust gas $y_{\mathrm{N_2,off}}$ together with the supplied substrate gas volume flow $\dot{m}_{\mathrm{G}} \cdot \rho_{\mathrm{G}}^{-1}$ can be used to calculate the off-gas volume flow $\dot{V}_{\mathrm{G,off}}$:

$$\dot{V}_{\mathrm{G,off}} = \frac{\dot{m}_{\mathrm{G}}}{\rho_{\mathrm{G}}} \cdot \frac{y_{\mathrm{N_2}}}{y_{\mathrm{N_2,off}}} \tag{4.1}$$

The individual gas uptake rates $r_{\mathrm{G,i}}$ can then be calculated using the difference between the measured inlet molar flux $\dot{n}_{\mathrm{i}}$ and the measured outlet molar flux $\dot{n}_{\mathrm{i,off}}$ of the individual gas i divided by the volume of the fermentation broth V_{W}:

$$r_{\mathrm{G,i}} = \frac{\dot{n}_{\mathrm{i}} - \dot{n}_{\mathrm{i,off}}}{V_{\mathrm{W}}} = \frac{\frac{y_{\mathrm{i}} \cdot \dot{m}_{\mathrm{G}}}{\rho_{\mathrm{G}} \cdot V_{\mathrm{m}}} - \frac{y_{\mathrm{i,off}} \cdot \dot{V}_{\mathrm{G,off}}}{V_{\mathrm{m}}}}{V_{\mathrm{W}}} \tag{4.2}$$

V_{m} represents the molar volume according to Equation 4.3:

$$V_{\mathrm{m}} = \frac{R \cdot T}{p} = \frac{8.314\,\frac{J}{mol\,K} \cdot 293.15\,K}{1.013\,bar} = 2405.97 \cdot 10^{-5}\,\frac{m^3}{mol} \tag{4.3}$$

A liquid sample can be taken from the reactor via a valve for offline measurement of cell density, carbon content and product concentrations. Cell density is determined using a UV-VIS spectrometer (VWR, Germany) via optical density at a wavelength of 600 nm. After centrifugation at 12000 x g for 15 minutes, the optical density of the supernatant is then determined and subtracted from the previous measured value of the sample. To calculate the cell dry weight β_{CDW} from the optical density OD_{600}, the optical density is multiplied by a conversion factor f_{CDW}:

$$\beta_{\mathrm{CDW}} = \mathrm{OD}_{600} \cdot f_{\mathrm{CDW}} \tag{4.4}$$

This conversion factor is determined gravimetrically according to STOLL [103] as follows: first the optical density of the sample with a clearly defined volume is measured, then the sample is centrifuged at 5000 x g and 4 °C for 10 minutes. The pellet is dried for 24 hours

at 90 °C and its mass is then determined. For the biocatalyst *C. ljungdahlii*, this results in a conversion factor of 0.53. The gravimetric determination of the conversion factor is carried out once in triplicates before a measurement campaign; the conversion factor is not determined again for each measurement. The conversion factor is valid up to an optical density of 0.45. For measured values $\mathrm{OD}_{600} > 0.45$, samples are diluted with a NaCl solution ($9\,\mathrm{g\,L^{-1}}$) and the measurement is repeated.

Cell separation is achieved by centrifugation at $12000\,\mathrm{x\,g}$ for 15 min. In the cell-free samples, the concentration of formic acid, acetic acid and ethanol is determined by HPLC using an Aminex HPX-87H column (Hitachi, Japan) and H_2SO_4 as eluent ($4\,\mathrm{mmol\,L^{-1}}$). The total organic carbon content TOC was determined by combustion catalytic oxidation and difference method TC-IC (DIMATEC, Germany).

4.3 Measurement campaigns

The measurement campaigns carried out as part of the present study are listed in Table 4.5.

The first experiment *HSF-Z-I* was used for commissioning the external circuit for retaining biomass and aimed to perform an initial functional test of the experimental setup. The reason for the shutdown of the experimental run after 167 hours was a damaged friction bearing on the agitator shaft coupling, see also Figure A.12 in the appendix.

In experiment *HSF-Z-II*, the influence of total biomass retention on the fermentation process was investigated. In addition, the influence of increased gas volume flows with unchanged gas composition was determined. The use of biomass retention significantly increased the cell density in the reactor. At the same time, considerable foam formation was observed, which led to blocking of the sterile filter in the off-gas pipe at irregular intervals and to strong measurement disturbances of the level probe due to rising foam in the probe casing. The experiment was stopped after 970 hours due to excessive foam formation.

In experiment *HSF-Z-III*, the amount of CO_2 in the substrate gas was reduced in order to investigate the influence on the fermentation process. In addition, the external circuit for retaining biomass was subsequently activated. Once again, a mechanical bearing defect occurred in the agitator shaft coupling, which led to a breakage of the agitator shaft, see also Figure A.13 in the appendix, so that the experiment had to be shut down after 392 hours.

For experiment *HSF-Z-IV*, a new coupling system consisting of long-term stable ceramic ball bearings was implemented due to the previous failures of the friction bearings on the agitator

Table 4.5: List of all measurement campaigns in continuous operation.

Name	Objective	Time period	Operating hours
HSF-Z-I	Start-up / Performance test CR	Nov. 2020	167
HSF-Z-II	CR, $\dot{V}_{\mathrm{G}} \uparrow$	Nov.-Dec. 2020	970
HSF-Z-III	$\mathrm{CO_2} \downarrow$	Feb. 2021	392
HSF-Z-IV	CR, $\dot{V}_{\mathrm{G}} \uparrow$, $\mathrm{CO_2} \downarrow$, FSS	March-May 2021	1683
ZP-I	CR, $p \uparrow$, C-limitation	Nov.-Dec. 2021	335
ZP-II	CR, $p/p_{\mathrm{H_2}} \uparrow$, $\mathrm{CO_2} \uparrow$, $\dot{V}_{\mathrm{G}} \uparrow$	Feb.-Apr. 2022	1970
ZpH-I	CR, $\dot{V}_{\mathrm{G}} \uparrow$, $pH \downarrow$, $D \uparrow$	Jun.-Nov. 2022	3097
			$\sum 8614$

shaft coupling. In addition, a glass vessel was used for the first time to separate foam and gas in the exhaust gas pipe, see Figure A.2 in Section 4.2.2 in the appendix. The amount of CO_2 in the substrate gas was also further reduced in this experimental campaign in order to investigate the influence on the fermentation process. The external circuit for retaining biomass was first activated after a stationary operating point was reached in order to again investigate the transition to increased cell densities and thus the reproducibility of the measurement results with cell retention. In addition, the influence of increased gas volume flows with an unchanged gas composition was determined. Information on the course of the experiment with stationary ranges and the process parameters set can be found in Table 5.1, Table 5.3 and Figure A.4.

The glass vessel for the separation of foam and gas in the exhaust gas pipe used in experiment *HSF-Z-IV* proved its worth, so in experiment *ZP-I* and for the other measurement campaigns, the glass vessel was replaced by a pressure-stable stainless steel vessel, supplemented by a stainless steel mesh in the exhaust gas pipe and an impeller on the agitator shaft above the liquid level; for details on the mechanical design of the foam separation system, see Figure 4.3. In experiment *ZP-I*, the biomass retention loop was activated right at the beginning, after which the influence of carbon limitation on the fermentation process was investigated. The carbon limitation was then overcome by increasing the substrate gas volume flow and the process pressure was subsequently increased by 1 bar. The experiment had to be terminated after 392 hours due to excessive foaming.

In experiment *ZP-II* the position of the impeller was optimized, see Section A.2 in the appendix. The other components of the antifoam system have not been changed. Cell retention was

activated directly at the beginning of the experiment, the influence of an increased amount of CO_2 and an overall increased substrate gas volume flow were investigated. The focus of the measurement campaign *ZP-II* was to investigate the influence of a gradually increased process pressure with a constant-volume hydrogen supply. The increase in pressure with constant-volume hydrogen supply was intended to increase hydrogen uptake. At a process overpressure of 4 bar, the experiment had to be shut down due to a damage to the peristaltic pump and hollow fiber membrane. Increased foam formation with spreading into the off-gas pipe did not occur during the experimental run. The configuration of the antifoam system was therefore used for all subsequent measurement campaigns. Information on the course of the experiment with stationary ranges and the process parameters set can be found in Table 5.7 and Figure A.6.

The focus of the last measurement campaign *ZpH-I* was to determine the influence of a reduced pH value as well as an increased dilution rate on the fermentation process. The pH reduction was intended to increase ethanol formation by the cells in order to counteract a further drop in pH. For this purpose, the external circuit for the retention of biomass was activated from the beginning, the substrate gas volume flow was adjusted so that the conversions of the individual gas components were less than 95 %. The pH value was then gradually lowered and then raised again to the initial value. In the next step, the dilution rate was gradually increased. Finally, the cell retention was deactivated to investigate the reproducibility of the measurement data with and without the operation of an external biomass retention cycle. Information on the course of the experiment with stationary ranges and the process parameters set can be found in Table 5.1, Table 5.9, Table 5.5, Figure A.7 and Figure A.5. The experiment *ZpH-I* was successfully completed after 3097 hours of operation.

5 Results

The measurement data presented in this chapter have been generated in fully continuous operation. In order to avoid the biocatalyst being washed out during the fully continuous operation of the CSTR, the first step was to implement an external circuit to retain the biomass. The influence of this biomass retention system on the fermentation process is shown in Section 5.1. Section 5.2 presents the results on the influence of the key process parameters substrate gas volume flow, dilution rate, gas partial pressure and pH value on the fermentation process at increased cell densities. All raw measurement data in the following sections are published in research data repositories, see PERRET ET AL. [179] and PERRET ET AL. [180]. The entire experimental runs, including the time allocation of the steady-state intervals, are shown in Appendix A.4.

5.1 Influence of a total biomass retention system

To investigate the influence of a total biomass retention system, the fermentation was first operated without biomass retention and a steady-state operating condition was waited for (interval $\overline{CR}$), then the external circuit for biomass retention was activated and waited again until a new steady-state operating condition was reached (interval CR). In a further experiment, after a process time of 2713 h with operation of the biomass retention system, biomass retention was deactivated in order to investigate whether the effects observed by activating the biomass retention are completely reversible (interval $\widetilde{\overline{CR}}$). The parameters set for the three intervals can be found in Table 5.1.

5.1.1 Cell density, product ratio, productivity

The first experimental interval $\overline{CR}$ was performed without cell retention. The dilution rate was $0.03\,\mathrm{h}^{-1}$ and the resulted cell density $1.19\,\mathrm{g\,L}^{-1}$. By activating cell retention (interval CR), cell density increases by 160 % to $3.15\,\mathrm{g\,L}^{-1}$, see Figure 5.1 E. Biomass-specific hydrogen uptake

Table 5.1: Experimental parameters to investigate the influence of biomass retention. The intervals $\overline{CR}$, CR and $\widetilde{\overline{CR}}$ represent steady-state areas from the experimental runs *HSF-Z-IV* and *ZpH-I* with $\overline{CR}$ and CR from *HSF-Z-IV* and $\widetilde{\overline{CR}}$ from experiment *ZpH-I*. $\overline{CR}$: the fermentation process is operated without a cell retention (CR) system; CR: cell retention is activated; $\widetilde{\overline{CR}}$: deactivation of biomass retention after 2713 hours of operation with cell retention.

	$\overline{\mathrm{CR}}$	CR	$\widetilde{\overline{\mathrm{CR}}}$
Cell retention	✗	✓	✗
p / barg	⟵ 0 ⟶		
$\dot{V}_\mathrm{G}$ / mL min^{-1}	⟵ 80 ⟶		62
$H_2/CO/CO_2/N_2$ / vol. %	⟵ 48/16/4/32 ⟶		59/16/7/19
$H_2 : CO : CO_2$	⟵ 70.5 : 23.5 : 6 ⟶		72 : 20 : 8
GRT / min	⟵ 27.5 ⟶		35.48
D / h^{-1}	⟵ 0.03 ⟶		
τ / h	⟵ 33.3 ⟶		
pH	⟵ 5.85 ⟶		5.9
duration of interval / h	52	55	64
number of gas samples	208	217	306
number of liquid samples	3	4	3

decreases from 14.16 mmol g^{-1} h^{-1} to 9.54 mmol g^{-1} h^{-1}, that of carbon monoxide decreases from 10.96 mmol g^{-1} h^{-1} by more than 50 % to 4.48 mmol g^{-1} h^{-1}, while q_{CO_2} increases from 0.14 mmol g^{-1} h^{-1} to 1 mmol g^{-1} h^{-1}, see Figure 5.1 A.

In contrast to the biomass-specific gas uptake rate, the gas uptake rate r increases for all three substrate gases: from 0.17 mmol L^{-1} h^{-1} to 3.17 mmol L^{-1} h^{-1} for carbon dioxide, from 13.09 mmol L^{-1} h^{-1} to 14.14 mmol L^{-1} h^{-1} for carbon monoxide and from 16.91 mmol L^{-1} h^{-1} to 30.09 mmol L^{-1} h^{-1} for hydrogen, see Figure 5.1 B. As the gas volume flow is not changed in the interval CR, the increased gas uptake leads to an increase in gas conversions resulting in a nearly complete conversion of CO with $X_{CO} = 0.97$, see Table 5.2.

The biomass-specific formation of acetic acid and ethanol and their sum as C_2 components are shown in Figure 5.1 C. By activating the biomass retention, the biomass-specific formation of acetic acid decreases from 3.73 mmol g^{-1} h^{-1} to 1.32 mmol g^{-1} h^{-1}, while q_{EtOH} is not affected by cell retention (1.60 mmol g^{-1} h^{-1} without cell retention and 1.63 mmol g^{-1} h^{-1} with cell

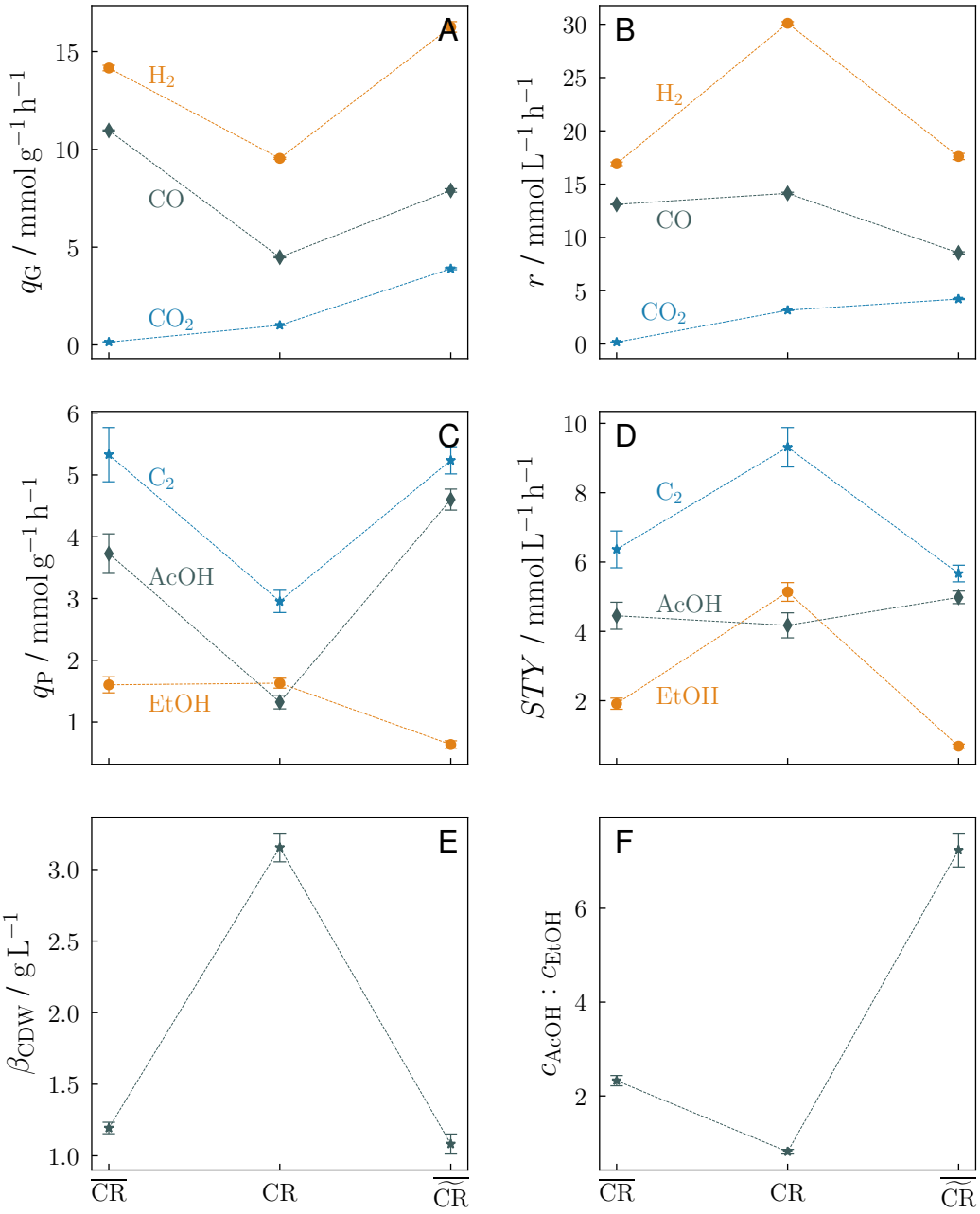

Figure 5.1: Influence of activation CR and deactivation $\widetilde{\overline{CR}}$ of cell retention vs. non-activated $\overline{CR}$ on biomass-specific gas uptake rate q_G (A), gas uptake rate r (B), biomass-specific productivity q_P (C), space–time yield STY (D), mass concentration of biomass β_{CDW} (E) and product ratio of acetic acid to ethanol (F). Averaged measured data of steady-state areas. For further details on experimental parameters, see Table 5.1.

retention). Due to the decreased acetic acid formation with cell retention, C_2 productivity decreases by 45 % from 5.33 $\mathrm{mmol\,g^{-1}\,h^{-1}}$ to 2.95 $\mathrm{mmol\,g^{-1}\,h^{-1}}$. However, as cell density increases by 160 %, there is still a 46 % increase of space-time yield of C_2 products during operation with cell retention (9.31 $\mathrm{mmol\,L^{-1}\,h^{-1}}$ for CR compared to 6.36 $\mathrm{mmol\,L^{-1}\,h^{-1}}$ for $\overline{CR}$), see Figure 5.1 D. This increase is a result entirely of the increased space-time yield of ethanol (5.14 $\mathrm{mmol\,L^{-1}\,h^{-1}}$ for CR compared to 1.91 $\mathrm{mmol\,L^{-1}\,h^{-1}}$ for $\overline{CR}$). The space-time yield of acetic acid is not significantly affected by cell retention and takes a value of 4.45 $\mathrm{mmol\,L^{-1}\,h^{-1}}$ ($\overline{CR}$) and 4.17 $\mathrm{mmol\,L^{-1}\,h^{-1}}$ (CR), respectively. As the space-time yield of ethanol increases, the acetic acid to ethanol product ratio reverses, from 2.33 without cell retention ($\overline{CR}$) to 0.81 with cell retention (CR), see Figure 5.1 F. This leads to a lower effort of neutralization of the C_2 product stream: the amount of potassium hydroxide decreases by more than 35 % from 0.7 $\mathrm{mmol_{KOH}\,mmol_{C_2}^{-1}}$ without cell retention to 0.45 $\mathrm{mmol_{KOH}\,mmol_{C_2}^{-1}}$ with cell retention, see Table 5.2.

This shift in the product ratio can be seen clearly in the selectivity S in Figure 5.2: without cell retention ($\overline{CR}$), two-thirds of the carbon uptake is converted to acetic acid, with cell retention (CR) it is 48 %, while 59 % is converted to ethanol.

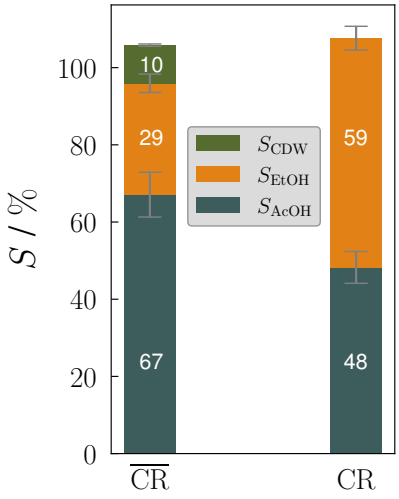

Figure 5.2: Influence of biomass retention on carbon-based selectivity S with standard deviation averaged in the steady-state intervals $\overline{CR}$ (without cell retention) and CR (cell retention activated).

In addition, without biomass retention ($\overline{CR}$), cells are continuously washed out with the product stream, so 10 % of the carbon uptake is used to continuously build up new biomass. With total cell retention (CR), a continuous build up of new biomass is not necessary, as the cells

are retained in the external circuit for biomass retention and therefore not washed out. Total selectivities greater than 100 % are presumably due to measurement inaccuracies, see also carbon balance in Table 5.2.

Table 5.2: Measurement data averaged in steady-state areas to investigate the influence of biomass retention. $\overline{CR}$: the fermentation process is operated without cell retention; CR: cell retention is activated; $\widetilde{\overline{CR}}$: deactivation of biomass retention after 2713 hours of operation with cell retention.

	$\overline{\mathrm{CR}}$	CR	$\widetilde{\overline{\mathrm{CR}}}$
carbon balance / %	106 ± 8	108 ± 7	98 ± 4
electron recovery / %	98 ± 8	107 ± 6	92 ± 4
X_{CO} / %	90 ± 0.2	97 ± 0.7	84 ± 1
$X_{\mathrm{CO_2}}$ / %	5 ± 0.7	84 ± 0.6	75 ± 1
$X_{\mathrm{H_2}}$ / %	39 ± 0.4	69 ± 0.3	45 ± 0.7
q_{CO} / $\mathrm{mmol\,g^{-1}\,h^{-1}}$	10.96 ± 0.03	4.48 ± 0.03	7.90 ± 0.09
$q_{\mathrm{CO_2}}$ / $\mathrm{mmol\,g^{-1}\,h^{-1}}$	0.14 ± 0.02	1.00 ± 0.01	3.90 ± 0.05
$q_{\mathrm{H_2}}$ / $\mathrm{mmol\,g^{-1}\,h^{-1}}$	14.16 ± 0.14	9.54 ± 0.05	16.26 ± 0.27
r_{CO} / $\mathrm{mmol\,L^{-1}\,h^{-1}}$	13.09 ± 0.03	14.14 ± 0.10	8.55 ± 0.10
$r_{\mathrm{CO_2}}$ / $\mathrm{mmol\,L^{-1}\,h^{-1}}$	0.17 ± 0.03	3.17 ± 0.02	4.22 ± 0.05
$r_{\mathrm{H_2}}$ / $\mathrm{mmol\,L^{-1}\,h^{-1}}$	16.91 ± 0.17	30.09 ± 0.15	17.60 ± 0.29
β_{CDW} / $\mathrm{g\,L^{-1}}$	1.19 ± 0.04	3.15 ± 0.10	1.08 ± 0.07
q_{AcOH} / $\mathrm{mmol\,g^{-1}\,h^{-1}}$	3.73 ± 0.32	1.32 ± 0.11	4.60 ± 0.17
$\mathrm{q_{EtOH}}$ / $\mathrm{mmol\,g^{-1}\,h^{-1}}$	1.60 ± 0.13	1.63 ± 0.08	0.64 ± 0.06
STY_{AcOH} / $\mathrm{mmol\,L^{-1}\,h^{-1}}$	4.45 ± 0.39	4.17 ± 0.36	4.98 ± 0.18
STY_{EtOH} / $\mathrm{mmol\,L^{-1}\,h^{-1}}$	1.91 ± 0.16	5.14 ± 0.27	0.69 ± 0.06
$c_{\mathrm{AcOH}} : c_{\mathrm{EtOH}}$ / $\frac{\mathrm{mmol_{AcOH}}}{\mathrm{mmol_{EtOH}}}$	2.33 ± 0.11	0.81 ± 0.05	7.24 ± 0.36
$n_{\mathrm{KOH}} : n_{\mathrm{C_2}}$ / $\frac{\mathrm{mmol_{KOH}}}{\mathrm{mmol_{C2}}}$	0.70 ± 0.01	0.45 ± 0.01	0.88 ± 0.01

5.1.2 Deactivation of cell retention - reversibility

Microorganisms can change and adapt over long experimental runs. When evaluating measurement data, a distinction must therefore be made between the influence of parameter changes and the influence of adaptation processes on the fermentation process. To investigate whether

the microorganisms have changed by switching on the external circuit for biomass retention, for example by adaptation, three intervals are considered: $\overline{CR}$, CR and $\widetilde{\overline{CR}}$, see Figure 5.1 and Table 5.2. In the interval $\overline{CR}$, as a reference, the fermentation process is started without the operation of a biomass retention system, then the biomass retention system is activated in interval CR. In another measurement campaign, biomass retention is deactivated ($\widetilde{\overline{CR}}$) from the on-going operation after 2713 h of operation with cell retention. If the microorganisms have changed due to the use of biomass retention, the measured values should differ significantly from those of the reference process $\overline{CR}$ after deactivation of cell retention.

By activating the biomass retention in the interval CR, the product ratio acetic acid to ethanol decreases from 2.33 to 0.81. After deactivation of biomass retention, this product ratio increases again significantly to 7.24, see Figure 5.1 F. In this case, as in the interval $\overline{CR}$, more acetic acid is formed than ethanol. The cell densities of both intervals without biomass retention are similar: $1.19\,\mathrm{g\,L^{-1}}$ in the interval $\overline{CR}$ and $1.08\,\mathrm{g\,L^{-1}}$ in the interval $\widetilde{\overline{CR}}$, see Figure 5.1 E. Furthermore, after deactivation of biomass retention ($\widetilde{\overline{CR}}$), there is a space-time yield of C_2 products of $5.67 \pm 0.24\,\mathrm{mmol\,L^{-1}\,h^{-1}}$, see Figure 5.1 D and is thus comparable to the space-time yield of the interval $\overline{CR}$ of $6.36 \pm 0.53\,\mathrm{mmol\,L^{-1}\,h^{-1}}$, taking into account the standard deviation. In addition, as already shown in Section 5.1.1, biomass retention leads to significantly reduced specific gas uptake rates: from $q_{\mathrm{CO+CO_2}} = 11.10\,\mathrm{mmol\,g^{-1}\,h^{-1}}$ without cell retention ($\overline{CR}$) to $5.48\,\mathrm{mmol\,g^{-1}\,h^{-1}}$ with cell retention (CR) and from $q_{\mathrm{H_2}} = 14.16\,\mathrm{mmol\,g^{-1}\,h^{-1}}$ without cell retention ($\overline{CR}$) to $9.54\,\mathrm{mmol\,g^{-1}\,h^{-1}}$ with cell retention (CR). After deactivation of biomass retention in the interval $\widetilde{\overline{CR}}$, again, specific gas uptake rates increase to $q_{\mathrm{CO+CO_2}} = 11.80\,\mathrm{mmol\,g^{-1}\,h^{-1}}$ and $q_{\mathrm{H_2}} = 17.60\,\mathrm{mmol\,g^{-1}\,h^{-1}}$, see Figure 5.1 A and Table 5.2 and thus are comparable to the specific gas uptake rates before activation of biomass retention.

5.1.3 Potential accumulation of carbon in the fermentation broth

By using a total cell retention system with a pore size of the hollow fiber of $0.2\,\mu\mathrm{m}$ and by not using a bleed flow, an accumulation of carbon could occur in the reactor over time. Therefore, as part of another long-term experiment, a total of 23 samples were taken from the reactor over a period of 2000 h (for measurement data see Table A.2 in appendix A.5) and the total carbon content of these non-centrifuged samples ($C_{\mathrm{total,measured}}$) was determined by TOC analysis. Samples were then centrifuged and both cell density and product concentrations of ethanol and acetic acid were determined so that the carbon content of each product C_{CDW}, C_{AcOH}, and C_{EtOH} can be calculated. According to INFANTES-LÓPEZ [181], a value of 0.44 was assumed for the carbon mass fraction of the biomass. The carbon fraction of the supplied nutrient

medium C_{NM} was determined by TOC analysis. Then the ratio of the measured total carbon content to the sum of the individual carbon amounts can be calculated:

$$\Delta C = \frac{C_{\mathrm{total,measured}}}{C_{\mathrm{NM}} + C_{\mathrm{CDW}} + C_{\mathrm{AcOH}} + C_{\mathrm{EtOH}}} - 1 \tag{5.1}$$

Positive values of ΔC indicate that the measured total carbon content is greater than the sum of the recorded individual components, whereas the other way around is the case for negative values. Figure 5.3 presents the values for ΔC over the duration of the experiment. The average is -6.63 percentage points and the median is -5.18 percentage points; consequently, the sum of the carbon from the culture medium, biomass, acetic acid and ethanol is greater than the total carbon measured. This is due to both measurement inaccuracies and simplifications made, such as assuming a carbon content of 0.44 of the biomass. If carbon were to accumulate, ΔC would have to increase and take positive values, but this is not evident in Figure 5.3. Accumulation of carbon in the fermentation broth due to the use of total cell retention can therefore be ruled out for the experimental setup.

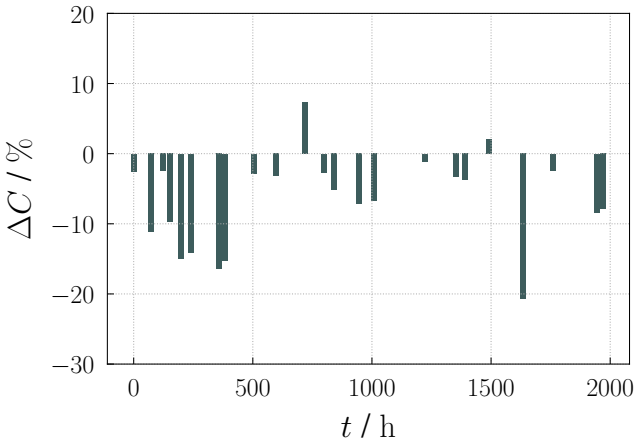

Figure 5.3: Relative difference between measured total carbon content and sum of calculated individual carbon contents over time with total cell retention.

5.2 Parameter study at increased cell densities

5.2.1 Influence of an increased substrate gas flow

As already shown in Section 5.1.1, the activation of cell retention leads to an increase of the gas conversions. This leads to a nearly complete conversion of CO, resulting in CO_2 serving as

the sole additional carbon source. To rule out the possibility that the increased space-time yield of ethanol and the shift in the product ratio are the results of these gas limitations and not a consequence of cell retention, the gas feed is increased in two steps to 105 $\mathrm{mL\,min^{-1}}$ in interval $CR_{\dot{V}_{G\uparrow}}$ and finally to 123 $\mathrm{mL\,min^{-1}}$ in interval $CR_{\dot{V}_{G\uparrow\uparrow}}$ with a constant ratio of $H_2 : CO : CO_2$. The parameters set for these intervals can be found in Table 5.3.

Table 5.3: Experimental parameters to investigate the influence of an increased substrate gas volume flow with activated biomass retention. The intervals CR, $CR_{\dot{V}_{G\uparrow}}$ and $CR_{\dot{V}_{G\uparrow\uparrow}}$ represent steady-state areas from the experimental run *HSF-Z-IV*. CR: fermentation process operated with a cell retention system; $CR_{\dot{V}_{G\uparrow}}$: increase of substrate gas flow while cell retention is still activated; $CR_{\dot{V}_{G\uparrow\uparrow}}$: second increase of substrate gas flow while cell retention is still activated.

	CR	$CR_{\dot{V}_{G\uparrow}}$	$CR_{\dot{V}_{G\uparrow\uparrow}}$
Cell retention	✓	✓	✓
p / barg		⟵ 0 ⟶	
$\dot{V}_G$ / $\mathrm{mL\,min^{-1}}$	80	105	123
$H_2/CO/CO_2/N_2$ / vol. %	⟵ 48/16/4/32 ⟶		61/20/5/14
$H_2 : CO : CO_2$		⟵ 70.5 : 23.5 : 6 ⟶	
GRT / min	27.5	20.95	17.89
D / $\mathrm{h^{-1}}$		⟵ 0.03 ⟶	
τ / h		⟵ 33.3 ⟶	
pH		⟵ 5.85 ⟶	
duration of interval / h	55	31	129
number of gas samples	217	122	516
number of liquid samples	4	3	7

Increasing the gas volume flow by 25 $\mathrm{ml\,min^{-1}}$, corresponding to 31 %, leads to increased biomass-specific gas uptake: q_{H_2} increases by 4 % to 9.96 $\mathrm{mmol\,g^{-1}\,h^{-1}}$, q_{CO} by 9 % to 4.88 $\mathrm{mmol\,g^{-1}\,h^{-1}}$ and q_{CO_2} by 13 % to 1.13 $\mathrm{mmol\,g^{-1}\,h^{-1}}$, see Figure 5.4 A and Table 5.4. In addition, the increase in gas volume flow leads to an increase in cell density by 19 % to 3.75 $\mathrm{g\,L^{-1}}$, see Figure 5.4 E, so that the gas uptake rate r for all three gases increases significantly: r_{H_2} by 24 % to 37.36 $\mathrm{mmol\,L^{-1}\,h^{-1}}$, r_{CO} by 29 % to 18.31 $\mathrm{mmol\,L^{-1}\,h^{-1}}$ and r_{CO_2} by 33 % to 4.22 $\mathrm{mmol\,L^{-1}\,h^{-1}}$, see Figure 5.4 B. The increase in the average gas uptake rate of all three substrate gases is 26 %, which is 5 percentage points below the increase in gas volume flow of 31 %. Biomass-specific ethanol formation decreases by 9 % to

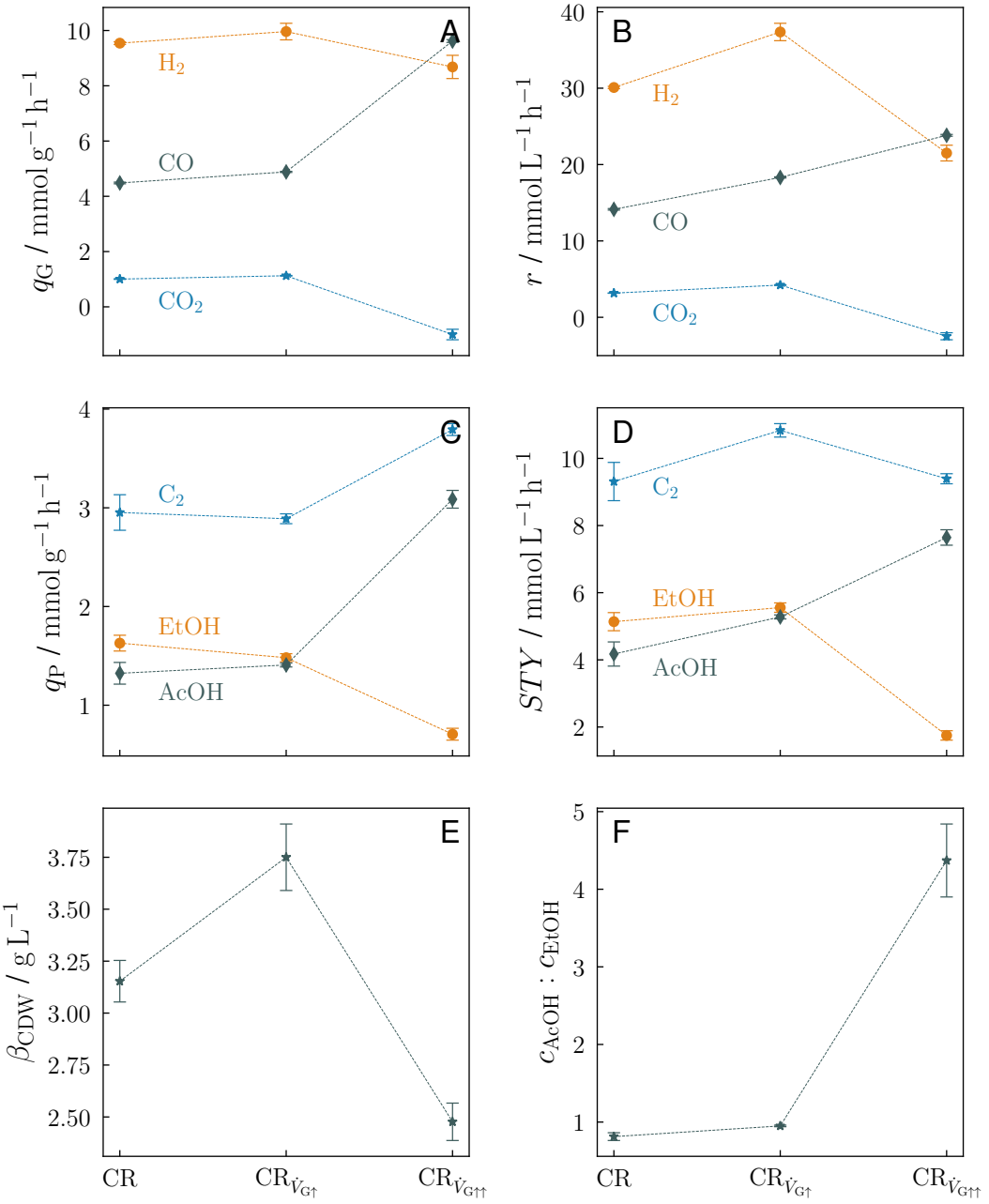

Figure 5.4: Influence of an increased substrate gas volume flow $CR_{\dot{V}_{G\uparrow}}$ and $CR_{\dot{V}_{G\uparrow\uparrow}}$ in comparison to CR with activated biomass retention on biomass-specific gas uptake rate q_G (A), gas uptake rate r (B), biomass-specific productivity q_P (C), space–time yield STY (D), mass concentration of biomass β_{CDW} (E) and product ratio of acetic acid to ethanol (F). Averaged measured data of steady-state areas. For further details on experimental parameters, see Table 5.3.

1.48 $\mathrm{mmol\,g^{-1}\,h^{-1}}$, while q_{AcOH} increases by 7 % to 1.41 $\mathrm{mmol\,g^{-1}\,h^{-1}}$, see Figure 5.4 C. In contrast to biomass-specific ethanol formation, there is an increase in the space-time yield of ethanol due to an increase in cell density: STY_{EtOH} increases by 8 % to 5.56 $\mathrm{mmol\,L^{-1}\,h^{-1}}$, STY_{AcOH} increases by 27 % to 5.28 $\mathrm{mmol\,L^{-1}\,h^{-1}}$, see Figure 5.4 D. The increase in the gas flow leads to an overall increase of C_2 space-time yield by 16 % to 10.84 $\mathrm{mmol\,L^{-1}\,h^{-1}}$. The product ratio of acetic acid to ethanol increases slightly, from 0.81 to 0.95, and is still significantly smaller compared to the product ratio of 2.33 without the operation of a cell retention system, see Section 5.1.1.

Table 5.4: Measurement data averaged in steady-state areas to investigate the influence of an increased substrate gas volume flow with activated biomass retention.

	CR	$\mathrm{CR}_{\dot{V}_{\mathrm{G}\uparrow}}$	$\mathrm{CR}_{\dot{V}_{\mathrm{G}\uparrow\uparrow}}$
carbon balance / %	108 ± 7	96 ± 2	88 ± 1
electron recovery / %	107 ± 6	98 ± 2	91 ± 1
X_{CO} / %	97 ± 0.7	96 ± 0.4	84 ± 0.4
$X_{\mathrm{CO_2}}$ / %	84 ± 0.6	81 ± 1	-32 ± 6
$X_{\mathrm{H_2}}$ / %	69 ± 0.3	65 ± 2	25 ± 1.2
q_{CO} / $\mathrm{mmol\,g^{-1}\,h^{-1}}$	4.48 ± 0.03	4.88 ± 0.02	9.62 ± 0.05
$q_{\mathrm{CO_2}}$ / $\mathrm{mmol\,g^{-1}\,h^{-1}}$	1.00 ± 0.01	1.13 ± 0.01	-1.00 ± 0.19
$q_{\mathrm{H_2}}$ / $\mathrm{mmol\,g^{-1}\,h^{-1}}$	9.54 ± 0.05	9.96 ± 0.30	8.68 ± 0.42
r_{CO} / $\mathrm{mmol\,L^{-1}\,h^{-1}}$	14.14 ± 0.10	18.31 ± 0.08	23.83 ± 0.12
$r_{\mathrm{CO_2}}$ / $\mathrm{mmol\,L^{-1}\,h^{-1}}$	3.17 ± 0.02	4.22 ± 0.05	-2.48 ± 0.46
$r_{\mathrm{H_2}}$ / $\mathrm{mmol\,L^{-1}\,h^{-1}}$	30.09 ± 0.15	37.36 ± 1.14	21.50 ± 1.03
β_{CDW} / $\mathrm{g\,L^{-1}}$	3.15 ± 0.10	3.75 ± 0.16	2.48 ± 0.09
q_{AcOH} / $\mathrm{mmol\,g^{-1}\,h^{-1}}$	1.32 ± 0.11	1.41 ± 0.02	3.09 ± 0.09
$\mathrm{q_{EtOH}}$ / $\mathrm{mmol\,g^{-1}\,h^{-1}}$	1.63 ± 0.08	1.48 ± 0.04	0.71 ± 0.06
STY_{AcOH} / $\mathrm{mmol\,L^{-1}\,h^{-1}}$	4.17 ± 0.36	5.28 ± 0.06	7.64 ± 0.23
STY_{EtOH} / $\mathrm{mmol\,L^{-1}\,h^{-1}}$	5.14 ± 0.27	5.56 ± 0.14	1.75 ± 0.14
$c_{\mathrm{AcOH}} : c_{\mathrm{EtOH}}$ / $\frac{\mathrm{mmol_{AcOH}}}{\mathrm{mmol_{EtOH}}}$	0.81 ± 0.05	0.95 ± 0.01	4.37 ± 0.47

The second increase in gas flow $CR_{\dot{V}_{G\uparrow\uparrow}}$ leads to a doubling of the biomass-specific gas uptake rate of CO to 9.62 $\mathrm{mmol\,g^{-1}\,h^{-1}}$ and to a reduction of $q_{\mathrm{H_2}}$ and $q_{\mathrm{CO_2}}$ by 13 % to 8.68 $\mathrm{mmol\,g^{-1}\,h^{-1}}$ and 88 % to -1.00 $\mathrm{mmol\,g^{-1}\,h^{-1}}$, respectively, see Figure 5.4 A. With that for the first time more CO_2 is formed than taken up by the microorganisms, responsible for this

is the oxidation of CO to CO_2. In contrast to the first gas flow increase $CR_{\dot{V}_{G\uparrow}}$, there is no further increase in cell density, but a reduction of 34 % to 2.48 $\mathrm{g\,L^{-1}}$, see Figure 5.4 E. The gas uptake rate r_{CO} increases by 30 % to 23.83 $\mathrm{mmol\,L^{-1}\,h^{-1}}$, $r_{\mathrm{H_2}}$ and $r_{\mathrm{CO_2}}$ decrease by 42 % and 159 % to 21.50 $\mathrm{mmol\,L^{-1}\,h^{-1}}$ and -2.48 $\mathrm{mmol\,L^{-1}\,h^{-1}}$, respectively, see Figure 5.4 B. The biomass-specific ethanol formation decreases by 52 % to 0.71 $\mathrm{mmol\,g^{-1}\,h^{-1}}$, while q_{AcOH} increases by 119 % to 3.09 $\mathrm{mmol\,g^{-1}\,h^{-1}}$, see Figure 5.4 C. The space-time yield of acetic acid increases by 45 % to 7.64 $\mathrm{mmol\,L^{-1}\,h^{-1}}$, STY_{EtOH} decreases by 68 % to 1.75 $\mathrm{mmol\,L^{-1}\,h^{-1}}$ and the total space-time yield of C_2 products decreases for the first time, by 13 % to 9.39 $\mathrm{mmol\,L^{-1}\,h^{-1}}$, see Figure 5.4 D. In addition, the second gas flow increase leads to a significant shift in the product ratio from 0.95 to 4.37: the concentration of acetic acid is thus more than four times higher than that of ethanol, see Figure 5.4 F.

5.2.2 Influence of an increased dilution rate

As already shown, by activating cell retention, cell density increases significantly, see Section 5.1.1. The supply of liquid nutrient medium ($D = 0.03\,\mathrm{h^{-1}}$) kept at a constant rate in this experiment could by now represent a limitation due to the increased cell density. Therefore, to investigate the influence of dilution rate on the fermentation process, the dilution rate is gradually increased in the following experiment from $D = 0.03\,\mathrm{h^{-1}}$ ($\mathrm{CR_{D=0.03}}$) to $D = 0.04\,\mathrm{h^{-1}}$ ($\mathrm{CR_{D=0.04}}$) and then to $D = 0.05\,\mathrm{h^{-1}}$ ($\mathrm{CR_{D=0.05}}$); for experimental parameters of these intervals see Table 5.5.

Increasing the dilution rate from 0.03 $\mathrm{h^{-1}}$ to 0.04 $\mathrm{h^{-1}}$, i. e., a reduction of the liquid retention time τ of 24 %, leads to a significant decrease in biomass-specific gas uptake rates: $q_{\mathrm{H_2}}$ decreases by 38 % to 3.67 $\mathrm{mmol\,g^{-1}\,h^{-1}}$, q_{CO} by 36 % to 1.34 $\mathrm{mmol\,g^{-1}\,h^{-1}}$ and $q_{\mathrm{CO_2}}$ by 33 % to 0.79 $\mathrm{mmol\,g^{-1}\,h^{-1}}$, see Figure 5.5 A and Table 5.6. The second increase in dilution rate from 0.04 $\mathrm{h^{-1}}$ to 0.05 $\mathrm{h^{-1}}$, i. e., a reduction of τ of 20 %, leads to a further, slight decrease in biomass-specific gas uptake rates: $q_{\mathrm{H_2}}$ drops by 6 % to 3.46 $\mathrm{mmol\,g^{-1}\,h^{-1}}$, q_{CO} by 7 % to 1.24 $\mathrm{mmol\,g^{-1}\,h^{-1}}$ and $q_{\mathrm{CO_2}}$ by 6 % to 0.74 $\mathrm{mmol\,g^{-1}\,h^{-1}}$. Cell density, on the other hand, increases with increasing dilution rate: by 29 % to 12.91 $\mathrm{g\,L^{-1}}$ and by 9 % to 14.11 $\mathrm{g\,L^{-1}}$ for $CR_{\mathrm{D=0.04}}$ and $CR_{\mathrm{D=0.05}}$, respectively, see Figure 5.5 E. The gas uptake rates in interval $CR_{\mathrm{D=0.04}}$ decrease compared to $CR_{\mathrm{D=0.03}}$ by 19 %, 17 % and 13 % to 47.45 $\mathrm{mmol\,L^{-1}\,h^{-1}}$, 17.33 $\mathrm{mmol\,L^{-1}\,h^{-1}}$ and 10.24 $\mathrm{mmol\,L^{-1}\,h^{-1}}$ for H_2, CO and CO_2, respectively, see Figure 5.5 B. A further increase in the dilution rate to 0.05 $\mathrm{h^{-1}}$ does not lead to a reduction in the gas uptake rates; instead, the gas uptake rates increase slightly by

Table 5.5: Experimental parameters to investigate the influence of an increased dilution rate with activated biomass retention. The intervals $CR_{\mathrm{D=0.03}}$, $CR_{\mathrm{D=0.04}}$ and $CR_{\mathrm{D=0.05}}$ represent steady-state areas from the experimental run *ZpH-I* with a dilution rate of 0.03 $\mathrm{h^{-1}}$, 0.04 $\mathrm{h^{-1}}$ and 0.05 $\mathrm{h^{-1}}$.

	$\mathrm{CR_{D=0.03}}$	$\mathrm{CR_{D=0.04}}$	$\mathrm{CR_{D=0.05}}$
Cell retention	✓	✓	✓
p / barg		⟵ 0 ⟶	
$\dot{V}_{\mathrm{G}}$ / $\mathrm{mL\,min^{-1}}$	126	⟵ 111 ⟶	
$\mathrm{H_2/CO/CO_2/N_2}$ / vol. %	65/18/7/9	65/18/7/11	
$\mathrm{H_2 : CO : CO_2}$		⟵ 72 : 20 : 8 ⟶	
GRT / min	17.46	⟵ 19.82 ⟶	
D / $\mathrm{h^{-1}}$	0.03	0.04	0.05
τ / h	33.3	25	20
pH		⟵ 5.9 ⟶	
duration of interval / h	85	75	53
number of gas samples	406	360	253
number of liquid samples	4	4	3

3 %, 1 %, and 2 % to 48.86 $\mathrm{mmol\,L^{-1}\,h^{-1}}$, 17.52 $\mathrm{mmol\,L^{-1}\,h^{-1}}$ and 10.47 $\mathrm{mmol\,L^{-1}\,h^{-1}}$ for H_2, CO and CO_2, respectively.

The biomass-specific ethanol formation, see Figure 5.5 C, decreases significantly by 54 % to 0.40 $\mathrm{mmol\,g^{-1}\,h^{-1}}$ in interval $CR_{\mathrm{D=0.04}}$ and increases slightly by 2.5 % to 0.41 $\mathrm{mmol\,g^{-1}\,h^{-1}}$ in case of $D = 0.05\,\mathrm{h^{-1}}$, while q_{AcOH} does not change for $D = 0.04\,\mathrm{h^{-1}}$ (0.57 $\mathrm{mmol\,g^{-1}\,h^{-1}}$), but decreases by 11 % to 0.51 $\mathrm{mmol\,g^{-1}\,h^{-1}}$ in interval $CR_{\mathrm{D=0.05}}$. Overall, as the dilution rate increases, the sum of specific ethanol and acetic acid formation, $q_{\mathrm{C_2}}$, decreases by 33 % and 5 % to 0.97 $\mathrm{mmol\,g^{-1}\,h^{-1}}$ and 0.92 $\mathrm{mmol\,g^{-1}\,h^{-1}}$ for $CR_{\mathrm{D=0.04}}$ and $CR_{\mathrm{D=0.05}}$, respectively. The space-time yield of ethanol decreases by 40 % to 5.19 $\mathrm{mmol\,L^{-1}\,h^{-1}}$ after increasing the dilution rate to 0.04 $\mathrm{h^{-1}}$, while STY_{AcOH} increases by 28 % to 7.35 $\mathrm{mmol\,L^{-1}\,h^{-1}}$, see Figure 5.5 D. A further increase of the dilution rate to 0.05 $\mathrm{h^{-1}}$ causes a slight increase in the space-time yield of ethanol by 13 % to 5.86 $\mathrm{mmol\,L^{-1}\,h^{-1}}$, while for acetic acid it remains almost constant at 7.25 $\mathrm{mmol\,L^{-1}\,h^{-1}}$ within the standard deviation. Overall, the space-time yield of acetic acid becomes larger than that of ethanol by increasing the dilution rate, thus

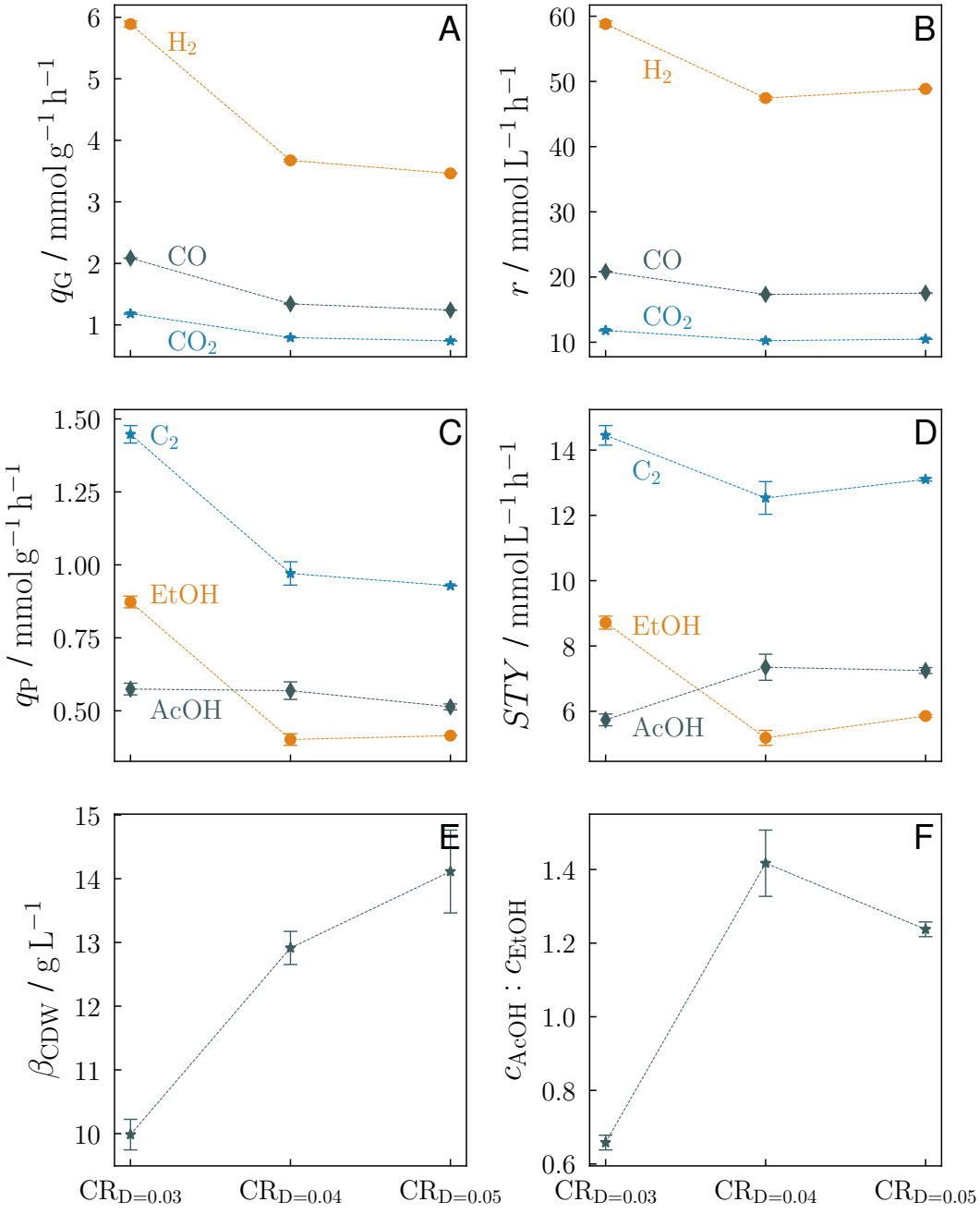

Figure 5.5: Influence of an increased dilution rate $CR_{D=0.04}$ and $CR_{D=0.05}$ in comparison to $CR_{D=0.03}$ with activated biomass retention on biomass-specific gas uptake rate q_G (A), gas uptake rate r (B), biomass-specific productivity q_P (C), space–time yield STY (D), mass concentration of biomass β_{CDW} (E) and product ratio of acetic acid to ethanol (F). Averaged measured data of steady-state areas. For further details on experimental parameters, see Table 5.5.

the product ratio of acetic acid to ethanol reverses from 0.66 in interval $CR_{\mathrm{D=0.03}}$ to 1.42 in interval $CR_{\mathrm{D=0.04}}$ and 1.24 in interval $CR_{\mathrm{D=0.05}}$, respectively, see Figure 5.5 F.

Table 5.6: Measurement data averaged in steady-state areas to investigate the influence of an increased dilution rate with activated biomass retention.

	$\mathrm{CR_{D=0.03}}$	$\mathrm{CR_{D=0.04}}$	$\mathrm{CR_{D=0.05}}$
carbon balance / %	89 ± 2	91 ± 4	94 ± 0
electron recovery / %	94 ± 2	93 ± 4	97 ± 0
X_{CO} / %	90 ± 0.2	87 ± 0.2	88 ± 0.1
$X_{\mathrm{CO_2}}$ / %	93 ± 0.7	94 ± 0.3	96 ± 0.2
$X_{\mathrm{H_2}}$ / %	68 ± 0.5	63 ± 0.4	65 ± 0.1
q_{CO} / $\mathrm{mmol\,g^{-1}\,h^{-1}}$	2.08 ± 0.00	1.34 ± 0.00	1.24 ± 0.00
$q_{\mathrm{CO_2}}$ / $\mathrm{mmol\,g^{-1}\,h^{-1}}$	1.18 ± 0.01	0.79 ± 0.00	0.74 ± 0.00
$q_{\mathrm{H_2}}$ / $\mathrm{mmol\,g^{-1}\,h^{-1}}$	5.89 ± 0.05	3.67 ± 0.02	3.46 ± 0.01
r_{CO} / $\mathrm{mmol\,L^{-1}\,h^{-1}}$	20.82 ± 0.04	17.33 ± 0.04	17.52 ± 0.02
$r_{\mathrm{CO_2}}$ / $\mathrm{mmol\,L^{-1}\,h^{-1}}$	11.81 ± 0.09	10.24 ± 0.028	10.47 ± 0.02
$r_{\mathrm{H_2}}$ / $\mathrm{mmol\,L^{-1}\,h^{-1}}$	58.81 ± 0.46	47.45 ± 0.28	48.86 ± 0.11
β_{CDW} / $\mathrm{g\,L^{-1}}$	9.98 ± 0.24	12.91 ± 0.26	14.11 ± 0.65
q_{AcOH} / $\mathrm{mmol\,g^{-1}\,h^{-1}}$	0.57 ± 0.02	0.57 ± 0.03	0.51 ± 0.01
$\mathrm{q_{EtOH}}$ / $\mathrm{mmol\,g^{-1}\,h^{-1}}$	0.87 ± 0.02	0.40 ± 0.02	0.41 ± 0.00
STY_{AcOH} / $\mathrm{mmol\,L^{-1}\,h^{-1}}$	5.74 ± 0.18	7.35 ± 0.40	7.25 ± 0.09
STY_{EtOH} / $\mathrm{mmol\,L^{-1}\,h^{-1}}$	8.71 ± 0.20	5.19 ± 0.23	5.86 ± 0.04
$c_{\mathrm{AcOH}} : c_{\mathrm{EtOH}}$ / $\frac{\mathrm{mmol_{AcOH}}}{\mathrm{mmol_{EtOH}}}$	0.66 ± 0.02	1.42 ± 0.09	1.24 ± 0.02

5.2.3 Influence of a pressure increase at a volume-constant hydrogen input

Figure 5.6 shows the gas uptake rates r, space-time yields STY, and cell density β_{CDW} over the time t to investigate the effect of an increased process pressure at a volume-constant hydrogen supply.

Table 5.7: Experimental parameters to investigate the influence of an increased process pressure at a constant volumetric hydrogen input with activated biomass retention. The intervals $0\,barg$, $1\,barg$, $1\,barg_{(CO_2\uparrow)}$, $2\,barg$ and $3\,barg$ represent steady-state areas from the experimental run *ZP-II*. Four different pressure levels were investigated, with the pressure-specific volumetric hydrogen input $\dot{V}_{H_2}/p$ kept constant. In interval $1\,barg_{(CO_2\uparrow)}$, the amount of supplied CO_2 in the substrate gas was increased.

	0 barg	1 barg	1 $\text{barg}_{(CO_2\uparrow)}$	2 barg	3 barg
Cell retention	✓	✓	✓	✓	✓
p / barg	0	1	1	2	3
$\dot{V}_{G,n}$ / $mL\,min^{-1}$	97	157	158	216	275
$H_2/CO/CO_2/N_2$ / vol. %	61/20/7/12	76/12/4/8	75/12/5/8	83/9/3/5	87/7/2/4
GRT / min	22.68	14.01	13.92	10.19	8
p_{H_2} / bar	0.61	1.52	1.5	2.49	3.48
p_{CO} / bar	0.2	0.24	0.24	0.27	0.28
p_{CO_2} / bar	0.07	0.08	0.1	0.09	0.08
$k_La(H_2)$ / $s^{-1} \cdot 10^{-2}$	0.96	0.95	0.95	0.96	0.96
$\frac{\dot{V}_{H_2}}{p}$ / $mL\,min^{-1}\,bar^{-1}$			⟵ 59.42 ⟶		
D / h^{-1}			⟵ 0.03 ⟶		
τ / h			⟵ 33.3 ⟶		
pH			⟵ 5.85 ⟶		
duration of interval / h	38.6	42	59.6	55	37.5
number of gas samples	155	168	235	220	150
number of liquid samples	3	4	5	3	3

Due to the constant volumetric hydrogen feed at increased pressure, the gas-liquid mass transfer coefficient k_La of hydrogen is kept constant. The estimation of the k_La of hydrogen is calculated according to STOLL [103]:

$$k_La_{H_2} = f_{H_2} \cdot 11.82 \cdot \left(\frac{P}{V_W}\right)^{0.26} \cdot \left(u_{G,H_2} \cdot \frac{p_0}{p_R}\right)^{0.97} \tag{5.2}$$

f_{H_2} with a value of 1.19 represents a conversion factor, P/V_W is the specific energy input into the CSTR, u_{G,H_2} represents the gas velocity of hydrogen, p_0 represents the ambient pressure in bar and p_R the pressure in the reactor in bar.

The experiment is started at ambient pressure conditions (0 barg) and the pressure is subsequently increased in 1 bar increments. After each pressure increase, the establishment of a steady-state condition is waited for, after which the next pressure increase takes place. The evaluation of the steady-state conditions is shown separately in Figure 5.7 and Table 5.8. For the experimental parameters of the intervals in steady-state areas, see Table 5.7.

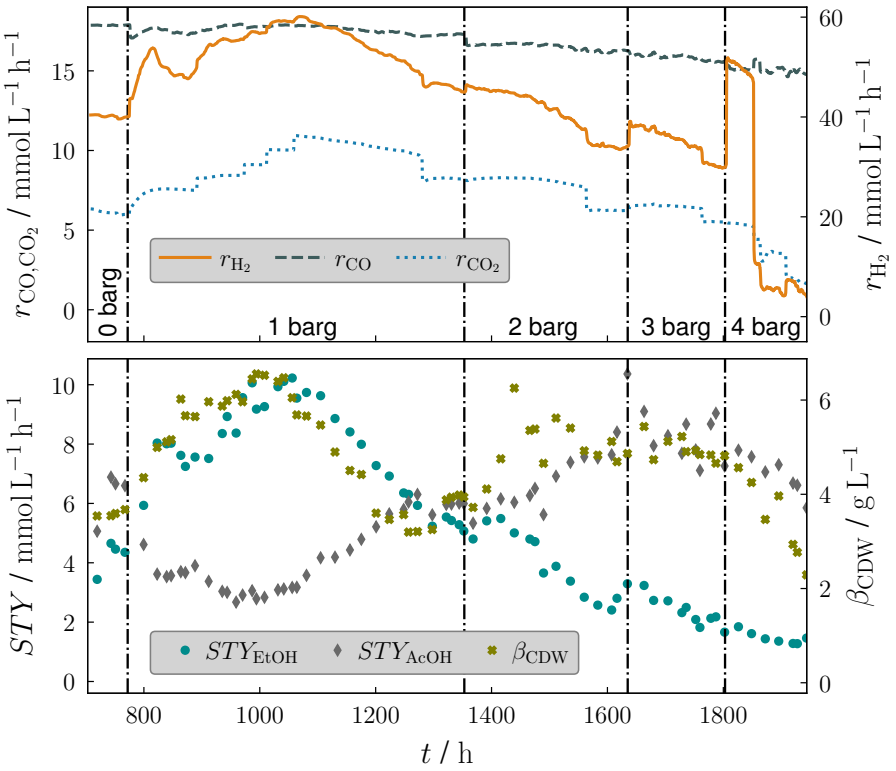

Figure 5.6: Non-averaged measurement data on gas uptake rate r, space-time yield STY and cell density β_{CDW} plotted over the time t to investigate the influence of a pressure increase with a constant-volume hydrogen supply. The pressure was increased from 0 barg in 1 bar increments to 4 barg. During the periods 729 - 768 h, 836 - 878 h, 1293 - 1353 h, 1575 - 1630 h and 1765 - 1803 h, steady-state conditions were established for the pressures 0 barg, 1 barg, 1 barg (at increased CO_2 gas flow), 2 barg and 3 barg. The measured data averaged over these intervals are shown in Figure 5.7. At a pressure of 4 barg, no steady-state condition was established.

After increasing the pressure from 0 barg to 1 barg, all three gas uptake rates as well as the cell density and the space-time yield for ethanol initially increase, see Figure 5.6. The gas conversion of CO_2 increases to 93 %. To avoid limitation in CO_2 feed, the gas feed of CO_2 is gradually increased by 10 % at hour 889, 971, 1010 and 1057, respectively. Immediately after the last increase of CO_2 in the substrate gas, at hour 1058, the gas uptake rates and space-time

yields for ethanol reach a local maximum. The space-time yield for ethanol of approximately $10\,\mathrm{mmol\,L^{-1}\,h^{-1}}$ corresponds to a product concentration of $15.33\,\mathrm{g\,L^{-1}}$. From this point on, the gas uptake rates for CO, CO_2 and H_2 as well as the space-time yield for ethanol decrease continuously until a steady-state condition is reached at hour 729. After increasing the pressure to 2 barg, the gas uptake rates drop again until steady-state, likewise at 3 barg. At 4 bar, the gas uptake rate of H_2 decreases significantly after a short temporary increase, and the cell density also decreases, so that no steady-state conditions are reached. Overall, an inverse behavior of the space-time yields can be seen from hour 1000: while ethanol continuously decreases, the space-time yield for acetic acid continuously increases up to the pressure increase to 4 barg. In addition, it can be seen in Figure 5.6 that after pressure increase to 2 barg, 3 barg and 4 barg, the gas uptake rate of CO_2 decreases with a time lag. Furthermore, after each pressure increase, the hydrogen uptake rate temporarily increases before continuously decreasing. This is most visible with the pressure increase to 4 barg at hour 1800 onwards.

The measured data averaged in the steady-state intervals from Figure 5.6 on the influence of an increased process pressure with constant-volume hydrogen feed are shown in Figure 5.7. The carbon and electron balances range from 88 % to 99 %, see Table 5.8.

At ambient pressure (interval $0\,barg$), the cell density is $3.60\,\mathrm{g\,L^{-1}}$ (Figure 5.7 E) and the product ratio is 1.50 (Figure 5.7 F). The space-time yield for acetic acid is consequently 50 % higher than that of ethanol, see Figure 5.7 D. The space-time yield of the C_2 products is $11.21\,\mathrm{mmol\,L^{-1}\,h^{-1}}$, and the biomass-specific productivity of the C_2 products is $3.11\,\mathrm{mmol\,g^{-1}\,h^{-1}}$, see Figure 5.7 C. In addition to hydrogen, both carbon monoxide and carbon dioxide are taken up by the bacteria. The ratios of the uptaken hydrogen to CO and CO_2 are 2.2 and 6.6, respectively.

The first increase of the process pressure to 1 barg leads to an increase of the cell density by 53 %, see Figure 5.7 E. At the same time, biomass-specific gas uptake decreases for all three substrate gases (Figure 5.7 A), this leads to a decreased biomass-specific C_2 productivity, see Figure 5.7 C. The biomass-specific productivity for acetic acid drops by 64 %, while the biomass-specific productivity for ethanol increases slightly by 13 %. Therefore, the pressure increase to 1 barg leads to a reduction of the product ratio from initially 1.5 to 0.47 (Figure 5.7 F) and consequently results in a higher space-time yield for ethanol compared to acetic acid, see Figure 5.7 D. The space-time yield of the C_2 products is not affected by the pressure increase to 1 barg.

In order to achieve a volume-constant hydrogen feed, the mass flow rate of hydrogen fed was doubled when the pressure was increased to 1 barg. The gas uptake rate for hydrogen

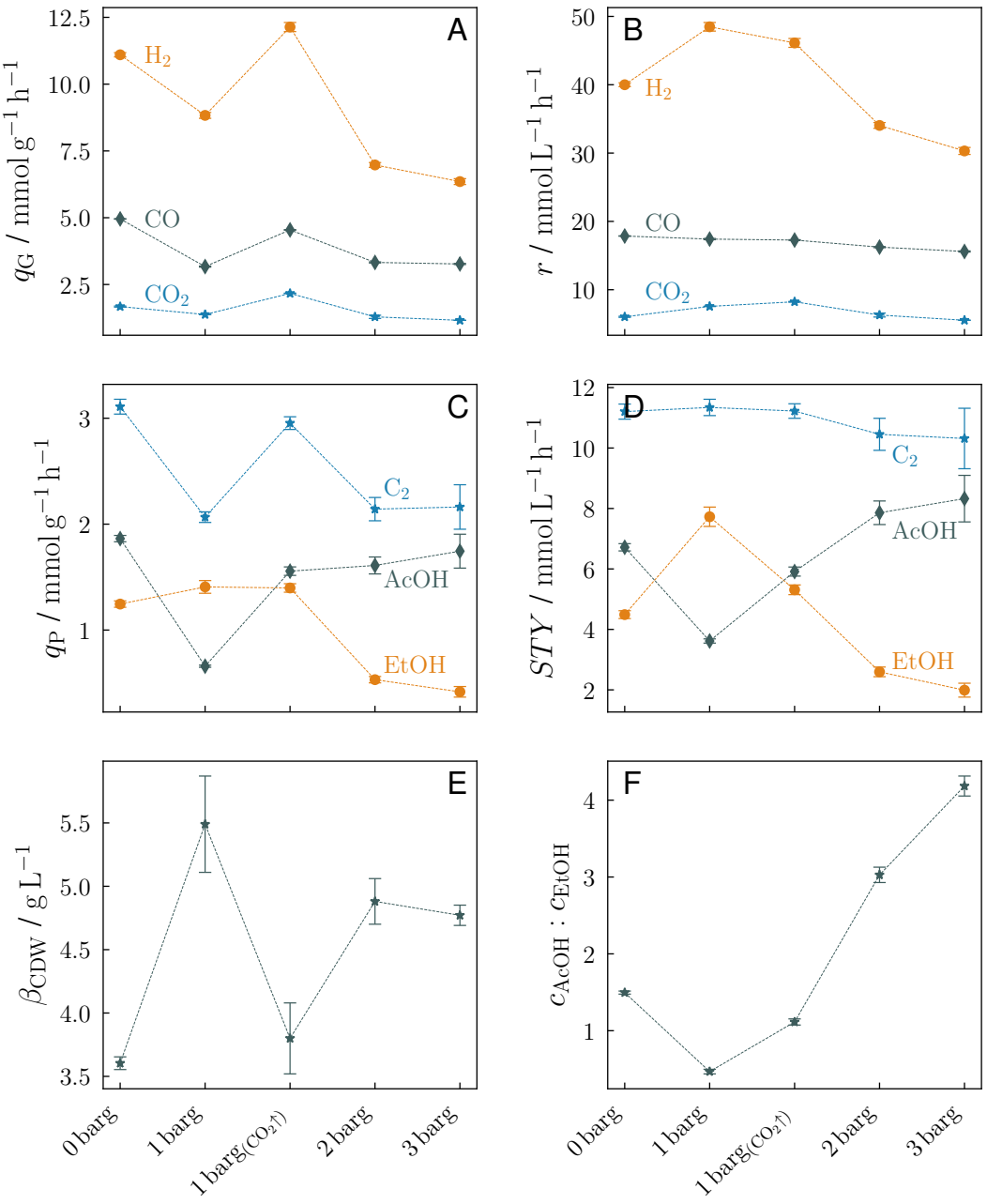

Figure 5.7: Influence of a gradual pressure increase to 3 bar gauge pressure with a constant volumetric supply of hydrogen on biomass-specific gas uptake rate q_G (A), gas uptake rate r (B), biomass-specific productivity q_P (C), space-time yield STY (D), mass concentration of biomass β_{CDW} (E), and product ratio of acetic acid to ethanol (F). Averaged measured data of steady-state areas. At one bar overpressure, the amount of CO_2 in the substrate gas was increased in a second step ($1\,barg_{(CO_2\uparrow)}$). For further details on experimental parameters, see Table 5.7.

increased with the pressure increase from initially 40 $\mathrm{mmol\,L^{-1}\,h^{-1}}$ to 48.48 $\mathrm{mmol\,L^{-1}\,h^{-1}}$, corresponding to an increase of 21 %, see Figure 5.7 B. In comparison to the supplied hydrogen feed, the gas uptake rate thus did not double, so that the conversion of hydrogen dropped from 62 % originally to 38 %. The conversion of CO_2 has increased from originally 75 % to 93 %, CO_2 is therefore almost completely taken up after the first pressure increase. In order to avoid a limitation in the availability of CO_2 during further pressure increases, the supplied volume flow of CO_2 is now increased by 21 % from initially 6.72 $\mathrm{ml\,min^{-1}}$ to 8.13 $\mathrm{ml\,min^{-1}}$ in an intermediate step, see interval $1\,barg_{(CO_2\uparrow)}$.

Increasing the supplied gas rate of CO_2 leads to a significant decrease in cell density by 30 %, see interval $1\,barg_{(CO_2\uparrow)}$ in Figure 5.7 E. The conversion of CO_2 decreases from 93 % to 85 %, the other gas conversions remain almost unchanged. The biomass-specific gas uptake increases for all three substrate gases, see Figure 5.7 A. The space-time yield of the C_2 products remains unchanged (-1 %), while the space-time yield for acetic acid increases by 63 % and decreases by 31 % for ethanol, see Figure 5.7 D. This reverses the product ratio again: from originally 0.47 in the interval 1 barg to 1.11 in the interval $1\,barg_{(CO_2\uparrow)}$, see Figure 5.7 F.

As it was already the case for the first pressure increase, the second pressure increase from 1 barg to 2 barg leads to an increase in cell density, too, the increase is 28 %, see Figure 5.7 E. The biomass-specific gas uptake decreases for all three gases, the reduction is largest for hydrogen with -42 % compared to CO_2 with -40 % and CO with -26 %, see Figure 5.7 A. The conversion of hydrogen drops from 36 % to 18 %. There is a further increase in the space-time yield of acetic acid, while the space-time yield of ethanol decreases again, see Figure 5.7 D. This increases the product ratio from 1.11 to 3.03, see Figure 5.7 F. Furthermore, there is a 7 % decrease in the space-time yield of the C_2 products for the first time.

The third and last pressure increase in Figure 5.7 from 2 barg to 3 barg, unlike the previous pressure increases, does not lead to a significant change in cell density. The 2 % reduction in cell density is within the standard deviation and therefore negligible. Gas conversions continue to drop, with the largest decrease for hydrogen at 33 % from 18 to 12 percentage points. There is a further increase in the space-time yield for acetic acid, while the space-time yield for ethanol assumes the lowest value of 1.99 $\mathrm{mmol\,L^{-1}\,h^{-1}}$ in this series of measurements, see Figure 5.7 D. The product ratio increases to 4.18 (Figure 5.7 F), which is the highest product ratio measured in this series of measurements. The ratio of uptaken hydrogen to CO and CO_2 is 1.9 and 5.5, respectively, which is lower than the ratio of 2.2 and 6.6 before the first pressure increase was applied.

Table 5.8: Measurement data averaged in steady-state areas to investigate the influence of an increased process pressure at a constant volumetric hydrogen input with activated biomass retention.

	0 barg	1 barg	1 barg$_{(CO_2\uparrow)}$	2 barg	3 barg
carbon balance / %	94 ± 2	91 ± 2	88 ± 2	93 ± 5	98 ± 9
electron recovery / %	93 ± 2	92 ± 3	88 ± 2	94 ± 5	99 ± 10
X_{CO} / %	88 ± 0.2	85 ± 0.5	86 ± 0.3	82 ± 0.4	79 ± 0.4
X_{CO_2} / %	75 ± 1	93 ± 0.3	85 ± 0.5	80 ± 3.7	79 ± 0.2
X_{H_2} / %	62 ± 0.4	38 ± 0.5	36 ± 0.5	18 ± 0.2	12 ± 0.2
q_{CO} / mmol g^{-1} h^{-1}	4.96 ± 0.01	3.17 ± 0.02	4.54 ± 0.01	3.33 ± 0.02	3.27 ± 0.02
q_{CO_2} / mmol g^{-1} h^{-1}	1.67 ± 0.02	1.38 ± 0.0	2.17 ± 0.01	1.29 ± 0.06	1.16 ± 0.0
q_{H_2} / mmol g^{-1} h^{-1}	11.10 ± 0.08	8.83 ± 0.11	12.14 ± 0.17	6.97 ± 0.09	6.35 ± 0.11
r_{CO} / mmol L^{-1} h^{-1}	17.86 ± 0.03	17.41 ± 0.09	17.27 ± 0.05	16.23 ± 0.08	15.6 ± 0.08
r_{CO_2} / mmol L^{-1} h^{-1}	6.03 ± 0.08	7.56 ± 0.02	8.23 ± 0.05	6.29 ± 0.29	5.53 ± 0.01
r_{H_2} / mmol L^{-1} h^{-1}	40.0 ± 0.28	48.48 ± 0.63	46.12 ± 0.65	34.04 ± 0.42	30.31 ± 0.51
β_{CDW} / g L^{-1}	3.60 ± 0.05	5.49 ± 0.38	3.80 ± 0.28	4.88 ± 0.18	4.77 ± 0.08
q_{AcOH} / mmol g^{-1} h^{-1}	1.86 ± 0.03	0.66 ± 0.01	1.56 ± 0.04	1.61 ± 0.08	1.74 ± 0.16
q_{EtOH} / mmol g^{-1} h^{-1}	1.25 ± 0.03	1.41 ± 0.06	1.40 ± 0.04	0.53 ± 0.03	0.42 ± 0.05
STY_{AcOH} / mmol L^{-1} h^{-1}	6.72 ± 0.12	3.62 ± 0.07	5.91 ± 0.15	7.86 ± 0.39	8.33 ± 0.77
STY_{EtOH} / mmol L^{-1} h^{-1}	4.49 ± 0.13	7.73 ± 0.32	5.31 ± 0.16	2.60 ± 0.16	1.99 ± 0.23
$c_{AcOH} : c_{EtOH}$ / $\frac{mmol_{AcOH}}{mmol_{EtOH}}$	1.50 ± 0.02	0.47 ± 0.03	1.11 ± 0.04	3.03 ± 0.10	4.18 ± 0.13

5.2.4 Influence of a gradually reduced pH value

The study on the influence of a reduced pH was first started at a pH of 5.9 ($pH\ 5.9$), subsequently the pH was reduced to 5.7 ($pH\ 5.7$) and 5.5 ($pH\ 5.5$) and then increased again to 5.9 ($pH\ \widetilde{5.9}$). For the experimental parameters of the intervals in steady-state areas, see Table 5.9.

Table 5.9: Experimental parameters to investigate the influence of a gradually reduced pH value with activated biomass retention. The intervals $pH\ 5.9$, $pH\ 5.7$, $pH\ 5.5$ und $pH\ \widetilde{5.9}$ represent steady-state areas at three different pH values from the experimental run *ZpH-I*. At the end of the experiment, the pH value of 5.9 investigated at the beginning in interval $pH\ 5.9$ was set again to test reproducibility in interval $pH\ \widetilde{5.9}$.

	pH 5.9	pH 5.7	pH 5.5	pH $\widetilde{5.9}$
Cell retention	✓	✓	✓	✓
pH	5.9	5.7	5.5	5.9
$\dot{V}_G$ / mL min^{-1}	⟵ 111 ⟶			126
$H_2/CO/CO_2/N_2$ / vol. %	⟵ 65.5/18/7/10.5 ⟶			66/18/7/9
$H_2 : CO : CO_2$	⟵ 72 : 20 : 8 ⟶			
GRT / min	⟵ 19.82 ⟶			17.46
D / h^{-1}	⟵ 0.03 ⟶			
τ / h	⟵ 33.3 ⟶			
p / barg	⟵ 0 ⟶			
duration of interval / h	38	102	78	91
number of gas samples	164	235	329	435
number of liquid samples	4	5	4	4

The averaged measured data on the influence of a reduced pH are shown in Figure 5.8. The carbon and electron balances are between 89 % and 99 %, see Table 5.10.

The first reduction of pH from 5.9 to 5.7 leads to a slight increase in cell density of 8 %, see Figure 5.8 E. The gas uptake rate of hydrogen also increases slightly by 5 %, see Figure 5.8 B. Furthermore, an opposite behavior can be seen in the product formation: while the product formation increases for ethanol, it decreases for acetic acid, see Figure 5.8 C and D. As a result, the product ratio decreases from 0.8 to 0.62 (Figure 5.8 F). The space-time yield of C_2 products increases by 8 % along with the pH reduction, and the biomass-specific C_2 product formation remains constant.

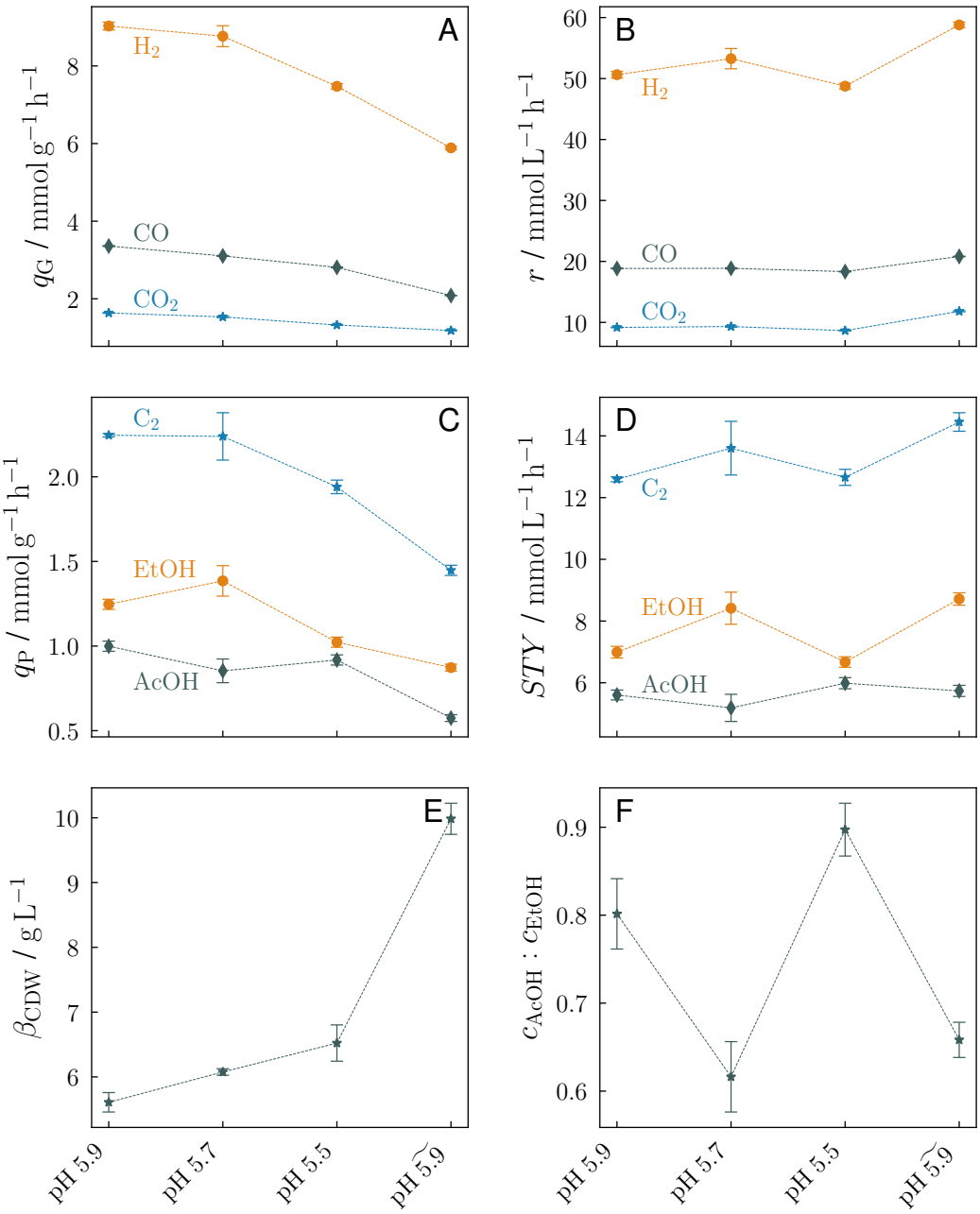

Figure 5.8: Influence of a gradually reduced pH value with activated biomass retention on biomass-specific gas uptake rate q_G (A), gas uptake rate r (B), biomass-specific productivity q_P (C), space-time yield STY (D), mass concentration of biomass β_{CDW} (E), and product ratio of acetic acid to ethanol (F). At the end of the experiment, the pH value of 5.9 investigated at the beginning in interval $pH\ 5.9$ was set again to test reproducibility in interval $pH\ \widetilde{5.9}$. Averaged measured data of steady-state areas. For further details on experimental parameters, see Table 5.9.

Table 5.10: Measurement data averaged in steady-state areas to investigate the influence of a gradually reduced pH value with activated biomass retention.

	pH 5.9	pH 5.7	pH 5.5	pH $\widetilde{5.9}$
carbon balance / %	90 ± 1	97 ± 6	94 ± 2	89 ± 2
electron recovery / %	93 ± 1	99 ± 6	95 ± 2	95 ± 2
X_{CO} / %	91 ± 0.2	91 ± 0.4	88 ± 0.3	90 ± 0.2
X_{CO_2} / %	91 ± 0.6	93 ± 1.1	86 ± 0.4	93 ± 0.7
X_{H_2} / %	65 ± 0.7	68 ± 2.1	62 ± 0.6	68 ± 0.5
q_{CO} / mmol g^{-1} h^{-1}	3.36 ± 0.01	3.10 ± 0.01	2.81 ± 0.01	2.08 ± 0.00
q_{CO_2} / mmol g^{-1} h^{-1}	1.64 ± 0.01	1.53 ± 0.02	1.32 ± 0.01	1.18 ± 0.01
q_{H_2} / mmol g^{-1} h^{-1}	9.03 ± 0.10	8.77 ± 0.27	7.47 ± 0.07	5.89 ± 0.04
r_{CO} / mmol L^{-1} h^{-1}	18.84 ± 0.04	18.87 ± 0.09	18.33 ± 0.05	20.81 ± 0.04
r_{CO_2} / mmol L^{-1} h^{-1}	9.17 ± 0.06	9.32 ± 0.11	8.64 ± 0.04	11.81 ± 0.09
r_{H_2} / mmol L^{-1} h^{-1}	50.63 ± 0.55	53.26 ± 1.66	48.75 ± 0.46	58.80 ± 0.45
β_{CDW} / g L^{-1}	5.61 ± 0.15	6.08 ± 0.05	6.52 ± 0.28	9.98 ± 0.24
q_{AcOH} / mmol g^{-1} h^{-1}	1.00 ± 0.03	0.85 ± 0.07	0.92 ± 0.03	0.57 ± 0.02
q_{EtOH} / mmol g^{-1} h^{-1}	1.25 ± 0.03	1.39 ± 0.09	1.02 ± 0.03	0.87 ± 0.02
STY_{AcOH} / mmol L^{-1} h^{-1}	5.60 ± 0.16	5.19 ± 0.44	5.99 ± 0.18	5.74 ± 0.18
STY_{EtOH} / mmol L^{-1} h^{-1}	6.99 ± 0.19	8.42 ± 0.52	6.67 ± 0.17	8.71 ± 0.20
$c_{AcOH} : c_{EtOH}$ / $\frac{mmol_{AcOH}}{mmol_{EtOH}}$	0.80 ± 0.04	0.62 ± 0.04	0.90 ± 0.03	0.66 ± 0.02

Further reduction of pH from 5.7 to 5.5 again leads to a moderate increase in cell density of 7 %, see Figure 5.8 E. However, for all three gases, the biomass-specific gas uptake rate decreases, by 9 % for CO, by 14 % for CO_2 and by 15 % for hydrogen, see Figure 5.8 A). Therefore, there is also a 13 % decrease in biomass-specific C_2 product formation, see Figure 5.8 C. Furthermore, ethanol productivity decreases in both mass and volume quantities, while acetic acid productivity increases for both benchmarks. Consequently, the product ratio of acetic acid to ethanol increases from 0.62 to 0.9, see Figure 5.8 F).

A further reduction of the pH to 5.3 leads to a decreasing gas uptake rate, especially for hydrogen, see Figure 5.9. Additionally, after reducing the pH to 5.1, the gas uptake rate of CO_2 decreases significantly. The space-time yield for ethanol decreases from the original 8 mmol L^{-1} h^{-1} at hour 1390 to 2 mmol L^{-1} h^{-1} at hour 1580. With the exception of cell density, no steady-state conditions are established, so the measured data at pH 5.3 and 5.1

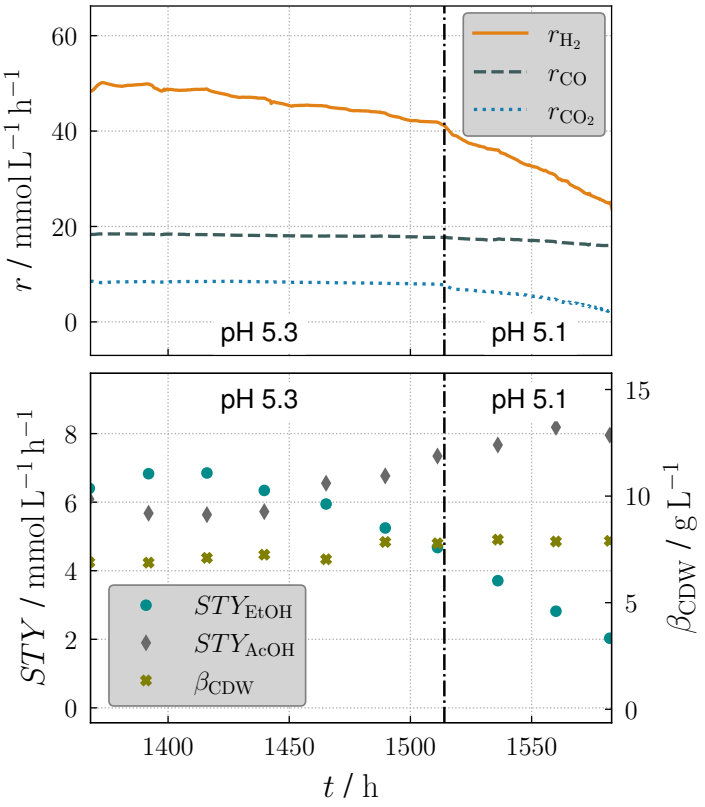

Figure 5.9: Non-averaged measured data of gas uptake rates r, space-time yields STY and cell density β_{CDW} over time t for pH 5.3 and 5.1.

cannot be averaged and therefore cannot be considered for further evaluation of steady-state intervals.

In a final step, the pH is set to the initial value of 5.9, see interval $pH\ \widetilde{5.9}$. In order to have similar gas conversions in this interval as in the interval $pH\ 5.9$, the gas volume flow rate was adjusted and increased in parallel with the increase of pH while keeping the gas composition constant.

The cell density increases significantly with 53 % after increasing the pH to 5.9 compared to the interval $pH\ 5.5$ in Figure 5.8 E. At the same time, the biomass-specific gas uptake rate decreases for all three substrate gases, see Figure 5.8 A. However, due to the high increase in cell density, there is an overall increase in the gas uptake rate for CO, CO_2 and H_2, see Figure 5.8 B. The biomass-specific product formation of ethanol and acetic acid decreases by 15 % and 38 %, respectively, but the increase in cell density by 53 % results in only a slight decrease in the space-time yield of acetic acid of 4 % and an increase in the space-time yield of ethanol of

31 %. As a result, the fraction of ethanol in the product flow increases, so that the product ratio of acetic acid to ethanol decreases from 0.9 to 0.66, see Figure 5.8 F. The space-time yields of ethanol with 8.71 $\mathrm{mmol\,L^{-1}\,h^{-1}}$ and C_2 products with 14.45 $\mathrm{mmol\,L^{-1}\,h^{-1}}$ in interval $pH\ \widetilde{5.9}$ are the highest measured space-time yields compared to the other intervals and higher than in interval $pH\ 5.9$ by 25 % and 15 %, respectively. The space-time yield of ethanol with 8.71 $\mathrm{mmol\,L^{-1}\,h^{-1}}$ corresponds to a product concentration of 13.36 $\mathrm{g\,L^{-1}}$.

6 Discussion

The experimental measurement results have shown that the use of a total biomass retention system increases the cell density by a factor of 2.6, while the total space-time yield is increased by a factor of 1.5. In addition, the product ratio reverses: without cell retention, more acetic acid is formed compared to ethanol, and with the use of a biomass retention system, more ethanol is formed compared to acetic acid. These observations are in contrast to the hypothesis established before the start of the experiments that cell retention would lead to an increase in cell density, but also to an increase in space-time yield proportional to cell density and to a product ratio that would remain constant. A shift in the product ratio due to adaptation of the microorganisms during operation of a biomass retention system is unlikely based on the measured data, see Section 5.1.2. Rather, another regulatory mechanism might have been responsible for the product shift. Therefore, in the following Section 6.1, three possible reasons that could lead to a product shift and to a decrease in biomass-specific product formation are discussed: (1.) Limitation of substrate gas and nutrients, (2.) Reduced biomass-specific partial pressure of CO and (3.) Growth stagnation. Furthermore, it is discussed why the use of a total cell retention system does not lead to a steadily increasing cell density but to a biomass concentration with steady-state areas in all performed experiments.

In addition, the increase in pressure at a constant volumetric hydrogen input and the lowering of the pH value in the reaction medium were aimed at shifting the product ratio in favor of ethanol. The increase in pressure with constant-volume hydrogen supply was intended to increase hydrogen uptake, while the pH reduction was intended to increase ethanol formation by the cells in order to counteract a further drop in pH. Therefore, the experimental results for pressure increase and pH decrease are discussed below in Section 6.2 and Section 6.4, respectively.

Furthermore, it was observed that high space-time yields of ethanol of $10\,\mathrm{mmol\,L^{-1}\,h^{-1}}$ can only be achieved in the short term. The influence of ethanol on long-term stability is therefore part of the discussion in Section 6.3.

6.1 Influence of high cell densities by using biomass retention

6.1.1 Limitation of substrate gas and nutrients

At high cell densities, substrate gases could be limited. However, the gas flow increase has shown that the biomass-specific gas uptake rates increase for all gases, including CO, but not linearly with the gas flow increase, see Section 5.2.1. A further, second gas increase led to a decrease in cell density, reduced conversion of CO and, for the first time, net CO_2 production. Despite a limitation in the substrate gas before increasing the gas volume flow at high cell densities, it is therefore unlikely that the limitation is responsible for the greatly reduced biomass-specific gas uptake rates, particularly for CO. However, reduced viability could be a possible cause, e. g. triggered by the peristaltic pump in the external circuit for biomass retention or by the absence of gas supply in this circuit. Therefore, determining viability could be important for future studies.

High cell densities with a constant supply of liquid nutrient medium can lead to limitations of individual nutrients [182]. The measured data on the effect of dilution rate, see Figure 5.5 in Section 5.2.2, show a significant increase in cell density of 29 % after increasing the dilution rate from $D = 0.03\,\mathrm{h}^{-1}$ to $D = 0.04\,\mathrm{h}^{-1}$. This indicates a limitation of cell growth at a dilution rate of $0.03\,\mathrm{h}^{-1}$. Furthermore, the product ratio reverses, the molar fraction of ethanol after increasing the dilution rate is 0.41 instead of 0.6 before, and that of acetic acid is 0.59 instead of 0.4 before, see Figure 6.1 $\mathrm{CR_{D=0.03}}$ and Figure 6.1 $\mathrm{CR_{D=0.04}}$.

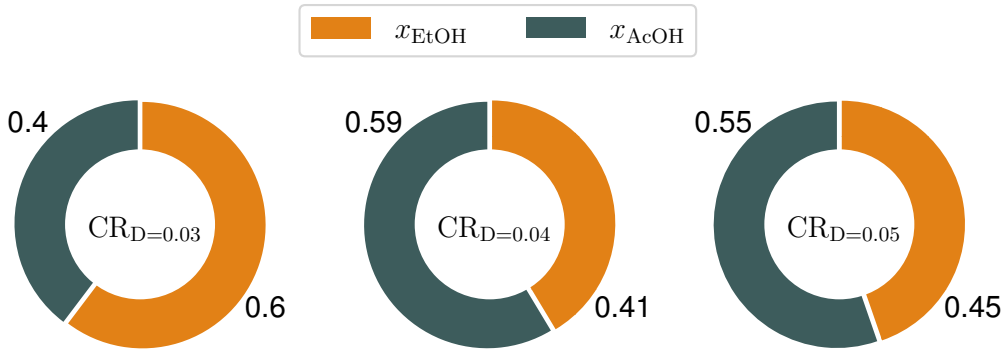

Figure 6.1: Mole fraction of ethanol (x_{EtOH}) and acetic acid (x_{AcOH}) of the product stream for three different dilution rates ($0.03\,\mathrm{h}^{-1}$, $0.04\,\mathrm{h}^{-1}$, $0.05\,\mathrm{h}^{-1}$) with activated cell retention (CR).

RICHTER ET AL. [120] have shown by proteomic analysis that an insufficient supply of sulphur via the addition of cysteine leads to reduced growth and the resulting excess of reduction potential leads to increased ethanol formation. GADDY ET AL. [15] have described in their patent the possibility of a reduction of calcium pantothenate and cobalt in the culture medium to slow down both the acetyl-CoA cycle relative to the carbonyl branch and the THF cycle rate. This also leads to increased reduction potential and eventually increased ethanol formation. WAN ET AL. [183] have observed reduced growth of *Clostridium carboxidivorans* during yeast extract limitation. In a study by PHILLIPS ET AL. [184], the product ratio of ethanol to acetic acid increased during phosphate limitation. Considering these experimental results, the measured data in the present study indicate that at a dilution rate of $D = 0.03\,\mathrm{h}^{-1}$ and activated cell retention, there is a limitation of biomass growth caused by the nutrient medium, resulting in an excess of reduction potential that is converted to ethanol. In contrast, a further increase in the dilution rate to $0.05\,\mathrm{h}^{-1}$ leads just to a slight increase in cell density and to no significant change in the product ratio, see Figure 6.1 $\mathrm{CR_{D=0.05}}$. It can be concluded that there is sufficient nutrient supply to the microorganisms already at a dilution rate of $D = 0.04\,\mathrm{h}^{-1}$. Further increasing the dilution rate, contrary to the assumption of RICHTER ET AL. [18], does not lead to an increase in product formation.

The experimental investigations on the influence of cell retention ($\overline{CR}$ vs. CR, see Figure 5.1 and Table 5.2 in Section 5.1.1) were performed at a constant dilution rate of $D = 0.03\,\mathrm{h}^{-1}$. Based on the above findings on the influence of the dilution rate, it must therefore be assumed that there was a limitation due to the nutrient medium after activation of the biomass retention. For this reason, the influence of this limiting effect on the measurement results will be discussed in the following. Activation of the biomass retention leads to increased biomass and to a reduced product ratio of acetic acid to ethanol from 2.33 to 0.81, and ethanol formation is thus favored at high cell densities. Increasing the dilution rate in order to overcome the limitation of the nutrient medium leads to an increase of the product ratio from initially 0.66 ($CR_{D=0.03}$) to 1.42 ($CR_{D=0.04}$), see Figure 5.5 F in Section 5.2.2. Thus, more acetic acid is again formed than ethanol, but this surplus of 42 % is significantly smaller compared to 133 % without cell retention. Furthermore, the biomass-specific productivities q_{AcOH} and q_{EtOH} decrease significantly with the use of biomass retention and do not increase again by increasing the dilution rate. Therefore, it is unlikely that limitation by the nutrient medium when biomass retention is used is the only reason for the significant shift in the product ratio and for the decrease in biomass-specific productivities.

6.1.2 Biomass-specific partial pressure of CO in the off-gas

As already shown, the operation of a biomass retention system increases the cell density from initially $1.19\,\mathrm{g\,L^{-1}}$ and $1.08\,\mathrm{g\,L^{-1}}$ to an average value of $3.13\,\mathrm{g\,L^{-1}}$ (measurement campaign *HSF-Z-IV*) and $12.33\,\mathrm{g\,L^{-1}}$ (measurement campaign *ZpH-I*), respectively. Figure 6.2 shows all measured data from *HSF-Z-IV* and *ZpH-I*, where both CO and CO_2 were taken up simultaneously.

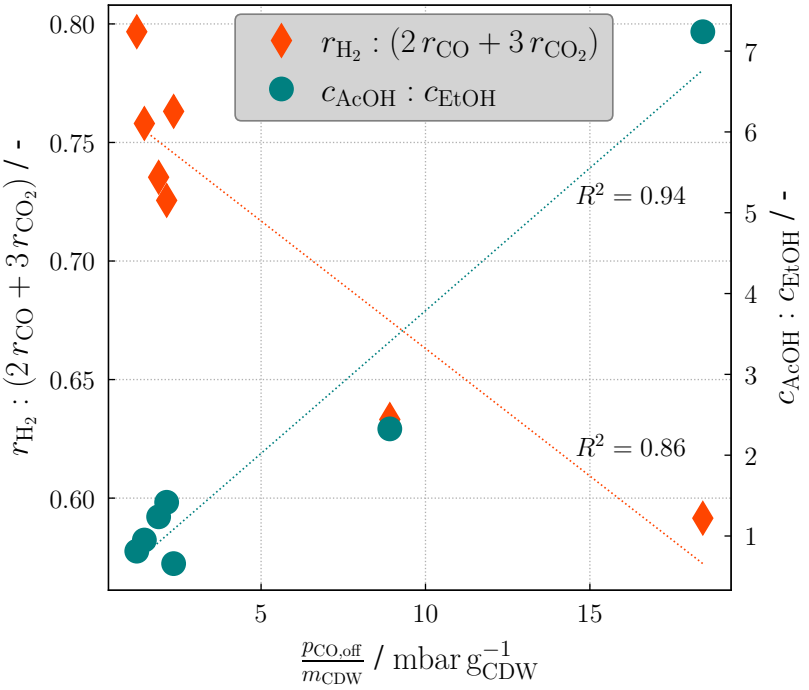

Figure 6.2: Hydrogen uptake ratio and product ratio as a function of biomass-specific CO partial pressure in the off-gas. The hydrogen uptake ratio takes into account that twice the molar amount of hydrogen is required for the complete conversion of CO to ethanol and three times the molar amount of hydrogen is required for the complete conversion of CO_2 to ethanol. This ratio is valid for data containing positive gas uptake rates. In addition to the measured points, linear fit of product ratio and hydrogen uptake ratio are shown.

It is clear that as the biomass-specific partial pressure of CO in the off-gas increases, the product ratio of acetic acid to ethanol increases proportionally, and the trend can be approximated by the following linear fit:

$$c_{\mathrm{AcOH}} : c_{\mathrm{EtOH}} = 0.3531\,\frac{g_{\mathrm{CDW}}}{\mathrm{mbar}} \cdot \frac{p_{\mathrm{CO,off}}}{m_{\mathrm{CDW}}} + 0.2569 \qquad and\ R^2 = 0.9424 \tag{6.1}$$

It is remarkable that all measurement points sampled with a cell retention system are in the range of low biomass-specific partial pressures of CO ($< 3\,\mathrm{mbar\,g_{CDW}^{-1}}$), whereas the measurement points without cell retention are assigned to significantly higher biomass-specific partial pressures of CO ($8.91\,\mathrm{mbar\,g_{CDW}^{-1}}$ from experiment ***HSF-Z-IV*** in interval $\overline{CR}$ and $18.43\,\mathrm{mbar\,g_{CDW}^{-1}}$ from experiment ***ZpH-I*** in interval $\widetilde{\overline{CR}}$). However, there is no clear tendency for the partial pressure of CO in the exhaust gas to decrease with higher cell density: e. g., at a cell density of $1.08\,\mathrm{g\,L^{-1}}$ in interval $\widetilde{\overline{CR}}$, the partial pressure of CO in the exhaust gas is 43.9 mbar, while at a higher cell density of $9.98\,\mathrm{g\,L^{-1}}$ in interval $CR_{\mathrm{D}=0.03}$ the partial pressure of CO in the exhaust gas is not smaller, but even higher with 51.4 mbar. Furthermore, the measured data shown in Figure 6.2 indicate that a high CO gas conversion alone does not necessarily lead to a low biomass-specific partial pressure of CO in the exhaust gas: for example, at a CO conversion of 0.9 (interval $\overline{CR}$, see Table 5.2 in Section 5.1.1), the biomass-specific partial pressure of CO in the exhaust gas is $8.91\,\mathrm{mbar\,g_{CDW}^{-1}}$, while at a slightly lower CO conversion of 0.87 (interval $CR_{\mathrm{D}=0.04}$, see Table 5.6 in Section 5.2.2), the biomass-specific partial pressure of CO in the off-gas is not higher, but significantly lower by 76 % at $2.13\,\mathrm{mbar\,g_{CDW}^{-1}}$. Of particular importance for the biomass-specific partial pressure of CO in the exhaust gas is therefore the cell density: only at high cell densities realized by the use of a biomass retention system, there are low biomass-specific partial pressures of CO in the off-gas as well as low product ratios of acetic acid to ethanol in the fermentation broth. In their studies, VALGEPEA ET AL. [185] have observed lower acetic acid to ethanol product ratios at higher cell densities, too, and they attribute this to the maintenance of ATP homeostasis at elevated concentrations of extracellular acetic acid. MOCK ET AL. [186] have a similar explanation approach and attribute high ethanol concentrations as a consequence of high acetic acid concentrations, as this could increase the intracellular acetic acid concentration compared to the intracellular acetaldehyde concentration, thus promoting ethanol formation via the AOR. MAYER ET AL. [21] observed in their studies with the microorganism *C. aceticum* an inhibitory effect of acetic acid exceeding a concentration of $10\,\mathrm{g\,L^{-1}}$, KANTZOW ET AL. [17] for *Acetobacterium woodii* from 8 - 12 $\mathrm{g\,L^{-1}}$. Moreover, an inhibitory effect of high acetic acid concentrations on the growth of microorganisms would explain the stagnation of cell growth despite total cell retention in the present study. Thus, the decrease in biomass-specific productivity of acetic acid after activation of cell retention in Figure 5.1 C in Section 5.1.1 would be explained by the fact that the decrease in biomass-specific productivity of acetic acid would counteract a further increase in intracellular acetic acid concentration. The graph in Figure 6.3 would be in agreement with this as well: A significant increase in ethanol concentration to $5\,\mathrm{g\,L^{-1}}$ or more is not observed until acetic acid concentrations are at least $8\,\mathrm{g\,L^{-1}}$. Therefore,

from Figure 6.3, it becomes clear that high ethanol concentrations only occur at high acetic acid concentrations. This can usually be achieved only with high cell densities due to the limited biomass-specific productivity of the microorganisms. This is consistent with VALGEPEA ET AL. [185] and MOCK ET AL. [186]. According to their findings, high ethanol concentrations were a consequence of high acetic acid concentrations. In contrast to acetic acid, ethanol concentrations up to $15\,\mathrm{g\,L^{-1}}$ do not have an inhibitory effect on the growth of *C. ljungdahlii* [187].

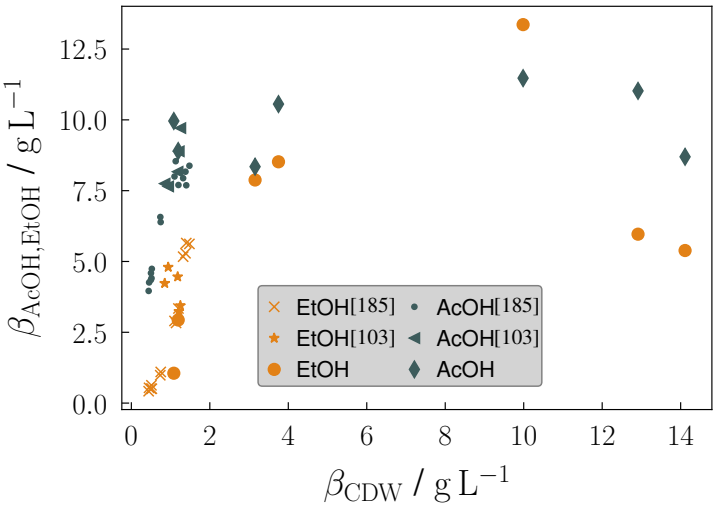

Figure 6.3: Product concentrations of acetic acid and ethanol as a function of cell density. Measured data of experiment *HSF-Z-IV* and *ZpH-I* are compared with those from STOLL [103] (chemostat, $D = 0.03\,\mathrm{h^{-1}}$, *C. ljungdahlii* DSM 13528) and VALGEPEA ET AL. [185] (chemostat, $D = 0.04\,\mathrm{h^{-1}}$, *C. autoethanogenum* DSM 19630). Cell densities of $12.91\,\mathrm{g\,L^{-1}}$ and $14.11\,\mathrm{g\,L^{-1}}$ were obtained at higher dilution rates of $0.04\,\mathrm{h^{-1}}$ and $0.05\,\mathrm{h^{-1}}$. Adapted with permission from [185]. Copyright 2017 Elsevier Inc.

In addition, VALGEPEA ET AL. [185] found that with the increase in cell density, the ratio q_{H_2}/q_{CO} decreased from 0.67 to 0.39, metabolic modeling demonstrated that the fraction of reduced ferredoxin generated by oxidation of CO to CO_2 increased by 19 %. In contrast, our measured data show that the ratio q_{H_2}/q_{CO} increases from 1.29 to 2.13 when cell density is increased by activation of biomass retention. Therefore, it is likely that reduced ferredoxin was increasingly formed by hydrogen uptake and hydrogenase activity. Accordingly, both CO and H_2 serve as reducing agents for ferredoxin. This is consistent with studies by BERTSCH and MÜLLER [188], LIEW ET AL. [36] and SCHUCHMANN and MÜLLER [13].

In addition, a linear relationship between the hydrogen uptake ratio and the biomass-specific partial pressure of CO in the exhaust gas is shown in Figure 6.2. The hydrogen uptake ratio takes into account that twice the molar amount of H_2 is required for the complete conversion of CO to ethanol, and three times the molar amount of H_2 is required for the complete conversion of CO_2. The hydrogen uptake ratio, from now on also called $r^*_{H_2}$, therefore represents a stoichiometric ratio. The course of this ratio as a function of the biomass-specific partial pressure of CO in the exhaust gas can be approximated by the following linear fit:

$$r^*_{H_2} = -0.0108 \frac{g_{CDW}}{mbar} \cdot \frac{p_{CO,off}}{m_{CDW}} + 0.7707 \qquad and\ R^2 = 0.8598 \tag{6.2}$$

From Figure 6.2, it can be seen that at low biomass-specific partial pressures of CO in the off-gas, the specific hydrogen uptake is high, while at large biomass-specific CO partial pressures, it is low. This relationship can be explained by the inhibitory effect of CO on hydrogenase. The CO-induced inhibition of hydrogenase has already been investigated in various studies, see [21, 105, 108, 109]. For example, BERTSCH and MÜLLER [188] were able to observe hydrogen uptake only above a conversion of CO of 90 %. It can also be seen from the measurement date of this present study that after a gas flow increase (interval $CR_{\dot{V}_{G\uparrow\uparrow}}$ see Figure 5.4 in Section 5.2.1), which resulted in a decrease of CO conversion to 84 %, the biomass-specific hydrogen uptake rate decreases significantly by 13 % from 9.96 $mmol\,g^{-1}\,h^{-1}$ to 8.68 $mmol\,g^{-1}\,h^{-1}$. Therefore, taking into account the studies mentioned previously, it is likely that the second gas flow increase resulted in an increase in CO-induced inhibition of hydrogenase.

In addition, the product ratio of acetic acid to ethanol decreases with an increase in specific hydrogen uptake, see Figure 6.2. This could be a result of excess reduction potential in the form of reduced ferredoxin and NADP due to increased activity of electron-bifurcating hydrogenase (Hyt). This excess can be reduced by the formation of ethanol via aldehyde ferredoxin oxidoreductase (AOR) or bifunctional acetaldehyde/alcohol dehydrogenase (AdhE), with AOR being the thermodynamically more favorable pathway [186, 188, 189].

6.1.3 Growth stagnation

Despite total cell retention, there has not been a continuous increase in cell density; instead, constant cell densities have occurred in the intervals. Therefore, in the following discussion, we assume that cell retention, together with the other process conditions, led to a stagnation of cell growth.

With cell retention, the energy efficiency increases from 80 % to 89 %, see Table 6.1. The reason for the increased energy efficiency may be the reduced energy requirement of the microorganisms due to stagnation of cell growth, requiring only energy for maintenance metabolism.

Table 6.1: Global reaction stoichiometry according to the measured data and energy efficiency of the process without cell retention ($\overline{CR}$) and with cell retention (CR). The energy efficiency is calculated by the lower heating value (LHV) of products ($\Delta H_{\mathrm{LHV_{AcOH}}} = 869.4\,\mathrm{kJ\,mol^{-1}}$ [190], $\Delta H_{\mathrm{LHV_{EtOH}}} = 1242\,\mathrm{kJ\,mol^{-1}}$ [191]) divided by the lower heating value of reactants ($\Delta H_{\mathrm{LHV_{H_2}}} = 241.84\,\mathrm{kJ\,mol^{-1}}$ [191], $\Delta H_{\mathrm{LHV_{CO}}} = 282.99\,\mathrm{kJ\,mol^{-1}}$ [191]). Idea of LHV-calculation is based on KÖPKE and SIMPSON [192].

Interval	Measured substrate uptake and product formation [mmol h^{-1}]	Energy efficiency [%]
$\overline{\mathrm{CR}}$	$37.2\,\mathrm{H_2} + 28.81\,\mathrm{CO} + 0.38\,\mathrm{CO_2}$	80 %
	$\longrightarrow 9.79\,\mathrm{AcOH} + 4.21\,\mathrm{EtOH}$	
CR	$66.20\,\mathrm{H_2} + 31.10\,\mathrm{CO} + 6.97\,\mathrm{CO_2}$	89 %
	$\longrightarrow 9.18\,\mathrm{AcOH} + 11.30\,\mathrm{EtOH}$	

In operation without cell retention, 80 % of ΔH_{LHV} taken up is captured in the products ethanol and acetic acid. It is now assumed that the remaining 20 %, i. e., the difference between the heating value of the reactant stream ($\sum \Delta H_{\mathrm{LHV_E}} \cdot \dot{n}_{\mathrm{E}}$) and the heating value of the product stream ($\sum \Delta H_{\mathrm{LHV_P}} \cdot \dot{n}_{\mathrm{P}}$), are necessary for the growth ($\beta_{\mathrm{CDW}} \cdot V_{\mathrm{W}} \cdot D \cdot e_{\mathrm{B}}$) and the maintenance metabolism ($\beta_{\mathrm{CDW}} \cdot V_{\mathrm{W}} \cdot p_{\mathrm{M}}$) of the microorganisms. Here, β_{CDW} represents the biomass concentration, V_{W} the working volume, D the dilution rate, e_{B} the specific energy to synthesize biomass and p_{M} represents the specific power for the maintenance metabolism:

$$\sum^{\overline{\mathrm{CR}}} \Delta H_{\mathrm{LHV_E}} \cdot \dot{n}_{\mathrm{E}} - \sum^{\overline{\mathrm{CR}}} \Delta H_{\mathrm{LHV_P}} \cdot \dot{n}_{\mathrm{P}} = \beta_{\mathrm{CDW}} \cdot V_{\mathrm{W}} \cdot D \cdot e_{\mathrm{B}} + \beta_{\mathrm{CDW}} \cdot V_{\mathrm{W}} \cdot p_{\mathrm{M}} \tag{6.3}$$

With the operation of cell retention, the term describing the specific energy to synthesize biomass can be neglected due to growth stagnation, thus Equation 6.3 is simplified:

$$\sum^{\mathrm{CR}} \Delta H_{\mathrm{LHV_E}} \cdot \dot{n}_{\mathrm{E}} - \sum^{\mathrm{CR}} \Delta H_{\mathrm{LHV_P}} \cdot \dot{n}_{\mathrm{P}} = \beta_{\mathrm{CDW}} \cdot V_{\mathrm{W}} \cdot p_{\mathrm{M}} \tag{6.4}$$

Using Equation 6.4, after inserting the values for heating value, biomass concentration and working volume, the necessary energy for maintenance metabolism $p_{\mathrm{M}} = 402.41\,\mathrm{J\,g^{-1}\,h^{-1}}$ is

obtained. In comparison, for another organism, *Rhodospirillum rubrum*, KARMANN ET AL. [193] reported a minimum supply necessary for maintenance metabolism of $0.2\,\mathrm{g_{CO}\,g_{CDW}^{-1}\,h^{-1}}$. Taking into account the lower heating value of CO, this results in a value for p_M of $2021\,\mathrm{J\,g^{-1}\,h^{-1}}$.

After inserting the value of $p_\mathrm{M} = 402.41\,\mathrm{J\,g^{-1}\,h^{-1}}$ together with the other values into Equation 6.3, a value of $e_\mathrm{B} = 29.808\,\mathrm{kJ\,g^{-1}}$ is obtained for the amount of energy required to build up the biomass (for comparison: $\Delta H_{\mathrm{LHV_{Glucose}}} = 14.47\,\mathrm{kJ\,g^{-1}}$). As a comparison, if, on the other hand, the energy required to build up the biomass is estimated assuming an average biomass composition of $\mathrm{CH_{1.81}O_{0.52}N_{0.21}}$ according to VILLADSEN ET AL. [194] and by the use of the method of calculating the lower heating value according to GROTE ET AL. [191], a value of $e_\mathrm{B} = 20.64\,\mathrm{kJ\,g^{-1}}$ is obtained.

At a dilution rate of $D = 0.03\,\mathrm{h^{-1}}$ and with the experimentally determined amount of energy for biomass growth of $e_\mathrm{B} = 29.808\,\mathrm{kJ\,g^{-1}}$, a specific power for biomass synthesis of $p_\mathrm{B} = 894.24\,\mathrm{J\,g^{-1}\,h^{-1}}$ is calculated. Hence, the power to synthesize biomass p_B is twice as high as for maintenance metabolism $p_\mathrm{M} = 402.41\,\mathrm{J\,g^{-1}\,h^{-1}}$. Due to stagnation of cell growth triggered by the use of biomass retention, no buildup of new biomass occurs. As a consequence, energy is directed entirely to the less energy-intensive maintenance metabolism, which leads to the increase in energy efficiency calculated in Table 6.1.

Furthermore, 4.77 mole of electrons per mole of biomass are required for the synthesis of biomass [74]. Therefore, for operation without cell retention in the interval $\overline{CR}$, $6.81 \cdot 10^{-3}$ mole of electrons per liter and hour are required for biomass buildup (at a dilution rate of $D = 0.03\,\mathrm{h^{-1}}$ and with $M_\mathrm{CDW} = 25.1\,\mathrm{g\,mol^{-1}}$ [194]). If cell growth is stagnating, as in the interval CR due to the operation of a cell retention system, the demand for electrons is reduced, resulting in a surplus of electrons. As a result, the electrons can be used elsewhere, e. g. for the reduction of acetic acid to ethanol, see Figure 6.4, with the product ratio shifting towards ethanol. For this reason, in the following section, the influence on the product ratio will be estimated if in the interval $\overline{CR}$, i. e., during operation without biomass retention, the electrons were used entirely for the reduction of acetic acid to ethanol and not for the synthesis of biomass.

Without cell retention, the product ratio of acetic acid to ethanol is 2.33. Eight mole of electrons are required per mole of acetic acid, and 12 mole of electrons are required per mole of ethanol, so by using the space-time yields from Table 5.2 in Section 5.1.1, the amount of electrons required can be calculated: $35.6 \cdot 10^{-3}$ mole of electrons per liter and hour for acetic acid formation and $23 \cdot 10^{-3}$ electrons per liter and hour for ethanol formation. We now assume that the $6.81 \cdot 10^{-3}$

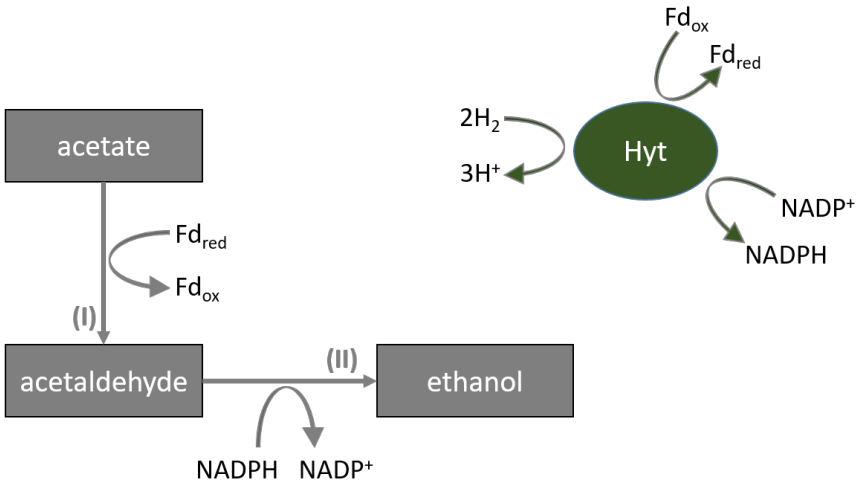

Figure 6.4: Reduction of acetate to ethanol in the WLP. Acetic acid is reduced to acetaldehyde via the AOR (I) and finally to ethanol via the AdhE (II). Four electrons are required for the reduction of acetate to ethanol, which can be provided, for example, via hydrogen uptake and electron-bifurcating hydrogenase (Hyt) with the carriers ferredoxin (Fd) and NADP.

mole of electrons per liter and hour initially required to build the biomass could be used to reduce acetic acid to ethanol. Four mole of electrons are needed to reduce one mole of acetic acid to one mole of ethanol, see Figure 6.4, thus $\frac{6.81 \cdot 10^{-3}}{4} = 1.7$ millimoles of ethanol per liter and hour could be additionally built by reducing acetic acid to ethanol. Theoretically, this would increase the space-time yield for ethanol by $1.7\,\mathrm{mmol\,L^{-1}\,h^{-1}}$ to a total of $3.61\,\mathrm{mmol\,L^{-1}\,h^{-1}}$ and reduce it for acetic acid to $2.75\,\mathrm{mmol\,L^{-1}\,h^{-1}}$. Thus, the product ratio would decrease from initially 2.33 to 0.76, being comparable to the product ratio of 0.81 in the interval CR when operating a biomass retention system. This theoretical calculation demonstrates that the continuous synthesis of biomass during the operation of a CSTR without biomass retention is associated with considerable electron demand. The experimentally measured product shift towards the more reduced product ethanol when using a biomass retention system could be a consequence of the reduced electron demand of non-growing cells. This would be consistent with the results of RICHTER ET AL. [120] that excess reduction potential as a result of reduced cell growth is dissipated by increased ethanol formation via solventogenesis. In addition, studies by LIU ET AL. [97] in the context of a genome-scale model indicate ethanol formation as a consequence of excess reduction potential.

6.2 Influence of a pressure increase at a constant volumetric hydrogen input

6.2.1 Increase in hydrogen uptake at moderate increased H_2 partial pressure

Only a moderate pressure increase to 1 barg with a constant-volume hydrogen supply led to an increased hydrogen uptake rate and increased ethanol formation. A further pressure increase to 2 barg and 3 barg resulted in a significantly reduced hydrogen uptake and reduced ethanol formation compared to atmospheric pressure conditions, see Figure 5.7 and Table 5.8 in Section 5.2.3. It can be ruled out that there was too low a concentration of hydrogen in the reaction medium responsible for this development, since the theoretical equilibrium concentration of hydrogen in the liquid phase increased with pressure increase at constant-volume hydrogen feed. The theoretical equilibrium concentration of hydrogen in the liquid phase $c^*_{\mathrm{l,H_2}}$ is calculated as follows [103]:

$$c^*_{\mathrm{l,H_2}} = y_{\mathrm{H_2}} \cdot p_{\mathrm{R}} \cdot H_{\mathrm{H_2}} \tag{6.5}$$

$y_{\mathrm{H_2}}$ represents the mole fraction of hydrogen in the gas phase in the reactor head, p_{R} the process pressure in the reactor, and $H_{\mathrm{H_2}}$ the Henry's law constant. For $37\,^{\circ}\mathrm{C}$, there is a value for $H_{\mathrm{H_2}}$ of $0.72\,\mathrm{mol\,m^{-3}\,bar^{-1}}$ [103]. Figure 6.5 shows the ratio of the hydrogen uptake rate to the carbon uptake rate and the space-time yield of ethanol as a function of the calculated theoretical equilibrium concentration of hydrogen in the liquid phase.

It can be clearly seen that at an equilibrium concentration of $c^*_{\mathrm{l,H_2}} = 1.2\,\mathrm{mmol\,L^{-1}}$ the ratio of the hydrogen uptake rate to the carbon uptake rate becomes maximum and drops sharply at higher concentrations. The plot of the space-time yield of ethanol shows great agreement with the plot of the ratio of hydrogen uptake rate to carbon uptake rate; similarly, the maximum space-time yield of ethanol is at an equilibrium concentration $c^*_{\mathrm{l,H_2}}$ of $1.2\,\mathrm{mmol\,L^{-1}}$. Figure 6.5 therefore suggests that above a critical equilibrium concentration of hydrogen in the liquid phase of $1.2\,\mathrm{mmol\,L^{-1}}$, an enzymatic reaction is inhibited. This might be the reason for the reduced ethanol formation, as seen in Figure 6.5.

Figure 6.6 shows the influence of the theoretical equilibrium concentrations in the liquid phase $c^*_{\mathrm{l,H_2}}$, $c^*_{\mathrm{l,CO}} = y_{\mathrm{CO}} \cdot p_{\mathrm{R}} \cdot H_{\mathrm{CO}}$, and $c^*_{\mathrm{l,CO_2}} = y_{\mathrm{CO_2}} \cdot p_{\mathrm{R}} \cdot H_{\mathrm{CO_2}}$ for all three substrate gases on the product ratio of acetic acid to ethanol.

Similarly, the product ratio of acetic acid to ethanol is smallest at a theoretical equilibrium concentration of hydrogen in the liquid phase of $1.2\,\mathrm{mmol\,L^{-1}}$, see Figure 6.6. Moreover, it

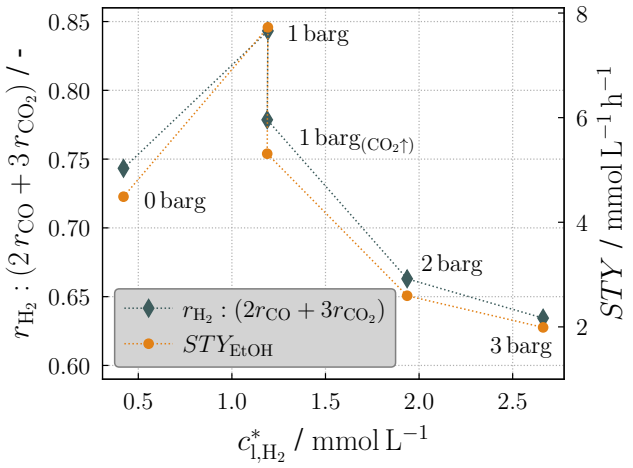

Figure 6.5: Gas uptake ratio of hydrogen to carbon and space-time yield of ethanol as a function of theoretical equilibrium concentration of hydrogen $c^*_{\mathrm{l,H_2}}$ in the fermentation liquid. The gas uptake ratio of hydrogen to carbon takes into account that twice the molar amount of hydrogen is required for the complete conversion of CO to ethanol and three times the molar amount of hydrogen is required for the complete conversion of CO_2 to ethanol. In addition, the process pressures to the corresponding equilibrium concentration are given.

is clear that the concentration of CO_2 in the liquid phase has no significant influence on the product ratio, no dependency between the product ratio and the CO_2 concentration can be seen. In contrast, for the theoretical equilibrium concentration of CO and the product ratio, there is a trend for the product ratio to be low at equilibrium concentrations of $0.052\,\mathrm{mmol\,L^{-1}}$ and smaller, while high product ratios are present at equilibrium concentrations greater than $0.052\,\mathrm{mmol\,L^{-1}}$. A clear relationship between hydrogen uptake, product ratio, and biomass-specific partial pressure of CO in the exhaust gas has already been shown in Section 6.1.2. Therefore, there are two novel findings from Figure 6.5 and Figure 6.6:

1.) Above a theoretical equilibrium concentration of hydrogen in the liquid phase of $c^*_{\mathrm{l,H_2}} = 1.2\,\mathrm{mmol\,L^{-1}}$, hydrogen uptake is inhibited.

2.) The theoretical equilibrium concentration of CO_2 in the liquid phase has been shown to have no effect on the product ratio in the studied range of $c^*_{\mathrm{l,CO_2}} = 0.3 \ldots 1.2\,\mathrm{mmol\,L^{-1}}$.

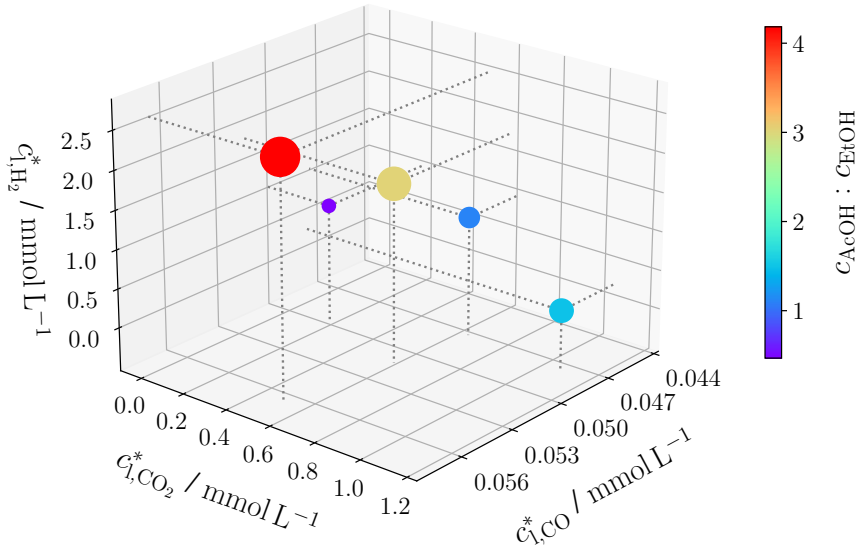

Figure 6.6: Molar product ratio of acetic acid to ethanol as a function of theoretical equilibrium concentration of CO, CO_2 and H_2 in the liquid phase. The size of the circle is proportional to the product ratio, the exact value of the product ratio can be taken from the color bar.

6.2.2 Inhibition of hydrogen uptake at high H_2 partial pressure

To achieve the above equilibrium concentration of hydrogen in the liquid phase of $1.2\,\mathrm{mmol\,L^{-1}}$, an elevated process pressure is necessary. Since at atmospheric pressure conditions and a mole fraction of hydrogen in the gas phase in the reactor head to a maximum value of 1, a theoretical equilibrium concentration according to Equation 6.5 of maximum $0.72\,\mathrm{mmol\,L^{-1}}$ would be possible. However, according to HÄUSLER ET AL. [195] it is unlikely that the process pressure itself has such an influence on the bacteria, it is rather the concentrations of reactants and products in the liquid phase that have a crucial influence on the bacteria. In their studies with a stirred-tank reactor (STR) and *C. ljungdahlii* at $c^*_{l,H_2} = 1.91\,\mathrm{mmol\,L^{-1}}$, OSWALD ET AL. [196] have detected a significant decrease in ethanol and acetic acid and a significant increase in the less reduced product formic acid compared to $c^*_{l,H_2} = 0.48\,\mathrm{mmol\,L^{-1}}$. Results of STOLL ET AL. [176] also show a decrease in ethanol productivity and an increase in acetic and formic acid productivity upon increasing c^*_{l,H_2} from $0.36\,\mathrm{mmol\,L^{-1}}$ to $1.47\,\mathrm{mmol\,L^{-1}}$ with the same organism in a STR. These results confirm the observation of inhibition above $c^*_{l,H_2} = 1.2\,\mathrm{mmol\,L^{-1}}$ in the present study.

Despite the reduced hydrogen uptake at increased theoretical equilibrium concentrations of H_2, the space-time yield of the C_2 products dropped only slightly, from 11.35 $\mathrm{mmol\,L^{-1}\,h^{-1}}$ at 1 barg by 9 % to 10.32 $\mathrm{mmol\,L^{-1}\,h^{-1}}$ at 3 barg, while the hydrogen uptake rate r_{H_2} dropped by 37 %. In contrast to CO inhibition, which significantly reduces C_2 productivity and cell density, see Section 5.2.1 and Section 6.1.2, a high hydrogen concentration in the liquid phase appears to significantly inhibit hydrogen uptake but not the other processes in metabolism. Therefore, at approximately constant C_2 productivity, there is only a shift in the product ratio towards acetic acid.

6.2.3 No inhibitory effect by CO_2

EIGENSTETTER and TAKORS [110] have found in studies with the yeast *Saccharomyces cerevisiae* that high CO_2 concentrations in the liquid phase increase the ATP requirement to maintain cell metabolism in the long term. In terms of syngas fermentation, this would mean that increased energy requirements for metabolism would result in the formation of fewer reduced products such as ethanol, and that the product ratio of acetic acid to ethanol would increase. However, Figure 6.6 does not show that as the theoretical equilibrium concentration of CO_2 in the liquid phase increases in the range of $0.3 \ldots 1.2\,\mathrm{mmol\,L^{-1}}$, the product ratio increases.

6.3 Limit of long-term stable ethanol concentrations

In Figure 5.6 in Section 5.2.3 over the period 750 h - 1300 h, acetic acid productivity initially starts to fall to a minimum of about 3 $\mathrm{mmol\,L^{-1}\,h^{-1}}$ and then rises again to a value of 6 $\mathrm{mmol\,L^{-1}\,h^{-1}}$. Ethanol productivity behaves in the opposite direction, first increasing to a maximum of 10 $\mathrm{mmol\,L^{-1}\,h^{-1}}$ and then decreasing to 5.5 $\mathrm{mmol\,L^{-1}\,h^{-1}}$. The space-time yield of 10 $\mathrm{mmol\,L^{-1}\,h^{-1}}$ for ethanol, corresponding to a product concentration of 15.36 $\mathrm{g\,L^{-1}}$ at a dilution rate of 0.03 $\mathrm{h^{-1}}$, is the highest space-time yield measured to date with the wild type of *C. ljungdahlii*. Measurement data from other research groups for space-time yields of ethanol measured in continuous operation are smaller, e. g. by 20 % (8.03 $\mathrm{mmol\,L^{-1}\,h^{-1}}$ RICHTER ET AL. [18]), by 58 % (4.23 $\mathrm{mmol\,L^{-1}\,h^{-1}}$ STOLL [103]) or even lower (3.65 $\mathrm{mmol\,L^{-1}\,h^{-1}}$ PHILLIPS ET AL. [19], 2.33 $\mathrm{mmol\,L^{-1}\,h^{-1}}$ MOHAMMADI ET AL. [156], 1.96 $\mathrm{mmol\,L^{-1}\,h^{-1}}$ RICHTER ET AL. [120], 1.78 $\mathrm{mmol\,L^{-1}\,h^{-1}}$ KLASK ET AL. [197], 1.52 $\mathrm{mmol\,L^{-1}\,h^{-1}}$ [198] SCHULZ ET AL., 0.64 $\mathrm{mmol\,L^{-1}\,h^{-1}}$ ACHARYA ET AL. [161], 0.2 $\mathrm{mmol\,L^{-1}\,h^{-1}}$ ROY ET AL. [89]). However, it can be seen in Figure 5.6 that this high space-time yield of ethanol is

obviously not stable over time. It is possible that this might be the result of inhibition by the high ethanol concentration due to the chaotropic characteristic of ethanol [185]. This would also explain the decrease in cell density. RAMIÓ-PUJOL ET AL. [187] did not observe any inhibitory effect in their studies with *C. ljungdahlii* at ethanol concentrations lower than $15\,\mathrm{g\,L^{-1}}$. The product concentration of $15.36\,\mathrm{g\,L^{-1}}$ in the present experiment is slightly above the study range of RAMIÓ-PUJOL ET AL. [187], so inhibition at this concentration cannot be ruled out. However, PHILLIPS ET AL. [19] achieved even higher ethanol concentrations of up to $48\,\mathrm{g\,L^{-1}}$ in continuous fermentation experiments with *C. ljungdahlii*, so inhibition by ethanol at concentrations as high as $15.36\,\mathrm{g\,L^{-1}}$ is unlikely.

Another possible cause for the drop in ethanol productivity starting at time 1060 h could be an imbalance in cell metabolism and a decrease in AcetylCoA pool, a finding made by VALGEPEA ET AL. [185]. Due to high ethanol productivity and the associated need for reduction potential, there would be a decrease in AcetylCoA pool and cell density due to a lagging WLP. This would explain the decrease in ethanol productivity and increase in acetic acid formation, as the reduced need for reduction potential to synthesize acetic acid compared to ethanol would restore the balance in cell metabolism.

6.4 Influence of a gradually reduced pH value

When the pH was reduced starting from 5.9 to 5.7, 5.5, 5.3, and 5.1, a lower acetic acid to ethanol ratio of 0.62 was observed only at pH 5.7 compared to 0.8 at pH 5.9, see Figure 5.8 in Section 5.2.4. At lower pH values, the ratio even increases and reaches a value of 4 in the non-steady state region of pH 5.1, see Figure 5.9 in Section 5.2.4.

In contrast, MOHAMMADI ET AL. [156] observed in their studies with *C. ljungdahlii* in a CSTR without cell retention an increase in ethanol concentration and a decrease in acetic acid concentration upon reduction of a non-regulated pH. This resulted in a reduction in the acetic acid to ethanol product ratio from initially 1.38 to 0.31. However, their measured space-time yields for ethanol and acetic acid of $1.79\,\mathrm{mmol\,L^{-1}\,h^{-1}}$ and $0.55\,\mathrm{mmol\,L^{-1}\,h^{-1}}$, respectively, are significantly lower than the space-time yields obtained in the present investigation of pH reduction. ABUBACKAR ET AL. [199] have been able to significantly reduce the acetic acid to ethanol product ratio with a similar organism, *C. autoethanogenum*, in STR by lowering the pH from 6 to 4.75, since at pH 4.75 the acetic acid concentration dropped from previously $900\,\mathrm{mg\,L^{-1}}$ to below $50\,\mathrm{mg\,L^{-1}}$ with an almost constant ethanol concentration. Also, in another study of cyclic lowering and raising of pH, ABUBACKAR ET AL. [200] found a significant

reduction in the product ratio of acetic acid to ethanol at lower pH values. However, in both studies, cell densities with concentrations of $0.3\,\mathrm{g\,L^{-1}}$ at maximum were significantly lower than in the present study with total cell retention and cell densities of up to $10\,\mathrm{g\,L^{-1}}$. On the other hand, INFANTES ET AL. [106] observed in their studies with *C. ljungdahlii* in a STR a nearly constant acetic acid to ethanol product ratio of 11.69 compared to 11.49 when the pH was reduced from 5.9 to 5.4. In a study using non-growing cells of *C. ljungdahlii*, COTTER ET AL. [201] found that lowering pH did not increase ethanol productivity and attributed this to reduced proton pump activity in non-growing cells [202].

The results of the above analyses show that a reduction in pH does not necessarily lead to a lower product ratio of acetic acid to ethanol. In the present study with total cell retention and constant cell density under steady-state conditions, it is likely that the growth of cells is very low and just enough to compensate for the isolated death of cells. It is therefore possible that the activity of the proton pumps of these cells is, in analogy to the non-growing cells at COTTER ET AL. [201], greatly reduced and therefore, despite reduction of pH to values below 5.7, there is no further decrease in the product ratio. At pH values of 5.3 and 5.1, gas uptake and ethanol productivity decrease steadily, and no steady-state is established. Cell density, on the other hand, remains constant, this could be an indication that although the cells do not die, viability decreases. This is supported by studies by COTTER ET AL. [201], showing that at a pH of 5.5, viability is only 44 %, and at a pH of 4.5, viability is only 11 %.

The re-raising of pH to the initial value of 5.9 after a gradually pH reduction, see Figure 5.8 and Table 5.10 in Section 5.2.4, and the renewed increase in ethanol productivity and C_2 productivity overall indicate that the cells have recovered from the unfavorable growth conditions at low pH values. However, the increase in cell density to $9.98\,\mathrm{g\,L^{-1}}$ and the decrease in biomass-specific productivity indicate that a certain amount of cells continue to have low or no viability, but these cells have nevertheless not died. However, it would also be possible, analogous to the studies of KWON ET AL. [203], that the cells have metabolically changed during the 1600 process hours due to lowering pH and due to increased acetic acid concentrations up to $16\,\mathrm{g\,L^{-1}}$. Increased cell density, higher space-time yield of ethanol, and at the same time lower biomass-specific productivity were reported by KWON ET AL. [203] and also found to be true for the measured results in the present study. Thus, the increased space-time yield of ethanol with $8.71\,\mathrm{mmol\,L^{-1}\,h^{-1}}$ after raising the pH to 5.9 compared to $6.99\,\mathrm{mmol\,L^{-1}\,h^{-1}}$ at the beginning of the experimental series *ZpH-I* at pH 5.9 could be attributed to mutational processes. However, the number of cell generations over a 1600 h run time is low when total cell retention is used: assuming that cells do not die and therefore do not have to be regenerated and assuming a dilution rate of $0.00244\,\mathrm{h^{-1}}$ due to daily sampling, the doubling time is 415.99 h

and the number of cell generations over a 1600 h run time is thus at least 4, see also HANISCH [204]. In fact, due to dying cells, among others, this number will be higher, but at most 49. This would correspond to operation without cell retention and assuming a growth rate of $\mu = D = 0.03\,\mathrm{h}^{-1}$. The focus of the present study is to obtain kinetic data and to determine the fundamentals of reaction engineering. However, further studies, in particular mutational genes analysis, are needed to determine to what extent the increased space-time yield of ethanol can really be attributed to mutational processes.

7 Conclusion

Synthesis gas fermentation and the associated mechanism of the Wood-Ljungdahl pathway, a C-C coupling, enable the conversion of CO, CO_2 and H_2 into C_2 compounds such as acetic acid and ethanol by acetogenic bacteria. As part of the present study, a comparison was made between synthesis gas fermentation and chemical catalysis, specifically heterogeneous methanol synthesis: In contrast to heterogeneous methanol synthesis, synthesis gas fermentation can be operated at mild conditions with pressures lower than 10 bar and temperatures lower than 65 °C. An almost complete gas conversion is possible under these conditions, eliminating the need for a cost-intensive high-pressure separation of the gas from the liquid in a gas recycling loop. In addition, sulphur is a nutrient medium component for the biocatalyst and does not lead to deactivation of the catalyst, so that gas purification with regard to sulphur can be omitted. With regard to gas composition and the ratio of COx to H_2, the biocatalyst is much more flexible and can regenerate itself even after unfavorable conditions. The catalyst mass-based productivities are in the same order of magnitude for both chemical and biological catalysis. However, the space-time yield for chemical catalysis is two to three orders of magnitude higher than that for biological catalysis. Low cell densities as well as low gas-liquid mass transfer rates are mentioned as important bottlenecks for syngas fermentation resulting in low volumetric productivities.

The aim of the present study was therefore to improve volumetric productivity and to determine the influence of key parameters such as dilution rate, substrate gas flow, H_2 partial pressure and pH on fermentation in continuous operating mode, thus leading to the answers of the following five research questions:

1.) When using a biomass retention system to increase the cell density, does cell retention affect the product ratio?

2.) Is the space-time yield proportional to the cell density?

3.) Does total cell retention lead to an accumulation of carbon in the reactor?

4.) When using a biomass retention system, is it possible to increase the hydrogen uptake rate by increasing the process pressure at a constant volumetric hydrogen input, thus

further increasing ethanol formation? The constant-volume hydrogen feed implies an increase in the hydrogen partial pressure in order to improve the gas-liquid mass transfer of H_2.

5.) With the use of a biomass retention system and already high space-time yields of ethanol, can the product ratio be shifted even further in the direction of ethanol by lowering the pH?

For this purpose, a test rig for continuous fermentation was operated as part of long-term experiments. A foam separator system was developed to prevent excessive foam formation, so that the addition of antifoam agents to the reactor could be completely dispensed with, even in long-term experimental runs of over 3000 hours.

The first step was to investigate the influence of an external circuit for the retention of biomass by switching the external circuit for biomass retention on or off as desired during experimental operation. By using biomass retention with wild-type strain *Clostridium ljungdahlii* (DSM 13528), biomass increases significantly leading to an overall increase of the C_2 product titer to $24.83\,\mathrm{g\,L^{-1}}$ and to an increase of the C_2 space-time yield to $0.75\,\mathrm{g\,L^{-1}\,h^{-1}}$. Furthermore, space-time yield of ethanol with a value of $8.71\,\mathrm{mmol\,L^{-1}\,h^{-1}}$ becomes greater than the space-time yield of acetic acid ($5.74\,\mathrm{mmol\,L^{-1}\,h^{-1}}$), leading to a shift in the product ratio towards ethanol (***answer to research question no. 1***). However, biomass-specific productivity decreases at high cell densities. As a result, there is no linear relationship between biomass concentration and space-time yield (***answer to research question no. 2***). Even an increase in gas volume flow or nutrient media supply does not contribute to a re-increase of the reduced biomass-specific productivities. An accumulation of carbon in the fermentation broth, which could influence the microorganisms, has not been detected when using total cell retention without a bleed flow (***answer to research question no. 3***). Furthermore, it was shown that the continuous growth of the biocatalyst is associated with a high demand for electrons. The product shift towards ethanol at high cell densities through the usage of a biomass retention system might be the result of an excess of reduction potential as a consequence of reduced or stagnated cell growth.

In addition, a correlation was found between the biomass-specific partial pressure of CO in the off-gas and hydrogen uptake and product ratio. This finding shows that an increase in gas flow, especially of CO, does not necessarily lead to increased electron uptake and thus ethanol formation, but on the contrary, in case of an increasing biomass-specific partial pressure of CO in the off-gas, can reduce hydrogen uptake and thus decrease the product ratio of ethanol to acetic acid.

In addition, an increase in the hydrogen partial pressure to 1.52 bar enhances hydrogen uptake and space-time yield of ethanol, and the product ratio can thus be shifted in the direction of ethanol (***answer to research question no. 4***). However, the measured data clearly show that above a partial pressure of hydrogen of 1.52 bar, corresponding to a theoretical equilibrium concentration of $c^*_{\mathrm{l,H_2}} = 1.2\,\mathrm{mmol\,L^{-1}}$, hydrogen uptake decreases significantly. Furthermore, a moderate reduction of the pH from 5.9 to 5.7 leads to increased hydrogen uptake and a shift of the product ratio towards ethanol (***answer to research question no. 5***). A further decrease in pH reduces hydrogen uptake and ethanol productivity.

The results of the present study have therefore not only contributed to a substantial increase in volumetric productivity through the detailed research of a biomass retention system, but also to a much better understanding of the influence of process parameters such as gas flow, dilution rate, H_2 partial pressure and pH on the fermentation process with *C. ljungdahlii*. Key influencing variables on productivity and product ratio such as biomass-specific partial pressure of CO in the off-gas or theoretical equilibrium concentration of H_2 in the fermentation broth have been identified and correlations have been developed. By taking measurements in steady state of continuous operation, a valuable database for future kinetic modeling has been built up.

These data and the correlations found could be transferred to a model as part of future work, initially for steady-state operating conditions and then also for dynamic operating conditions. For dynamic modelling, in addition to online optimization with the help of control engineering approaches, a state estimation for the next steady-state operating condition would also be helpful in order to shorten the time-consuming procedure until a steady-state operating condition is reached. The implementation of such a model would enable further optimization and increased efficiency of the fermentation process. Finally, in a further step, an additional conversion stage could be coupled with the previous one so that the products ethanol and acetic acid can be converted into high added-value products such as single-cell oil and single-cell protein with the help of other microorganisms such as yeasts. These products would not only be of high value, but could also be separated from the fermentation broth much more easily and therefore more economically than the products ethanol and acetic acid from the first stage. This would cover the entire value chain, from the conversion of gases, e. g. from waste gases, to the formation of proteins and lipids, e. g. for the food industry.

A Appendix

A.1 Detailed process flow diagram

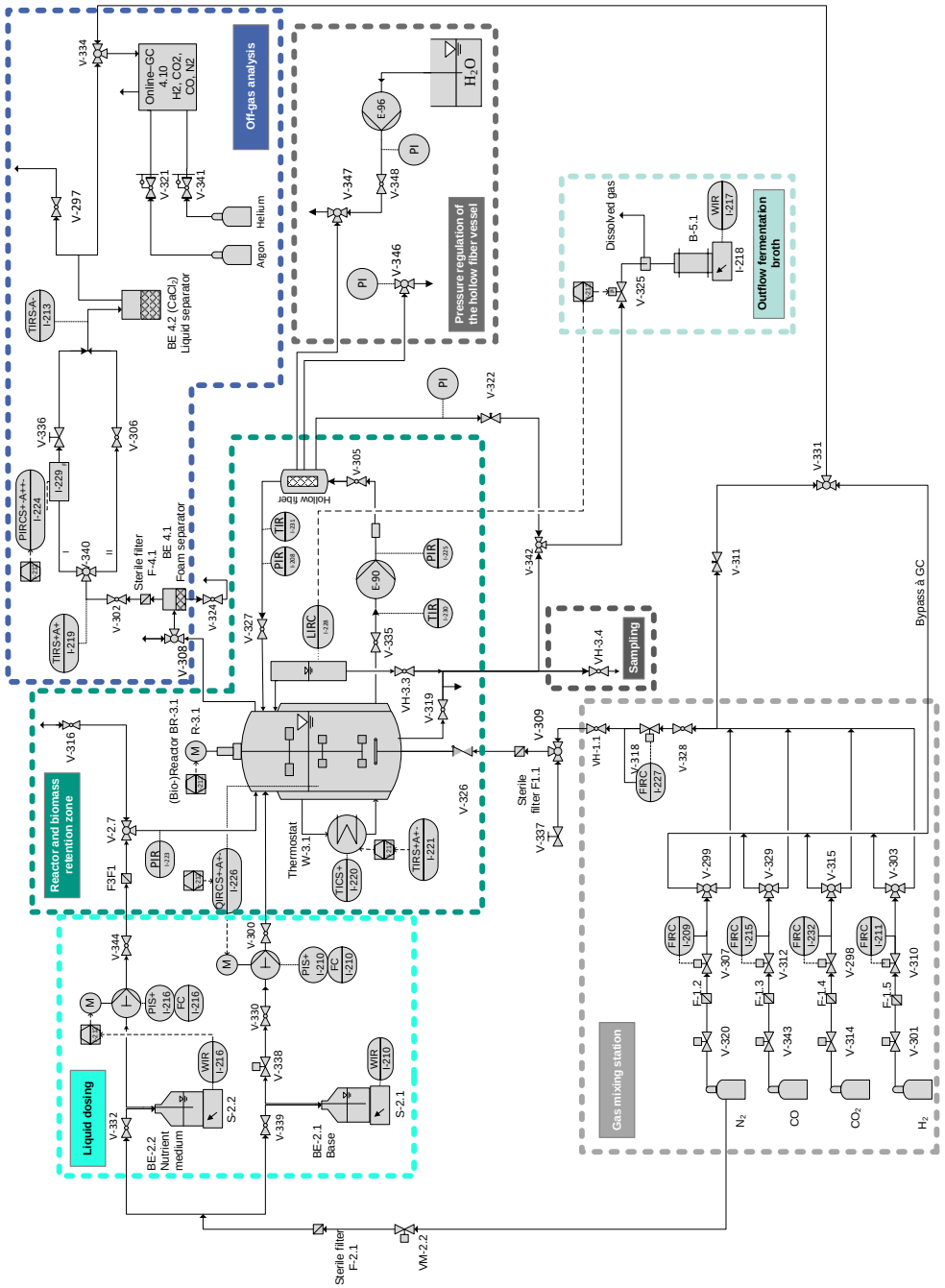

Figure A.1: Detailed process flow diagram of the experimental test rig for continuous fermentation of synthesis gas.

A.2 Development of a foam separation system

The use of a total cell retention system significantly increases the cell density in the reactor. This can lead to increased foam formation. This foam can rise both into the level probe and into the exhaust gas pipe. On the one hand, this influences the measurement of the level probe, as the rise of foam can be mistaken as an increase of the level. On the other hand, the foam can rise into the exhaust gas pipe and irreversibly block the sterile filter placed there. This leads to an increase in pressure and thus to a system failure.

To prevent foam formation, liquid antifoam agents could be added into the reactor. However, as already explained in Section 4.2.1, the addition of antifoam agents is avoided in order to not influence the gas-liquid mass transfer. An alternative system was therefore developed to prevent foam formation.

(a) Glass vessel for separation before the experimental run.

(b) Glass vessel for separation filled with foam during the experimental run.

(c) Anti-foam agent and collapsed foam at the bottom of the glass vessel.

Figure A.2: Glass vessel for separating foam from the off-gas for operation at atmospheric pressure conditions. The exhaust gas from the reactor is directed deep into the glass vessel through a hose and leaves the vessel for off-gas analysis via a further opening in the cap.

The first step was to implement a glass bottle with two connections on the cap to separate foam from the exhaust gas, see Figure A.2a. The exhaust gas from the reactor is led to the bottom of the bottle via a hose, while the gas for off-gas analysis can leave via a second opening on the cap. Rising foam from the reactor would thus remain at the bottom of the bottle and no longer block the pipe for off-gas analysis. A functional test of this glass separator was successful, rising foam could be retained in the glass bottle, see Figure A.2b. However, long-term experiments have shown that under unfavorable cultivation conditions for the biocatalyst, the foam separator can be completely filled after a short time, as the foam does not collapse immediately and therefore occupies a large volume. For this reason, antifoam agent is added to the glass separator before

the start of the experimental run so that the bottom is covered. This causes the foam hitting the bottom to collapse immediately, so that the volume of the glass bottle is sufficient. The liquefied foam accumulates at the bottom of the vessel, while the antifoam agent, a synthetic oil (A 4050 HAC, Zschimmer & Schwarz, Germany), remains on top and thus continues to collapse the incoming foam, see Figure A.2c.

In a next step, a lab-scale experiment was carried out to investigate whether the installation of an impeller on the agitator shaft above the liquid level is appropriate for the reduction of foam, see Figure A.3. For this purpose, a glass vessel (5 liters) resembling the reactor was used, baffles were placed and the agitator shaft was equipped with agitator blades. The agitator shaft was then rotated at 600 - 1000 rpm, initially without an impeller and then with an impeller, while detergent was added to the vessel to simulate foam formation. The result of the investigation clearly showed that placing an impeller above the liquid level significantly reduced the rise of foam. An increase in foam above the impeller cannot be seen, see Figure A.3b. The optimal axial position of the impeller on the agitator shaft was determined iteratively, it is 153 mm measured from the lower end of the agitator shaft.

(a) Foam formation without an impeller. **(b)** Foam formation with an impeller.

Figure A.3: Lab-scale experiment to investigate the influence of an impeller placed above the liquid phase on the agitator shaft on foam formation. Rinsing agent is used to simulate foam formation.

In a final step, the results of the developments on the glass separator and impeller were transferred into a pressure-stable, three-part system for preventing and separating foam. The technical details of this system are described in Section 4.2.2. This system has proven to be very successful under experimental conditions. Problems with rising foam in the level probe or exhaust gas pipe did not occur even during long-term experimental runs of over 3000 hours.

A.3 Calculation of the reactor wall thickness depending temperature and pressure

The calculation of the necessary reactor wall thickness is carried out according to the AD 2000 standard and DIN EN 10028, resulting in the following formula for the cylindrical wall thickness:

$$s = \frac{D_\mathrm{o} \cdot p}{20\frac{K}{S_\mathrm{f}} \cdot v + p} + c_1 + c_2 \tag{A.1}$$

The outer diameter D_o is specified as one meter, the pressure p results from the operating conditions, see Figure 3.1. Strength parameter K, safety factor S_f, weld factor v and allowances c_1 and c_2 are taken from AD 2000 and DIN EN 10028, see Table A.1.

Table A.1: Calculation of the reactor wall thickness s_R and the resulting stainless steel raw material costs.

	Fermentation	MeOH synthesis
Applied pressure / bar	10	80
Applied temperature / °C	45	250
D_o / m	1	1
V_R / m^3	1	1
K / $10^6\,\mathrm{N\,m^{-2}}$	230	293
S_f / -	1.5	1.5
v / -	1	1
$c_1 + c_2$ / mm	1	1
Material	1.4301	1.7362
Raw material costs / € kg^{-1}	3.219 [205]	3.219 [205]
Density stainless steel / $\mathrm{kg\,m^{-3}}$	7900 [206]	7900 [206]
Calculated s_R / mm	1.33	3.04
Calculated m_R / kg	58.5	134.8
Calculated raw material cost for reactor wall / € $\mathrm{m_R^{-3}}$	188	434

The assumption that the bottom and the top of the reactor are flat and have the same wall thickness as the cylindrical wall is made. For Equation A.1, this results in a minimum wall thickness of 1.33 mm for the fermentation reactor and 3.04 mm for the methanol reactor. This

allows the calculation of the material volume and finally the raw material price for the reactor with an internal volume of one cubic meter (see also Table A.1): $188\,€/\mathrm{m}^3_\mathrm{R}$ and $434\,€/\mathrm{m}^3_\mathrm{R}$ for fermentation and MeOH synthesis, respectively.

A.4 Measurement data of the long-term experiments

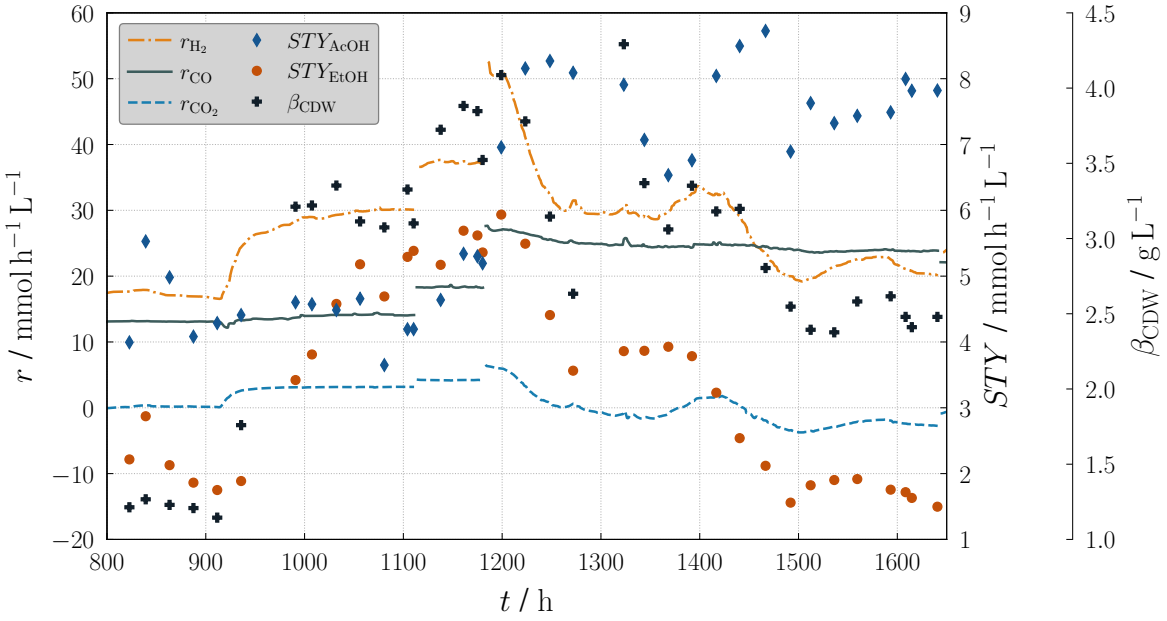

Figure A.4: Measurement data on gas uptake rate r, space-time yield STY and cell density β_{CDW} plotted over the time t of measurement campaign *HSF-Z-IV* to investigate the influence of cell retention and increased substrate gas flow at high cell density. Cell retention was activated at 913 h, substrate gas flow was increased at 1111 h and 1181 h. During the periods 860 - 912 h, 1056 - 1111 h, 1150 - 1180.5 h and 1512 - 1641 h, steady-state conditions were established for $\overline{CR}$, CR, $CR_{\dot{V}_{G\uparrow}}$ and $CR_{\dot{V}_{G\uparrow\uparrow}}$. $\overline{CR}$: the fermentation process is operated without a cell retention (CR) system. CR: fermentation process operated with a cell retention system. $CR_{\dot{V}_{G\uparrow}}$: increase of substrate gas flow while cell retention is still activated. $CR_{\dot{V}_{G\uparrow\uparrow}}$: second increase of substrate gas flow while cell retention is still activated. Further process parameters can be taken from Table 5.1 and Table 5.3. The measured data averaged over these intervals are shown in Figure 5.1, Figure 5.4, Table 5.2 and Table 5.4.

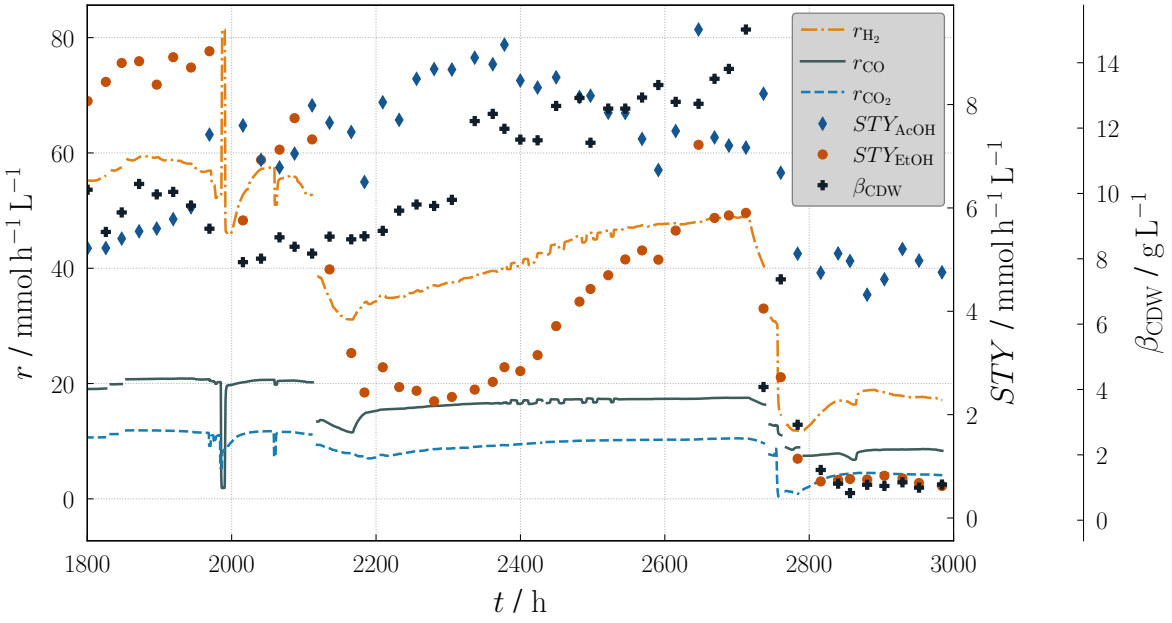

Figure A.5: Measurement data on gas uptake rate r, space-time yield STY and cell density β_{CDW} plotted over the time t of measurement campaign *ZpH-I* to investigate the influence of dilution rate and cell retention deactivation. Dilution rate is increased at 1949 h and 2617 h, cell retention is deactivated at 2714 h. During the periods 1862 - 1947 h, 2541 - 2616 h, 2660 - 2713 h and 2920 - 2984 h, steady-state conditions were established for $CR_{D=0.03}$, $CR_{D=0.04}$, $CR_{D=0.05}$ and $\overline{\widetilde{CR}}$. Further process parameters can be taken from Table 5.1 and Table 5.5. The measured data averaged over these intervals are shown in Figure 5.1, Figure 5.5, Table 5.2 and Table 5.6.

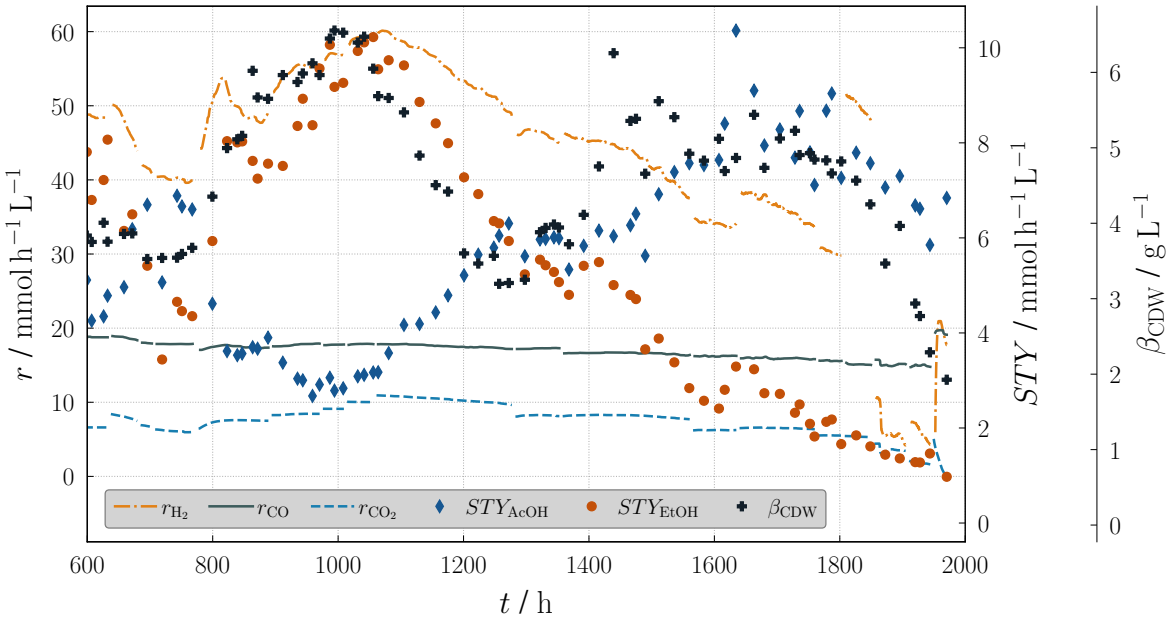

Figure A.6: Measurement data on gas uptake rate r, space-time yield STY and cell density β_{CDW} plotted over the time t of measurement campaign *ZP-II* to investigate the influence of pressure increase at a constant volumetric hydrogen input and activated cell retention. The pressure was increased from 0 barg to 1 barg, 2 barg, 3 barg, and 4 barg at hour 743, 1353, 1636, and 1803, respectively. At hour 889, the amount of supplied CO_2 in the substrate gas was increased. During the periods 729 - 767.6 h, 836 - 878 h, 1293 - 1352.6 h, 1575 - 1630 h and 1765 - 1802.5 h, steady-state conditions were established for $0\,barg$, $1\,barg$, $1\,barg_{(CO_2\uparrow)}$, $2\,barg$, and $3\,barg$. Further process parameters can be taken from Table 5.7. The measured data averaged over these intervals are shown in Figure 5.7 and Table 5.8.

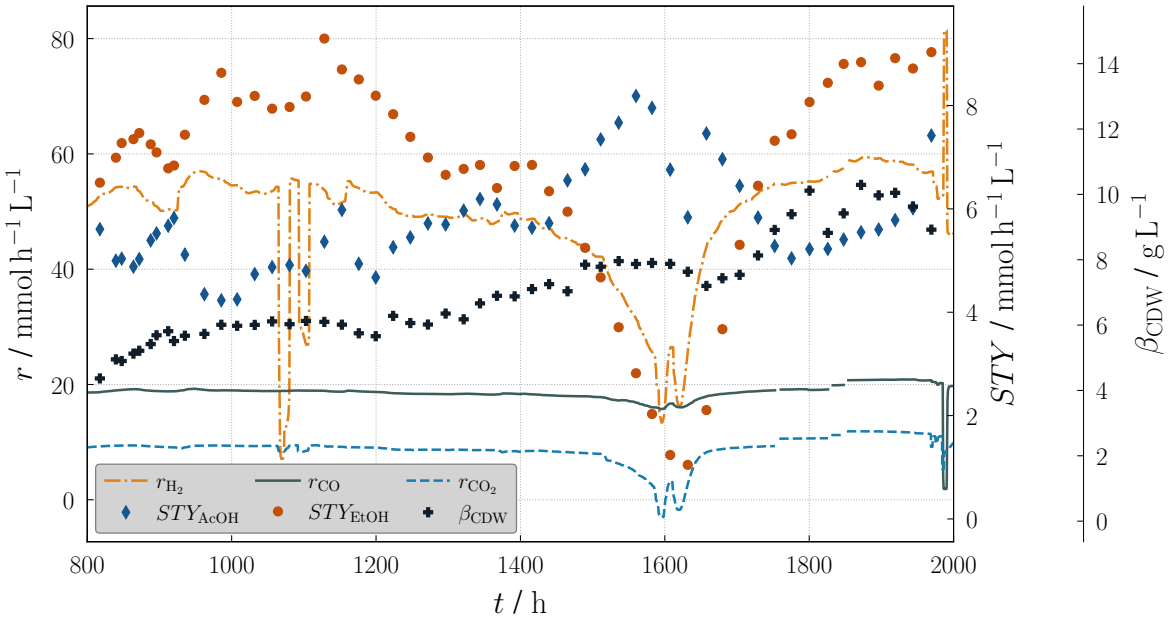

Figure A.7: Measurement data on gas uptake rate r, space-time yield STY and cell density β_{CDW} plotted over the time t of measurement campaign *ZpH-I* to investigate the influence of reduced pH at high cell densities with activated cell retention. The pH was reduced from 5.9 to 5.7, 5.5, 5.3, and 5.1 at hour 921, 1154, 1368, and 1514, respectively, and then increased again to 5.9 at hour 1584. During the periods 882 - 920.3 h, 1051 - 1153 h, 1289 - 1367.5 h and 1856 - 1947 h, steady-state conditions were established for $pH\,5.9$, $pH\,5.7$, $pH\,5.5$ and $pH\,\widetilde{5.9}$. The fluctuations in the measured hydrogen uptake rate between hour 1050 and 1104 are due to problems with the micro gas chromatograph pump, which were successfully resolved by replacing the pump. Further process parameters can be taken from Table 5.9. The measured data averaged over these intervals are shown in Figure 5.8 and Table 5.10.

A.5 Measurement data of potential carbon accumulation

Table A.2: Data of measurement campaign *ZP-II* for the investigation of potential carbon accumulation in the fermentation broth over a test period of 2000 hours. The carbon content C_{CDW}, C_{AcOH}, and C_{EtOH} used in equation 5.1 can be calculated from the mass concentrations β_{CDW}, β_{AcOH} and β_{EtOH}. According to INFANTES-LÓPEZ [181], a value of 0.44 was assumed for the carbon mass fraction of the biomass.

Sample	Process time [h]	$C_{\mathrm{total,measured}}$ [mg L^{-1}]	β_{CDW} [g L^{-1}]	β_{AcOH} [mg L^{-1}]	β_{EtOH} [mg L^{-1}]	C_{NM} [mg L^{-1}]
1	0.1	7760	0.10	273	180	7713
2	72.4	12456	2.57	5018	6052	7713
3	122.1	14706	2.79	5740	8157	7290
4	154.4	15239	2.64	9232	9084	7290
5	199.7	15204	3.30	5825	10570	8573
6	239.1	16190	4.15	6543	11159	8573
7	359.9	16661	4.48	8279	12731	7999
8	384.5	17304	4.40	9033	13150	7999
9	503.2	17004	3.45	12440	8213	6711
10	599.2	17091	3.84	10227	11972	5611
11	719.4	17129	3.54	10127	5276	7580
12	799.5	17250	4.35	9230	9099	7364
13	839.3	17879	5.11	7064	12280	7364
14	943.7	18795	5.99	6007	13689	8064
15	1008.1	19225	6.53	5671	14203	8064
16	1223.5	19245	3.47	11294	10614	7876
17	1352.2	18137	3.94	11988	7774	8163
18	1391.6	18314	4.11	11665	8299	8211
19	1489.7	18052	4.66	11247	5605	8207
20	1634.5	16518	4.87	20726	5048	7760
21	1759.7	17466	4.84	14225	2792	8616
22	1943.7	14378	2.29	11702	2243	8833
23	1970.5	14676	1.93	13681	1492	8833

A.6 History of evolution of the test rig for the fermentation of synthesis gas

To expand functionality and improve process stability, the test rig was modified and expanded as part of three major revisions. The achievable experimental run times were successfully increased after each modification, from the original 970 hours (Figure A.8), to 1683 hours (Figure A.9), 1970 hours (Figure A.10) and finally to 3097 hours (Figure A.11) of continuous fermentation of synthesis gas at high cell densities. The following list is a selection of modifications and hardware upgrades:

- Implementation of long-term stable ceramic ball bearings on the agitator shaft coupling
- Implementation of a pressure-stable foam separator system
- Pressure-stable construction of the biomass retention system
- Capacity expansion of the nutrient medium feed system (up to 15 liters)
- Upgrade to a two-module syringe pump for the feed system
- Upgrade to a new micro gas chromatograph
- Integration of an inline NIR-absorbance sensor for biomass measurement monitoring
- Replacement of the peristaltic pump in the external circuit for biomass retention with a micro annular gear pump
- Installation of an uninterruptible power supply
- Development and implementation of an automated analysis tool with Python
- Expansion of measurement equipment for recording pressure, temperature and mass flow
- Mechanical modifications to feed pipes, exhaust pipes and fittings to improve user-friendliness and to reduce maintenance time

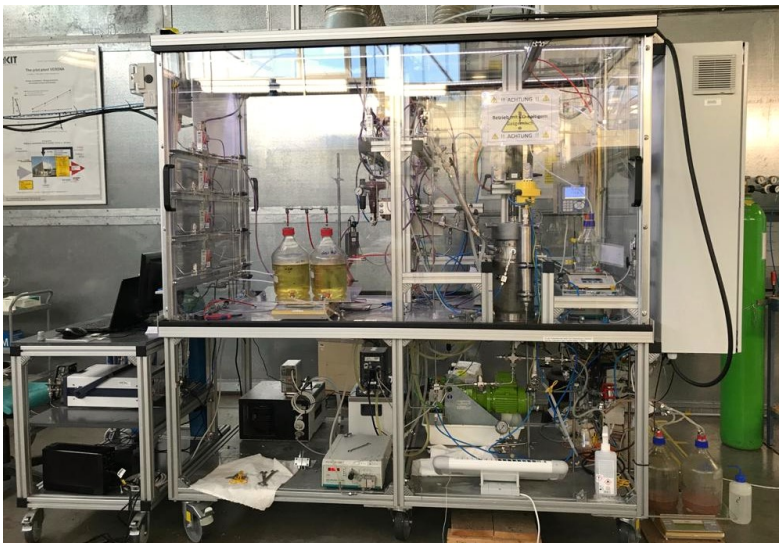

Figure A.8: Experimental setup for continuous fermentation of synthesis gas with an external circuit for the retention of biomass. Released in November 2020. Longest time of operation achieved: 970 hours (*HSF-Z-II*).

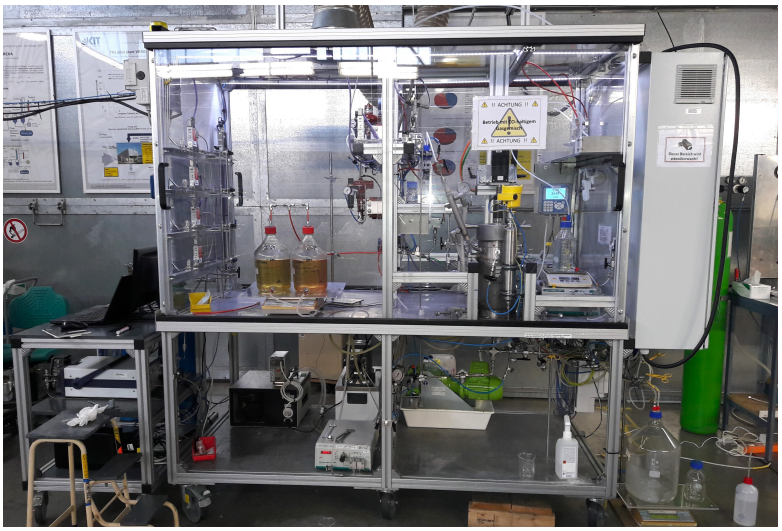

Figure A.9: Upgraded experimental setup for continuous fermentation of synthesis gas with an external circuit for the retention of biomass. Released in March 2021. Longest time of operation achieved: 1683 hours (*HSF-Z-IV*).

Figure A.10: Further developed experimental setup for continuous fermentation of synthesis gas with an external circuit for the retention of biomass and the possibility of operation at increased process pressures. Released in November 2021. Longest time of operation achieved: 1970 hours (*ZP-II*). Photography: T. Zevaco, 2021.

Figure A.11: Final experimental setup for continuous fermentation of synthesis gas with an external circuit for the retention of biomass and the possibility of operation at increased process pressures. Released in June 2022. Longest time of operation achieved: 3097 hours (*ZpH-I*).

A.7 Maximum hours of operation of the agitator coupling with friction bearings

(a) Friction bearing running dry

(b) Particle attrition at the head of the coupling system

(c) Particle attrition on the spring groove

Figure A.12: Mechanical breakdown of the agitator coupling system with friction bearing after 167 hours of operation.

Figure A.13: Breakage of the agitator shaft at the interface to the coupling system after 392 hours of operation.

A.8 List of chemicals

Table A.3: Detailed description of all substances used for the operation of the synthesis gas fermentation process (Part I).

Name	CAS No.	Distributor
Agar	9002-18-0	Carl Roth, DE
4-Aminobenzoic acid	150-13-0	Alfa Aesar, USA
Ammonium chloride	12125-02-9	Carl Roth, DE
Antifoam A 4050 HAC	-	Zschimmer & Schwarz, DE
Biotin (Vitamin B7)	58-85-5	AppliChem, DE
Calcium chloride dihydrate	10035-04-8	Carl Roth, DE
Cobalt(II) chloride hexahydrate	7791-13-1	Acros Organics, USA
Copper(II) chloride dihydrate	10125-13-0	VWR Chemicals, DE
Cyanocobalamin (Vitamin B12)	68-19-9	Carl Roth, DE
D-(-)-Fructose	57-48-7	Merck, DE
D-Pantothenic Acid Calcium Salt (Vitamin B5)	137-08-6	Acros Organics, USA
Folic acid (Vitamin B9)	59-30-3	Merck, DE
Glycerol bidistilled 99.5 %	56-81-5	VWR Chemicals, DE
Iron(II) sulfate heptahydrate	7782-63-0	VWR Chemicals, DE
L-Cysteine hydrochloride monohydrate	7048-04-6	Carl Roth, DE
Lipoic acid	1077-28-7	Merck, DE
Magnesium sulfate heptahydrate	10034-99-8	Carl Roth, DE
Manganese(II) sulfate monohydrate	10034-96-5	Merck, DE
MES	4432-31-9	Carl Roth, DE
Nickel(II) chloride hexahydrate	7791-20-0	VWR Chemicals, DE
Nicotinic acid (Vitamin B3)	59-67-6	Merck, DE
Nitrilotriacetic acid	139-13-9	Merck, DE
Peracetic Acid 15 % pure	79-21-0	AppliChem, DE

Table A.3: Detailed description of all substances used for the operation of the synthesis gas fermentation process (Part II).

Name	CAS No.	Distributor
Potassium chloride	7447-40-7	Merck, DE
Potassium dihydrogen phosphate	7778-77-0	Carl Roth, DE
Potassium hydroxide	1310-58-3	Merck, DE
Pyridoxine hydrochloride (Vitamin B6)	58-56-0	AppliChem, DE
Resazurin sodium salt	62758-13-8	Alfa Aesar, USA
Riboflavin (Vitamin B2)	83-88-5	VWR Chemicals, DE
Sodium chloride	7647-14-5	Merck, DE
Sodium molybdate dihydrate	10102-40-6	Merck, DE
Sodium selenite pentahydrate	26970-82-1	Honeywell, USA
Sodium tungstate dihydrate	10213-10-2	VWR Chemicals, DE
Thiamine hydrochloride (Vitamin B1)	67-03-8	Carl Roth, DE
Tryptone	91079-40-2	Carl Roth, DE
Yeast Extract	8013-01-2	Carl Roth, DE
Zinc sulfate heptahydrate	7446-20-0	Bernd Kraft, DE

List of Tables

2.1 Acetogenic microorganisms: a selection of key organisms of different genus. 5

3.1 Characteristics of pure chemical catalysts versus biochemical catalysts for the production of synthetic carbon-neutral and oxygenated hydrocarbons. 12
3.2 Most common syngas impurities and their influence on process performance in comparison for fermentation and heterogeneous MeOH synthesis. 14

4.1 Composition of the culture medium for pre-cultivation and process. 24
4.2 Composition of the vitamin solution. 25
4.3 Composition of the trace element solution. 25
4.4 Typical operating range for the process parameters at the test rig. 30
4.5 List of all measurement campaigns in continuous operation. 33

5.1 Experimental parameters to investigate the influence of biomass retention. . . 36
5.2 Measurement data averaged in steady-state areas to investigate the influence of biomass retention. 39
5.3 Experimental parameters to investigate the influence of an increased substrate gas volume flow with activated biomass retention. 42
5.4 Measurement data averaged in steady-state areas to investigate the influence of an increased substrate gas volume flow with activated biomass retention. . . . 44
5.5 Experimental parameters to investigate the influence of an increased dilution rate with activated biomass retention. 46
5.6 Measurement data averaged in steady-state areas to investigate the influence of an increased dilution rate with activated biomass retention. 48
5.7 Experimental parameters to investigate the influence of an increased process pressure at a volume-constant hydrogen input with activated biomass retention. 49
5.8 Measurement data averaged in steady-state areas to investigate the influence of an increased process pressure at a constant volumetric hydrogen input with activated biomass retention. 54

5.9 Experimental parameters to investigate the influence of a gradually reduced pH value with activated biomass retention. 55
5.10 Measurement data averaged in steady-state areas to investigate the influence of a gradually reduced pH value with activated biomass retention. 57

6.1 Global reaction stoichiometry according to the measured data and energy efficiency of the process without cell retention and with cell retention. 67

A.1 Calculation of the reactor wall thickness and the resulting stainless steel raw material costs. 84
A.2 Measurement data for the investigation of potential carbon accumulation. . . 90
A.3 Detailed description of all substances used for the operation of the synthesis gas fermentation process. 95

List of Figures

2.1 Overview of the Wood-Ljungdahl pathway and a model for chemiosmotic energy conservation in Ech and Rnf acetogens. 7
2.2 Components of process development for acetogenic syngas fermentation. . . 8

3.1 Operating windows for anaerobic syngas fermentation and MeOH synthesis. . 16
3.2 Theoretical CO_2 equilibrium conversion of methanol synthesis and ethanol synthesis at stoichiometric conditions, different temperatures and two different pressures. 17
3.3 A comparative perspective of productivities between heterogeneous catalysis and syngas fermentation for mass-specific productivity and space-time yield. 19
3.4 Process scheme of product separation for fermentation broth recovery. 21
3.5 Two-column methanol distillation for product recovery. 22

4.1 Experimental setup for a continuous fermentation. 26
4.2 Hollow fiber membrane with periphery and pressure-stable vessel. 27
4.3 Three-part pressure-stable system for the prevention and separation of rising foam. 29

5.1 Influence of activation and deactivation of biomass retention on the fermentation process. 37
5.2 Influence of biomass retention on carbon-based selectivity. 38
5.3 Relative difference between measured total carbon content and sum of calculated individual carbon contents over time with total cell retention. 41
5.4 Influence of an increased substrate gas volume flow with activated biomass retention. 43
5.5 Influence of an increased dilution rate with activated biomass retention. . . . 47
5.6 Non-averaged measurement data to investigate the influence of pressure increase with a constant-volume hydrogen supply. 50

5.7 Influence of a gradual pressure increase to 3 bar gauge pressure with a constant volumetric supply of hydrogen. 52
5.8 Influence of a gradually reduced pH value with activated biomass retention. . 56
5.9 Non-averaged measured data of gas uptake rates, space-time yields and cell density over time for pH 5.3 and 5.1. 58

6.1 Mole fraction of ethanol and acetic acid of the product stream for three different dilution rates with activated cell retention. 61
6.2 Hydrogen uptake ratio and product ratio as a function of biomass-specific CO partial pressure in the off-gas. 63
6.3 Product concentrations of acetic acid and ethanol as a function of cell density. 65
6.4 Reduction of acetate to ethanol in the WLP. 69
6.5 Gas uptake ratio of hydrogen to carbon and space-time yield of ethanol as a function of theoretical equilibrium concentration of hydrogen in the fermentation liquid. 71
6.6 Molar product ratio of acetic acid to ethanol as a function of theoretical equilibrium concentration of CO, CO_2 and H_2 in the liquid phase. 72

A.1 Detailed process flow diagram of the experimental test rig for continuous fermentation of synthesis gas. 81
A.2 Glass vessel for separating foam from the off-gas for operation at atmospheric pressure conditions. 82
A.3 Lab-scale experiment to investigate the influence of an impeller placed above the liquid phase on the agitator shaft on foam formation. 83
A.4 Measurement data on gas uptake rate, space-time yield and cell density plotted over the time of measurement campaign *HSF-Z-IV* to investigate the influence of cell retention and increased substrate gas flow at high cell density. 86
A.5 Measurement data on gas uptake rate, space-time yield and cell density plotted over the time of measurement campaign *ZpH-I* to investigate the influence of dilution rate and cell retention deactivation. 87
A.6 Measurement data on gas uptake rate, space-time yield and cell density plotted over the time of measurement campaign *ZP-II* to investigate the influence of pressure increase at a constant volumetric hydrogen input and activated cell retention. 88

A.7 Measurement data on gas uptake rate, space-time yield and cell density plotted over the time of measurement campaign *ZpH-I* to investigate the influence of reduced pH at high cell densities with activated cell retention. 89
A.8 Experimental setup for continuous fermentation of synthesis gas released in November 2020. 92
A.9 Upgraded experimental setup for continuous fermentation of synthesis gas released in March 2021. 92
A.10 Further developed experimental setup for continuous fermentation of synthesis gas released in November 2021. 93
A.11 Final experimental setup for continuous fermentation of synthesis gas released in June 2022. 93
A.12 Mechanical breakdown of the agitator coupling system with friction bearing after 167 hours of operation. 94
A.13 Breakage of the agitator shaft at the interface to the coupling system after 392 hours of operation. 94

Bibliography

[1]
P. TCVETKOV; A. CHEREPOVITSYN; S. FEDOSEEV: *The Changing Role of CO2 in the Transition to a Circular Economy: Review of Carbon Sequestration Projects*. Sustainability 11.20 (2019), p. 5834. DOI: 10.3390/su11205834.

[2]
M. PAVAN; K. REINMETS; S. GARG; A. P. MUELLER; E. MARCELLIN; M. KÖPKE; K. VALGEPEA: *Advances in systems metabolic engineering of autotrophic carbon oxide-fixing biocatalysts towards a circular economy*. Metab. Eng. 71 (2022), pp. 117–141. DOI: 10.1016/j.ymben.2022.01.015.

[3]
L. DITTRICH; M. NOHL; E. E. JAEKEL; S. FOIT; L. DE HAART; R.-A. EICHEL: *High-Temperature Co-Electrolysis: A Versatile Method to Sustainably Produce Tailored Syngas Compositions*. J. Electrochem. Soc. 166.13 (2019), F971–F975. DOI: 10.1149/2.0581913jes.

[4]
D. TANG; G.-L. TAN; G.-W. LI; J.-G. LIANG; S. M. AHMAD; A. BAHADUR; M. HUMAYUN; H. ULLAH; A. KHAN; M. BOUOUDINA: *State-of-the-art hydrogen generation techniques and storage methods: A critical review*. J. Energy Storage 64 (2023), p. 107196. DOI: 10.1016/j.est.2023.107196.

[5]
J. J. BOLÍVAR CABALLERO; I. N. ZAINI; W. YANG: *Reforming processes for syngas production: A mini-review on the current status, challenges, and prospects for biomass conversion to fuels*. Appl. Energy Combust. Sci. 10 (2022), p. 100064. DOI: 10.1016/j.jaecs.2022.100064.

[6]
V. SINGH; L. C. BUELENS; H. POELMAN; M. SAEYS; G. B. MARIN; V. V. GALVITA: *Carbon monoxide production using a steel mill gas in a combined chemical looping process*. J. Energy Chem. 68 (2022), pp. 811–825. DOI: 10.1016/j.jechem.2021.12.042.

[7]
D. Y. LEUNG; G. CARAMANNA; M. M. MAROTO-VALER: *An overview of current status of carbon dioxide capture and storage technologies*. Renewable Sustainable Energy Rev. 39 (2014), pp. 426–443. DOI: 10.1016/j.rser.2014.07.093.

[8]
C. FERNÁNDEZ-BLANCO; M. C. VEIGA; C. KENNES: *Efficient production of n-caproate from syngas by a co-culture of Clostridium aceticum and Clostridium kluyveri*. J. Environ. Manage. 302.Pt A (2022), p. 113992. DOI: 10.1016/j.jenvman.2021.113992.

[9]
X. SUN; H. K. ATIYEH; R. L. HUHNKE; R. S. TANNER: *Syngas fermentation process development for production of biofuels and chemicals: A review*. Bioresour. Technol. Rep. 7 (2019), p. 100279. DOI: 10.1016/j.biteb.2019.100279.

[10]
T. HAAS; R. KRAUSE; R. WEBER; M. DEMLER; G. SCHMID: *Technical photosynthesis involving CO2 electrolysis and fermentation*. Nat. Catal. 1.1 (2018), pp. 32–39. DOI: 10.1038/s41929-017-0005-1.

[11]
C. FERNÁNDEZ-BLANCO; R. ROBLES-IGLESIAS; C. NAVEIRA-PAZOS; M. C. VEIGA; C. KENNES: *Production of biofuels from C1-gases with Clostridium and related bacteria - Recent advances*. Microb. Biotechnol. 16.4 (2023), pp. 726–741. DOI: 10.1111/1751-7915.14220.

[12]
H. G. WOOD: *Life with CO or CO2 and H2 as a source of carbon and energy*. FASEB j. 5.2 (1991), pp. 156–163. DOI: 10.1096/fasebj.5.2.1900793.

[13]
K. SCHUCHMANN; V. MÜLLER: *Autotrophy at the thermodynamic limit of life: a model for energy conservation in acetogenic bacteria*. Nat. Rev. Microbiol. 12.12 (2014), pp. 809–821. DOI: 10.1038/nrmicro3365.

[14]
F. P. ROSENBAUM; V. MÜLLER: *Energy conservation under extreme energy limitation: the role of cytochromes and quinones in acetogenic bacteria*. Extremophiles 25.5-6 (2021), pp. 413–424. DOI: 10.1007/s00792-021-01241-0.

[15]
J. L. GADDY; D. K. ARORA; C.-W. KO; J. R. PHILLIPS; R. BASU; C. V. WIKSTROM; E. C. CLAUSEN: "Methods for increasing the production of ethanol from microbial fermentation". US Patent 2003/0211585 A1. 2003.

[16]
E. M. DE MEDEIROS; J. A. POSADA; H. NOORMAN; R. M. FILHO: *Dynamic modeling of syngas fermentation in a continuous stirred-tank reactor: Multi-response parameter estimation and process optimization*. Biotechnol. Bioeng. 116.10 (2019), pp. 2473–2487. DOI: 10.1002/bit.27108.

[17]
C. KANTZOW; A. MAYER; D. WEUSTER-BOTZ: *Continuous gas fermentation by Acetobacterium woodii in a submerged membrane reactor with full cell retention*. J. Biotechnol. 212 (2015), pp. 11–18. DOI: 10.1016/j.jbiotec.2015.07.020.

[18]
H. RICHTER; M. MARTIN; L. ANGENENT: *A Two-Stage Continuous Fermentation System for Conversion of Syngas into Ethanol*. Energies 6.8 (2013), pp. 3987–4000. DOI: 10.3390/en6083987.

[19]
J. R. PHILLIPS; K. T. KLASSON; E. C. CLAUSEN; J. L. GADDY: *Biological production of ethanol from coal synthesis gas*. Appl. Biochem. Biotechnol. 39-40.1 (1993), pp. 559–571. DOI: 10.1007/BF02919018.

[20]
H. N. ABUBACKAR; M. C. VEIGA; C. KENNES: *Production of acids and alcohols from syngas in a two-stage continuous fermentation process*. Bioresour. Technol. 253 (2018), pp. 227–234. DOI: 10.1016/j.biortech.2018.01.026.

[21]
A. MAYER; T. SCHÄDLER; S. TRUNZ; T. STELZER; D. WEUSTER-BOTZ: *Carbon monoxide conversion with Clostridium aceticum*. Biotechnol. Bioeng. 115.11 (2018), pp. 2740–2750. DOI: 10.1002/bit.26808.

[22]
B. MOLITOR; A. MISHRA; L. T. ANGENENT: *Power-to-protein: converting renewable electric power and carbon dioxide into single cell protein with a two-stage bioprocess*. Energy Environ. Sci. 12.12 (2019), pp. 3515–3521. DOI: 10.1039/c9ee02381j.

[23]
H. YOUNESI; G. NAJAFPOUR; A. R. MOHAMED: *Ethanol and acetate production from synthesis gas via fermentation processes using anaerobic bacterium, Clostridium ljungdahlii*. Biochem. Eng. J. 27.2 (2005), pp. 110–119. DOI: 10.1016/j.bej.2005.08.015.

[24]
B. GEINITZ; A. HÜSER; M. MANN; J. BÜCHS: *Gas Fermentation Expands the Scope of a Process Network for Material Conversion*. Chem. Ing. Tech. 92.11 (2020), pp. 1665–1679. DOI: 10.1002/cite.202000086.

[25]
J. LI; D. HAN; Z. ZI; T. HE; G. LIU; Z. WANG; J. WU; J. WU: *The synthesis of H[Fe,Al]ZSM-5 zeolites with uniform nanocrystals for dimethyl ether to gasoline reaction*. Fuel 313 (2022), p. 122643. ISSN: 00162361. DOI: 10.1016/j.fuel.2021.122643.

[26]
N. FACKLER; B. D. HEIJSTRA; B. J. RASOR; H. BROWN; J. MARTIN; Z. NI; K. M. SHEBEK; R. R. ROSIN; S. D. SIMPSON; K. E. TYO; R. J. GIANNONE; R. L. HETTICH; T. J. TSCHAPLINSKI; C. LEANG; S. D. BROWN; M. C. JEWETT; M. KÖPKE: *Stepping on the Gas to a Circular Economy: Accelerating Development of Carbon-Negative Chemical Production from Gas Fermentation*. Annu. Rev. Chem. Biomol. Eng. 12 (2021), pp. 439–470. DOI: 10.1146/annurev-chembioeng-120120-021122.

[27]
C. BRIGHAM: *Perspectives for the biotechnological production of biofuels from CO2 and H2 using Ralstonia eutropha and other 'Knallgas' bacteria*. Appl. Microbiol. Biotechnol. 103.5 (2019), pp. 2113–2120. DOI: 10.1007/s00253-019-09636-y.

[28]
P. DÜRRE; B. J. EIKMANNS: *C1-carbon sources for chemical and fuel production by microbial gas fermentation*. Curr. Opin. Biotechnol. 35 (2015), pp. 63–72. DOI: 10.1016/j.copbio.2015.03.008.

[29]
J. SIPMA; A. M. HENSTRA; S. M. PARSHINA; P. N. LENS; G. LETTINGA; A. J. M. STAMS: *Microbial CO conversions with applications in synthesis gas purification and bio-desulfurization*. Crit. Rev. Biotechnol. 26.1 (2006), pp. 41–65. DOI: 10.1080/07388550500513974.

[30]
K. K. SAHOO; G. GOSWAMI; D. DAS: *Biotransformation of Methane and Carbon Dioxide Into High-Value Products by Methanotrophs: Current State of Art and Future Prospects*. Front. Microbiol. 12 (2021), p. 636486. DOI: 10.3389/fmicb.2021.636486.

[31]
P. J. STRONG; M. KALYUZHNAYA; J. SILVERMAN; W. P. CLARKE: *A methanotroph-based biorefinery: Potential scenarios for generating multiple products from a single fermentation*. Bioresour. Technol. 215 (2016), pp. 314–323. DOI: 10.1016/j.biortech.2016.04.099.

[32]
K. C. COSTA; J. A. LEIGH: *Metabolic versatility in methanogens*. Curr. Opin. Biotechnol. 29 (2014), pp. 70–75. DOI: 10.1016/j.copbio.2014.02.012.

[33]
LANZATECH: *World's leading steel company, ArcelorMittal and LanzaTech announce first ethanol samples from commercial flagship carbon capture and utilisation facility in Ghent, Belgium*. Chicago, 2023. URL: https://lanzatech.com/worlds-leading-steel-company-arcelormittal-and-lanzatech-announce-first-ethanol-samples-from-commercial-flagship-carbon-capture-and-utilisation-facility-in-ghent-belgium/ (visited on 12/10/2023).

[34]
H. L. DRAKE; A. S. GÖSSNER; S. L. DANIEL: *Old acetogens, new light*. Ann. N. Y. Acad. Sci. 1125 (2008), pp. 100–128. DOI: 10.1196/annals.1419.016.

[35]
F. E. FONTAINE; W. H. PETERSON; E. MCCOY; M. J. JOHNSON; G. J. RITTER: *A New Type of Glucose Fermentation by Clostridium thermoaceticum*. J. Bacteriol. 43.6 (1942), pp. 701–715. DOI: 10.1128/jb.43.6.701-715.1942.

[36]
F. LIEW; M. E. MARTIN; R. C. TAPPEL; B. D. HEIJSTRA; C. MIHALCEA; M. KÖPKE: *Gas Fermentation - A Flexible Platform for Commercial Scale Production of Low-Carbon-Fuels and Chemicals from Waste and Renewable Feedstocks*. Front. Microbiol. 7 (2016), p. 694. DOI: 10.3389/fmicb.2016.00694.

[37]
M. KOEPKE; F. LIEW: "Recombinant microorganism and methods of production thereof". US Patent 2011/0236941 A1. 2011.

[38]
K. ARSLAN; T. SCHOCH; F. HÖFELE; S. HERRSCHAFT; C. OBERLIES; F. BENGELSDORF; M. C. VEIGA; P. DÜRRE; C. KENNES: *Engineering Acetobacterium woodii for the production of isopropanol and acetone from carbon dioxide and hydrogen*. Biotechnol. J. 17.5 (2022), e2100515. DOI: 10.1002/biot.202100515.

[39]

B. R. GENTHNER; C. L. DAVIS; M. P. BRYANT: *Features of rumen and sewage sludge strains of Eubacterium limosum, a methanol- and H2-CO2-utilizing species*. Appl. Environ. Microbiol. 42.1 (1981), pp. 12–19. DOI: 10.1128/aem.42.1.12-19.1981.

[40]

W. E. BALCH; S. SCHOBERTH; R. S. TANNER; R. S. WOLFE: *Acetobacterium, a New Genus of Hydrogen-Oxidizing, Carbon Dioxide-Reducing, Anaerobic Bacteria*. Int. J. Syst. Bacteriol. 27.4 (1977), pp. 355–361. DOI: 10.1099/00207713-27-4-355.

[41]

S. HOFFMEISTER; M. GERDOM; F. R. BENGELSDORF; S. LINDER; S. FLÜCHTER; H. ÖZTÜRK; W. BLÜMKE; A. MAY; R.-J. FISCHER; H. BAHL; P. DÜRRE: *Acetone production with metabolically engineered strains of Acetobacterium woodii*. Metab. Eng. 36 (2016), pp. 37–47. DOI: 10.1016/j.ymben.2016.03.001.

[42]

R. HEISE; V. MÜLLER; G. GOTTSCHALK: *Sodium dependence of acetate formation by the acetogenic bacterium Acetobacterium woodii*. J. Bacteriol. 171.10 (1989), pp. 5473–5478. DOI: 10.1128/jb.171.10.5473-5478.1989.

[43]

K. P. NEVIN; S. A. HENSLEY; A. E. FRANKS; Z. M. SUMMERS; J. OU; T. L. WOODARD; O. L. SNOEYENBOS-WEST; D. R. LOVLEY: *Electrosynthesis of organic compounds from carbon dioxide is catalyzed by a diversity of acetogenic microorganisms*. Appl. Environ. Microbiol. 77.9 (2011), pp. 2882–2886. DOI: 10.1128/AEM.02642-10.

[44]

M. F. LUX; H. L. DRAKE: *Re-examination of thee metabolic potentials of the acetogens Clostridium aceticum and Clostridium formicoaceticum: Chemolithoautotrophic and aromatic-dependent growth*. FEMS Microbiol. Lett. 95.1 (1992), pp. 49–56. DOI: 10.1111/j.1574-6968.1992.tb05341.x.

[45]

F. U. BECKER; G. GRUND; M. ORSCHEL; K. DODERER; G. LOEHDEN; G. BRAND; P. DUERRE; S. THUM; H. J. BAHL; R.-J. FISCHER; A. MAY: "Cells and method for producing acetone". US Patent 2012/0101304 A1. 2010.

[46]

S. D. SIMPSON; M. KOEPKE; F. LIEW; W. Y. CHENG: "Recombinant Microorganisms and uses therefor". WO Patent 2012/115527. 2012.

[47]
S. D. BROWN; S. NAGARAJU; S. UTTURKAR; S. DE TISSERA; S. SEGOVIA; W. MITCHELL; M. L. LAND; A. DASSANAYAKE; M. KÖPKE: *Comparison of single-molecule sequencing and hybrid approaches for finishing the genome of Clostridium autoethanogenum and analysis of CRISPR systems in industrial relevant Clostridia*. Biotechnol. Biofuels 7 (2014), p. 40. DOI: 10.1186/1754-6834-7-40.

[48]
E. MARCELLIN; J. B. BEHRENDORFF; S. NAGARAJU; S. DETISSERA; S. SEGOVIA; R. W. PALFREYMAN; J. DANIELL; C. LICONA-CASSANI; L.-e. QUEK; R. SPEIGHT; M. P. HODSON; S. D. SIMPSON; W. P. MITCHELL; M. KÖPKE; L. K. NIELSEN: *Low carbon fuels and commodity chemicals from waste gases – systematic approach to understand energy metabolism in a model acetogen*. Green Chem. 18.10 (2016), pp. 3020–3028. DOI: 10.1039/c5gc02708j.

[49]
M. KÖPKE; C. MIHALCEA; F. LIEW; J. H. TIZARD; M. S. ALI; J. J. CONOLLY; B. AL-SINAWI; S. D. SIMPSON: *2,3-butanediol production by acetogenic bacteria, an alternative route to chemical synthesis, using industrial waste gas*. Appl. Environ. Microbiol. 77.15 (2011), pp. 5467–5475. DOI: 10.1128/AEM.00355-11.

[50]
B. BOURGADE; C. M. HUMPHREYS; J. MILLARD; N. P. MINTON; M. A. ISLAM: *Design, Analysis, and Implementation of a Novel Biochemical Pathway for Ethylene Glycol Production in Clostridium autoethanogenum*. ACS Synth. Biol. 11.5 (2022), pp. 1790–1800. DOI: 10.1021/acssynbio.1c00624.

[51]
M. KOEPKE; W. Y. CHEN: "Recombinant microorganisms and uses therefor". US Patent 2013/0323806 A1. 2013.

[52]
A. P. MUELLER; M. KOEPKE; S. NAGARAJU: "Recombinant microorganisms and usese therefor". US Patent 2013/0330809 A1. 2013.

[53]
A. P. MUELLER; M. KOEPKE: "Recombinant microorganisms comprising stereospecific diol dehydratase enzyme and methods related thereto". US Patent 9,284,564 B2. 2013.

[54]
M. KOEPKE; S. SIMPSON; F. LIEW; C. WENDY: "Fermentation process for producing isopropanol using a recombinant microorganism". US Patent 2012/0252083 A1. 2012.

[55]
W. Y. CHEN; F. LIEW; M. KOEPKE: "Recombinant microorganisms and uses therefor". US Patent 2013/0323820 A1. 2013.

[56]
R. DE SOUZA PINTO LEMGRUBER; K. VALGEPEA; R. TAPPEL; J. B. BEHRENDORFF; R. W. PALFREYMAN; M. PLAN; M. P. HODSON; S. D. SIMPSON; L. K. NIELSEN; M. KÖPKE; E. MARCELLIN: *Systems-level engineering and characterisation of Clostridium autoethanogenum through heterologous production of poly-3-hydroxybutyrate (PHB)*. Metab. Eng. 53 (2019), pp. 14–23. DOI: 10.1016/j.ymben.2019.01.003.

[57]
J. S.-C. LIOU; D. L. BALKWILL; G. R. DRAKE; R. S. TANNER: *Clostridium carboxidivorans sp. nov., a solvent-producing clostridium isolated from an agricultural settling lagoon, and reclassification of the acetogen Clostridium scatologenes strain SL1 as Clostridium drakei sp. nov*. Int. J. Syst. Evol. Microbiol. 55.Pt 5 (2005), pp. 2085–2091. DOI: 10.1099/ijs.0.63482-0.

[58]
Á. FERNÁNDEZ-NAVEIRA; M. C. VEIGA; C. KENNES: *Effect of pH control on the anaerobic H-B-E fermentation of syngas in bioreactors*. J. Chem. Technol. Biotechnol. 92.6 (2017), pp. 1178–1185. DOI: 10.1002/jctb.5232.

[59]
M. KÖPKE; C. HELD; S. HUJER; H. LIESEGANG; A. WIEZER; A. WOLLHERR; A. EHRENREICH; W. LIEBL; G. GOTTSCHALK; P. DÜRRE: *Clostridium ljungdahlii represents a microbial production platform based on syngas*. Proc. Natl. Acad. Sci. U. S. A. 107.29 (2010), pp. 13087–13092. DOI: 10.1073/pnas.1004716107.

[60]
T. UEKI; K. P. NEVIN; T. L. WOODARD; D. R. LOVLEY: *Converting carbon dioxide to butyrate with an engineered strain of Clostridium ljungdahlii*. mBio 5.5 (2014), e01636–14. DOI: 10.1128/mBio.01636-14.

[61]
R. S. TANNER; L. M. MILLER; D. YANG: *Clostridium ljungdahlii sp. nov., an acetogenic species in clostridial rRNA homology group I*. Int. J. Syst. Bacteriol. 43.2 (1993), pp. 232–236. DOI: 10.1099/00207713-43-2-232.

[62]
H. NAGARAJAN; M. SAHIN; J. NOGALES; H. LATIF; D. R. LOVLEY; A. EBRAHIM; K. ZENGLER: *Characterizing acetogenic metabolism using a genome-scale metabolic reconstruction of Clostridium ljungdahlii*. Microb. Cell Fact. 12 (2013), p. 118. DOI: 10.1186/1475-2859-12-118.

[63]
A. BANERJEE; C. LEANG; T. UEKI; K. P. NEVIN; D. R. LOVLEY: *Lactose-inducible system for metabolic engineering of Clostridium ljungdahlii*. Appl. Environ. Microbiol. 80.8 (2014), pp. 2410–2416. DOI: 10.1128/AEM.03666-13.

[64]
Z. BECK; M. CERVIN; C. GOPAL; B. DINER; J. FAN; C. PERES; K. SANFORD; M. SCOTCHER; D. WELLS; G. WHITED: "Recombinant anaerobic acetogenic bacteria for production of isoprene and/or industrial bio-products using synthesis gas". US Patent 2014/0234926 A1. 2014.

[65]
I. LAUER; G. PHILIPPS; S. JENNEWEIN: *Metabolic engineering of Clostridium ljungdahlii for the production of hexanol and butanol from CO2 and H2*. Microb. Cell Fact. 21.1 (2022), p. 85. DOI: 10.1186/s12934-022-01802-8.

[66]
W. H. LOROWITZ; M. P. BRYANT: *Peptostreptococcus productus strain that grows rapidly with CO as the energy source*. Appl. Environ. Microbiol. 47.5 (1984), pp. 961–964. DOI: 10.1128/aem.47.5.961-964.1984.

[67]
G. GEERLIGS; H. C. ALDRICH; W. HARDER; G. DIEKERT: *Isolation and characterization of a carbon monoxide utilizing strain of the acetogen Peptostreptococcus productus*. Arch. Microbiol. 148.4 (1987), pp. 305–313. DOI: 10.1007/BF00456709.

[68]
R. KERBY; J. G. ZEIKUS: *Growth of Clostridium thermoaceticum on H2/CO2 or CO as energy source*. Curr. Microbiol. 8.1 (1983), pp. 27–30. DOI: 10.1007/BF01567310.

[69]
J. KATO; K. TAKEMURA; S. KATO; T. FUJII; K. WADA; Y. IWASAKI; Y. AOI; A. MATSUSHIKA; K. MURAKAMI; Y. NAKASHIMADA: *Metabolic engineering of Moorella thermoacetica for thermophilic bioconversion of gaseous substrates to a volatile chemical*. AMB Express 11.1 (2021), p. 59. ISSN: 2191-0855. DOI: 10.1186/s13568-021-01220-w.

[70]
V. HESS; K. SCHUCHMANN; V. MÜLLER: *The ferredoxin:NAD+ oxidoreductase (Rnf) from the acetogen Acetobacterium woodii requires Na+ and is reversibly coupled to the membrane potential*. J. Biol. Chem. 288.44 (2013), pp. 31496–31502. DOI: 10.1074/jbc.M113.510255.

[71]
G. DIEKERT; M. RITTER: *Nickel requirement of Acetobacterium woodii*. J. Bacteriol. 151.2 (1982), pp. 1043–1045. DOI: 10.1128/jb.151.2.1043-1045.1982.

[72]
S. I. HU; H. L. DRAKE; H. G. WOOD: *Synthesis of acetyl coenzyme A from carbon monoxide, methyltetrahydrofolate, and coenzyme A by enzymes from Clostridium thermoaceticum*. J. Bacteriol. 149.2 (1982), pp. 440–448. DOI: 10.1128/jb.149.2.440-448.1982.

[73]
J. YI; H. HUANG; J. LIANG; R. WANG; Z. LIU; F. LI; S. WANG: *A Heterodimeric Reduced-Ferredoxin-Dependent Methylenetetrahydrofolate Reductase from Syngas-Fermenting Clostridium ljungdahlii*. Microbiol. Spectrum 9.2 (2021), e0095821. DOI: 10.1128/Spectrum.00958-21.

[74]
M. HERMANN; A. TELEKI; S. WEITZ; A. NIESS; A. FREUND; F. R. BENGELSDORF; R. TAKORS: *Electron availability in CO2 , CO and H2 mixtures constrains flux distribution, energy management and product formation in Clostridium ljungdahlii*. Microb. Biotechnol. 13.6 (2020), pp. 1831–1846. DOI: 10.1111/1751-7915.13625.

[75]
C. E. ISOM; M. A. NANNY; R. S. TANNER: *Improved conversion efficiencies for n-fatty acid reduction to primary alcohols by the solventogenic acetogen "Clostridium ragsdalei"*. J. Ind. Microbiol. Biotechnol. 42.1 (2015), pp. 29–38. DOI: 10.1007/s10295-014-1543-z.

[76]
A. NEUMANN; S. DÖRSAM; F. OSWALD; K. OCHSENREITHER: *Microbial Production of Value-Added Chemicals from Pyrolysis Oil and Syngas*. *Sustainable Production of Bulk Chemicals*. Ed. by M. XIAN. Vol. 281. Dordrecht: Springer Netherlands, 2015, pp. 69–105. ISBN: 978-94-017-7473-4. DOI: 10.1007/978-94-017-7475-8_4.

[77]
J. PHILLIPS; R. HUHNKE; H. ATIYEH: *Syngas Fermentation: A Microbial Conversion Process of Gaseous Substrates to Various Products*. Fermentation 3.2 (2017), p. 28. DOI: 10.3390/fermentation3020028.

[78]
A. AYOL; L. PEIXOTO; T. KESKIN; H. N. ABUBACKAR: *Reactor Designs and Configurations for biological and Bioelectrochemical C1 Gas Conversion: A Review*. Int. J. Environ. Res. Public Health 18.21 (2021). DOI: 10.3390/ijerph182111683.

[79]
B. GUNES: *A critical review on biofilm-based reactor systems for enhanced syngas fermentation processes*. Renewable Sustainable Energy Rev. 143.October 2019 (2021), p. 110950. DOI: 10.1016/j.rser.2021.110950.

[80]
I. K. STOLL; N. BOUKIS; J. SAUER: *Syngas Fermentation to Alcohols: Reactor Technology and Application Perspective*. Chem. Ing. Tech. 92.1-2 (2020), pp. 125–136. DOI: 10.1002/cite.201900118.

[81]
BREDWELL; SRIVASTAVA; WORDEN: *Reactor Design Issues for Synthesis-Gas Fermentations*. Biotechnol. Prog. 15.5 (1999), pp. 834–844. DOI: 10.1021/bp990108m.

[82]
R. TAKORS; M. KOPF; J. MAMPEL; W. BLUEMKE; B. BLOMBACH; B. EIKMANNS; F. R. BENGELSDORF; D. WEUSTER-BOTZ; P. DÜRRE: *Using gas mixtures of CO, CO2 and H2 as microbial substrates: the do's and don'ts of successful technology transfer from laboratory to production scale*. Microb. Biotechnol. 11.4 (2018), pp. 606–625. DOI: 10.1111/1751-7915.13270.

[83]
J. J. ORGILL; H. K. ATIYEH; M. DEVARAPALLI; J. R. PHILLIPS; R. S. LEWIS; R. L. HUHNKE: *A comparison of mass transfer coefficients between trickle-bed, hollow fiber membrane and stirred tank reactors*. Bioresour. Technol. 133 (2013), pp. 340–346. DOI: 10.1016/j.biortech.2013.01.124.

[84]
M. P. ELISIÁRIO; H. DE WEVER; W. VAN HECKE; H. NOORMAN; A. J. J. STRAATHOF: *Membrane bioreactors for syngas permeation and fermentation*. Crit. Rev. Biotechnol. 42.6 (2022), pp. 856–872. DOI: 10.1080/07388551.2021.1965952.

[85]
X. LI; B. J. COSSEY; S. R. TREVETHICK: "Fermentation of gaseous substrates". US Patent 9,617,509 B2. 2015.

[86]
S. R. TREVETHICK; J. C. BROMLEY; G. W. WATERS; M. KOEPKE; L. P. TRAN; R. J. OVERGAARD: "Multi-stage bioreactor processes". US Patent 2016/0115505 A1. 2016.

[87]
L. PUIMAN; E. ALMEIDA BENALCÁZAR; C. PICIOREANU; H. J. NOORMAN; C. HARINGA: *Downscaling Industrial-Scale Syngas Fermentation to Simulate Frequent and Irregular Dissolved Gas Concentration Shocks*. Bioengineering 10.5 (2023). DOI: 10.3390/bioengineering10050518.

[88]
R. TAKORS; M. WILD; Y. MAST; S. BALTACI; U. SCHLIESSMANN; A. ZIMMERMAN; J. SCHMIDTKE; I. BEUTER: *Machbarkeitsstudie im Themenfeld Carbon Economy: Modulare Abgas-Raffinerie mit biologischen und hybriden Technologien mit Schwerpunkt auf C02-Recycling aus CO2-Punktquellen*. Ed. by LANDESAGENTUR FÜR UMWELTTECHNIK UND RESSOURCENEFFIZIENZ BADEN-WÜRTTEMBERG. 2021. URL: https://www.pure-bw.de/sites/default/files/2022-06/210613_Machbarkeitsstudie_Abgasrafffinerie_barrierefrei.pdf (visited on 07/23/2022).

[89]
P. ROY; A. DUTTA; S. CHANG: *Development and evaluation of a functional bioreactor for CO fermentation into ethanol*. Bioresour. Bioprocess. 3.1 (2016). DOI: 10.1186/s40643-016-0082-z.

[90]
B. M. ENNIS; I. S. MADDOX: *Production of solvents (ABE fermentation) from whey permeate by continuous fermentation in a membrane bioreactor*. Bioprocess Eng. 4.1 (1989), pp. 27–34. DOI: 10.1007/BF00612667.

[91]
J. M. NEWTON; D. SCHOFIELD; J. VLAHOPOULOU; Y. ZHOU: *Detecting cell lysis using viscosity monitoring in E. coli fermentation to prevent product loss*. Biotechnol. Prog. 32.4 (2016), pp. 1069–1076. DOI: 10.1002/btpr.2292.

[92]
C. A. VEES; C. S. NEUENDORF; S. PFLÜGL: *Towards continuous industrial bioprocessing with solventogenic and acetogenic clostridia: challenges, progress and perspectives*. J. Ind. Microbiol. Biotechnol. 47.9-10 (2020), pp. 753–787. DOI: 10.1007/s10295-020-02296-2.

[93]
M. C. SCOTCHER; F. B. RUDOLPH; G. N. BENNETT: *Expression of abrB310 and SinR, and effects of decreased abrB310 expression on the transition from acidogenesis to solventogenesis, in Clostridium acetobutylicum ATCC 824*. Appl. Environ. Microbiol. 71.4 (2005), pp. 1987–1995. DOI: 10.1128/AEM.71.4.1987-1995.2005.

[94]
M. STRAUB; M. DEMLER; D. WEUSTER-BOTZ; P. DÜRRE: *Selective enhancement of autotrophic acetate production with genetically modified Acetobacterium woodii*. J. Biotechnol. 178 (2014), pp. 67–72. DOI: 10.1016/j.jbiotec.2014.03.005.

[95]
F. E. LIEW; R. NOGLE; T. ABDALLA; B. J. RASOR; C. CANTER; R. O. JENSEN; L. WANG; J. STRUTZ; P. CHIRANIA; S. DE TISSERA; A. P. MUELLER; Z. RUAN; A. GAO; L. TRAN; N. L. ENGLE; J. C. BROMLEY; J. DANIELL; R. CONRADO; T. J. TSCHAPLINSKI; R. J. GIANNONE; R. L. HETTICH; A. S. KARIM; S. D. SIMPSON; S. D. BROWN; C. LEANG; M. C. JEWETT; M. KÖPKE: *Carbon-negative production of acetone and isopropanol by gas fermentation at industrial pilot scale*. Nat. Biotechnol. 40.3 (2022), pp. 335–344. DOI: 10.1038/s41587-021-01195-w.

[96]
J. STRUTZ; J. MARTIN; J. GREENE; L. BROADBELT; K. TYO: *Metabolic kinetic modeling provides insight into complex biological questions, but hurdles remain*. Curr. Opin. Biotechnol. 59 (2019), pp. 24–30. DOI: 10.1016/j.copbio.2019.02.005.

[97]
J. K. LIU; C. LLOYD; M. M. AL-BASSAM; A. EBRAHIM; J.-N. KIM; C. OLSON; A. AKSENOV; P. DORRESTEIN; K. ZENGLER: *Predicting proteome allocation, overflow metabolism, and metal requirements in a model acetogen*. PLoS Comput. Biol. 15.3 (2019), pp. 1–16. DOI: 10.1371/journal.pcbi.1006848.

[98]
C. FOSTER; K. CHARUBIN; E. T. PAPOUTSAKIS; C. D. MARANAS: *Modeling Growth Kinetics, Interspecies Cell Fusion, and Metabolism of a Clostridium acetobutylicum/Clostridium ljungdahlii Syntrophic Coculture*. mSystems 6.1 (2021). ISSN: 2379-5077. DOI: 10.1128/mSystems.01325-20.

[99]
J. GREENE; J. DANIELL; M. KÖPKE; L. BROADBELT; K. E. TYO: *Kinetic ensemble model of gas fermenting Clostridium autoethanogenum for improved ethanol production*. Biochem. Eng. J. 148 (2019), pp. 46–56. DOI: 10.1016/j.bej.2019.04.021.

[100]
C. KANTZOW; D. WEUSTER-BOTZ: *Effects of hydrogen partial pressure on autotrophic growth and product formation of Acetobacterium woodii*. Bioprocess Biosyst. Eng. 39.8 (2016), pp. 1325–1330. DOI: 10.1007/s00449-016-1600-2.

[101]
J. BERTSCH; V. MÜLLER: *Bioenergetic constraints for conversion of syngas to biofuels in acetogenic bacteria*. Biotechnol. Biofuels 8 (2015), p. 210. DOI: 10.1186/s13068-015-0393-x.

[102]
K. M. HURST; R. S. LEWIS: *Carbon monoxide partial pressure effects on the metabolic process of syngas fermentation*. Biochem. Eng. J. 48.2 (2010), pp. 159–165. DOI: 10.1016/j.bej.2009.09.004.

[103]
I. K. STOLL: *Einfluss eines erhöhten Prozessdrucks bei der Fermentation von Synthesegas: Charakterisierung der Druckfermentation im Rührkesselreaktor*. Dissertation. Karlsruhe: Karlsruhe Institute of Technology, 2021.

[104]
K. VALGEPEA; R. DE SOUZA PINTO LEMGRUBER; T. ABDALLA; S. BINOS; N. TAKEMORI; A. TAKEMORI; Y. TANAKA; R. TAPPEL; M. KÖPKE; S. D. SIMPSON; L. K. NIELSEN; E. MARCELLIN: *H2 drives metabolic rearrangements in gas-fermenting Clostridium autoethanogenum*. Biotechnol. Biofuels 11 (2018), p. 55. DOI: 10.1186/s13068-018-1052-9.

[105]
J. JACK; J. LO; P.-C. MANESS; Z. J. REN: *Directing Clostridium ljungdahlii fermentation products via hydrogen to carbon monoxide ratio in syngas*. Biomass Bioenergy 124 (2019), pp. 95–101. DOI: 10.1016/j.biombioe.2019.03.011.

[106]
A. INFANTES; M. KUGEL; K. RAFFELT; A. NEUMANN: *Side-by-Side Comparison of Clean and Biomass-Derived, Impurity-Containing Syngas as Substrate for Acetogenic Fermentation with Clostridium ljungdahlii*. Fermentation 6.3 (2020), p. 84. DOI: 10.3390/fermentation6030084.

[107]
E. D. CARLSON; E. T. PAPOUTSAKIS: *Heterologous Expression of the Clostridium carboxidivorans CO Dehydrogenase Alone or Together with the Acetyl Coenzyme A Synthase Enables both Reduction of CO2 and Oxidation of CO by Clostridium acetobutylicum*. Appl. Environ. Microbiol. 83.16 (2017). DOI: 10.1128/AEM.00829-17.

[108]
M. MOHAMMADI; G. D. NAJAFPOUR; H. YOUNESI; P. LAHIJANI; M. H. UZIR; A. R. MOHAMED: *Bioconversion of synthesis gas to second generation biofuels: A review*. Renewable Sustainable Energy Rev. 15.9 (2011), pp. 4255–4273. DOI: 10.1016/j.rser.2011.07.124.

[109]
S. W. RAGSDALE: *Life with carbon monoxide*. Crit. Rev. Biochem. Mol. Biol. 39.3 (2004), pp. 165–195. DOI: 10.1080/10409230490496577.

[110]
G. EIGENSTETTER; R. TAKORS: *Dynamic modeling reveals a three-step response of Saccharomyces cerevisiae to high CO2 levels accompanied by increasing ATP demands*. FEMS Yeast Res. 17.1 (2017). DOI: 10.1093/femsyr/fox008.

[111]
R. P. JONES; P. F. GREENFIELD: *Effect of carbon dioxide on yeast growth and fermentation*. Enzyme Microb. Technol. 4.4 (1982), pp. 210–223. DOI: 10.1016/0141-0229(82)90034-5.

[112]
D. XU; D. R. TREE; R. S. LEWIS: *The effects of syngas impurities on syngas fermentation to liquid fuels*. Biomass Bioenergy 35.7 (2011), pp. 2690–2696. DOI: 10.1016/j.biombioe.2011.03.005.

[113]
A. RÜCKEL; J. HANNEMANN; C. MAIERHOFER; A. FUCHS; D. WEUSTER-BOTZ: *Studies on Syngas Fermentation With Clostridium carboxidivorans in Stirred-Tank Reactors With Defined Gas Impurities*. Front. Microbiol. 12 (2021), p. 655390. DOI: 10.3389/fmicb.2021.655390.

[114]
C. BENEVENUTI; P. AMARAL; T. FERREIRA; P. SEIDL: *Impacts of Syngas Composition on Anaerobic Fermentation*. Reactions 2.4 (2021), pp. 391–407. DOI: 10.3390/reactions2040025.

[115]
L. OLIVEIRA; S. RÖHRENBACH; V. HOLZMÜLLER; D. WEUSTER-BOTZ: *Continuous sulfide supply enhanced autotrophic production of alcohols with Clostridium ragsdalei*. Bioresour. Bioprocess. 9.1 (2022). DOI: 10.1186/s40643-022-00506-6.

[116]
D. K. KUNDIYANA; M. R. WILKINS; P. MADDIPATI; R. L. HUHNKE: *Effect of temperature, pH and buffer presence on ethanol production from synthesis gas by "Clostridium ragsdalei"*. Bioresour. Technol. 102.10 (2011), pp. 5794–5799. DOI: 10.1016/j.biortech.2011.02.032.

[117]
S. RAMIÓ-PUJOL; R. GANIGUÉ; L. BAÑERAS; J. COLPRIM: *Incubation at 25 °C prevents acid crash and enhances alcohol production in Clostridium carboxidivorans P7*. Bioresour. Technol. 192 (2015), pp. 296–303. DOI: 10.1016/j.biortech.2015.05.077.

[118]
S. SHEN; Y. GU; C. CHAI; W. JIANG; Y. ZHUANG; Y. WANG: *Enhanced alcohol titre and ratio in carbon monoxide-rich off-gas fermentation of Clostridium carboxidivorans through combination of trace metals optimization with variable-temperature cultivation*. Bioresour. Technol. 239 (2017), pp. 236–243. DOI: 10.1016/j.biortech.2017.04.099.

[119]
S. SHEN; G. WANG; M. ZHANG; Y. TANG; Y. GU; W. JIANG; Y. WANG; Y. ZHUANG: *Effect of temperature and surfactant on biomass growth and higher-alcohol production during syngas fermentation by Clostridium carboxidivorans P7*. Bioresour. Bioprocess. 7.1 (2020). DOI: 10.1186/s40643-020-00344-4.

[120]
H. RICHTER; B. MOLITOR; H. WEI; W. CHEN; L. ARISTILDE; L. T. ANGENENT: *Ethanol production in syngas-fermenting Clostridium ljungdahlii is controlled by thermodynamics rather than by enzyme expression*. Energy Environ. Sci. 9.7 (2016), pp. 2392–2399. DOI: 10.1039/c6ee01108j.

[121]
A. INFANTES; M. KUGEL; A. NEUMANN: *Evaluation of Media Components and Process Parameters in a Sensitive and Robust Fed-Batch Syngas Fermentation System with Clostridium ljungdahlii*. Fermentation 6.2 (2020), p. 61. DOI: 10.3390/fermentation6020061.

[122]
H. N. ABUBACKAR; M. C. VEIGA; C. KENNES: *Biological conversion of carbon monoxide to ethanol: effect of pH, gas pressure, reducing agent and yeast extract*. Bioresour. Technol. 114 (2012), pp. 518–522. DOI: 10.1016/j.biortech.2012.03.027.

[123]
B. AHN; S. PARK; Y.-K. KIM: *Effect of Medium Composition on Cell Growth and Bioethanol Production in Clostridium ljungdahlii Culture*. Appl. Chem. Eng. 29.4 (2018), pp. 419–424. DOI: 10.14478/ace.2018.1032.

[124]
J. R. PHILLIPS; N. M. REMONDET; H. K. ATIYEH; M. R. WILKINS; R. L. HUHNKE: *Designing Syngas Fermentation Medium for Fuels and Bulk Chemicals Production*. ASABE (2011). DOI: 10.13031/2013.37400.

[125]
H. IM; T. AN; R. KWON; S. PARK; Y.-K. KIM: *Effect of Organic Nitrogen Supplements on Syngas Fermentation Using Clostridium autoethanogenum*. Biotechnol. Bioprocess Eng. 26.3 (2021), pp. 476–482. DOI: 10.1007/s12257-020-0221-4.

[126]
M. MOHAMMADI; A. R. MOHAMED; G. NAJAFPOUR; H. YOUNESI; M. H. UZIR: *Clostridium ljungdahlii for production of biofuel from synthesis gas*. Energy Sources, Part A 38.3 (2016), pp. 427–434. DOI: 10.1080/15567036.2012.729254.

[127]
F. OSWALD; S. DÖRSAM; N. VEITH; M. ZWICK; A. NEUMANN; K. OCHSENREITHER; C. SYLDATK: *Sequential Mixed Cultures: From Syngas to Malic Acid*. Front. Microbiol. 7 (2016), p. 891. DOI: 10.3389/fmicb.2016.00891.

[128]
S. PARK; B. AHN; Y.-K. KIM: *Growth enhancement of bioethanol-producing microbe Clostridium autoethanogenum by changing culture medium composition*. Bioresour. Technol. Rep. 6 (2019), pp. 237–240. DOI: 10.1016/j.biteb.2019.03.012.

[129]
K. DOLL; A. RÜCKEL; P. KÄMPF; M. WENDE; D. WEUSTER-BOTZ: *Two stirred-tank bioreactors in series enable continuous production of alcohols from carbon monoxide with Clostridium carboxidivorans*. Bioprocess Biosyst. Eng. 41.10 (2018), pp. 1403–1416. DOI: 10.1007/s00449-018-1969-1.

[130]
M. E. MARTIN; H. RICHTER; S. SAHA; L. T. ANGENENT: *Traits of selected Clostridium strains for syngas fermentation to ethanol*. Biotechnol. Bioeng. 113.3 (2016), pp. 531–539. DOI: 10.1002/bit.25827.

[131]
H. K. ATIYEH; J. R. PHILLIPS; R. L. HUHNKE: "Systems and method for feedback control of gas supply for ethanol production via syngas fermentation using pH as a key control indicator". US Patent 10,017,789 B2. 2018.

[132]
D. CHICHE; C. DIVERCHY; A.-C. LUCQUIN; F. PORCHERON; F. DEFOORT: *Synthesis Gas Purification*. Oil Gas Sci. Technol. – Rev. IFP Energies nouvelles 68.4 (2013), pp. 707–723. DOI: 10.2516/ogst/2013175.

[133]

J. SCHITTKOWSKI; H. RULAND; D. LAUDENSCHLEGER; K. GIROD; K. KÄHLER; S. KALUZA; M. MUHLER; R. SCHLÖGL: *Methanol Synthesis from Steel Mill Exhaust Gases: Challenges for the Industrial Cu/ZnO/Al2O3 Catalyst*. Chem. Ing. Tech. 90.10 (2018), pp. 1419–1429. DOI: 10.1002/cite.201800017.

[134]

P. J. WOOLCOCK; R. C. BROWN: *A review of cleaning technologies for biomass-derived syngas*. Biomass Bioenergy 52.6 (2013), pp. 54–84. DOI: 10.1016/j.biombioe.2013.02.036.

[135]

N. ABDOULMOUMINE; S. ADHIKARI; A. KULKARNI; S. CHATTANATHAN: *A review on biomass gasification syngas cleanup*. Appl. Energy 155 (2015), pp. 294–307. DOI: 10.1016/j.apenergy.2015.05.095.

[136]

V. DIETERICH; A. BUTTLER; A. HANEL; H. SPLIETHOFF; S. FENDT: *Power-to-liquid via synthesis of methanol, DME or Fischer–Tropsch-fuels: a review*. Energy Environ. Sci. 13.10 (2020), pp. 3207–3252. DOI: 10.1039/d0ee01187h.

[137]

E. HERACLEOUS; V. KOIDI; A. A. LAPPAS; A. HAUSER; S. HAAG: *Valorization of steel-work off-gases: Influence of impurities on the performance of Cu-based methanol synthesis catalyst*. Chem. Eng. J. 444 (2022), p. 136571. DOI: 10.1016/j.cej.2022.136571.

[138]

J. HE; D. LAUDENSCHLEGER; J. SCHITTKOWSKI; A. MACHOKE; H. SONG; M. MUHLER; R. SCHLÖGL; H. RULAND: *Influence of Contaminants in Steel Mill Exhaust Gases on Cu/ZnO/Al2O3 Catalysts Applied in Methanol Synthesis*. Chem. Ing. Tech. 92.10 (2020), pp. 1525–1532. DOI: 10.1002/cite.202000045.

[139]

A. AHMED; B. G. CATENI; R. L. HUHNKE; R. S. LEWIS: *Effects of biomass-generated producer gas constituents on cell growth, product distribution and hydrogenase activity of Clostridium carboxidivorans P7T*. Biomass Bioenergy 30.7 (2006), pp. 665–672. DOI: 10.1016/j.biombioe.2006.01.007.

[140]

R. QUINN; T. DAHL; B. TOSELAND: *An evaluation of synthesis gas contaminants as methanol synthesis catalyst poisons*. Appl. Catal., A 272.1-2 (2004), pp. 61–68. DOI: 10.1016/j.apcata.2004.05.015.

[141]

INEOS NEW PLANET BIOENERGY: *Technical evaluation & preliminary determination: Biomass to Ethanol Production: Permit Modification - Installation of Hydrogen Cyanide Scrubber*. Florida, 2014. URL: http://www.ascension-publishing.com/INEOS-FIX-090514.pdf (visited on 07/10/2022).

[142]

F. OSWALD; M. ZWICK; O. OMAR; E. N. HOTZ; A. NEUMANN: *Growth and Product Formation of Clostridium ljungdahlii in Presence of Cyanide*. Front. Microbiol. 9 (2018), p. 1213. DOI: 10.3389/fmicb.2018.01213.

[143]

M. V. TWIGG: *Deactivation of copper metal catalysts for methanol decomposition, methanol steam reforming and methanol synthesis*. Top. Catal. 22.3/4 (2003), pp. 191–203. DOI: 10.1023/A:1023567718303.

[144]

S. KAWASAKI; Y. WATAMURA; M. ONO; T. WATANABE; K. TAKEDA; Y. NIIMURA: *Adaptive responses to oxygen stress in obligatory anaerobes Clostridium acetobutylicum and Clostridium aminovalericum*. Appl. Environ. Microbiol. 71.12 (2005), pp. 8442–8450. DOI: 10.1128/AEM.71.12.8442-8450.2005.

[145]

J. M. WHITHAM; O. TIRADO-ACEVEDO; M. S. CHINN; J. J. PAWLAK; A. M. GRUNDEN: *Metabolic response of Clostridium ljungdahlii to oxygen exposure*. Appl. Environ. Microbiol. 81.24 (2015), pp. 8379–8391. DOI: 10.1128/AEM.02491-15.

[146]

CLARIANT INTERNATIONAL LTD: *Catalysts for methanol synthesis*. 2017. URL: https://www.clariant.com/-/media/Files/Solutions/Products/Additional-Files/M/18/Clariant-Brochure-Methanol-Synthesis-201711-EN.pdf (visited on 07/19/2022).

[147]

T. CORDERO-LANZAC; A. RAMIREZ; A. NAVAJAS; L. GEVERS; S. BRUNIALTI; L. M. GANDÍA; A. T. AGUAYO; S. MANI SARATHY; J. GASCON: *A techno-economic and life cycle assessment for the production of green methanol from CO2: catalyst and process bottlenecks*. J. Energy Chem. 68 (2022), pp. 255–266. DOI: 10.1016/j.jechem.2021.09.045.

[148]

A. AHMED; R. S. LEWIS: *Fermentation of biomass-generated synthesis gas: effects of nitric oxide*. Biotechnol. Bioeng. 97.5 (2007), pp. 1080–1086. DOI: 10.1002/bit.21305.

[149]
N. DHAKAL; B. ACHARYA: *Syngas Fermentation for the Production of Bio-Based Polymers: A Review*. Polymers 13.22 (2021). DOI: 10.3390/polym13223917.

[150]
J. OTT; V. GRONEMANN; F. PONTZEN; E. FIEDLER; G. GROSSMANN; D. B. KERSEBOHM; G. WEISS; C. WITTE: *Methanol. Ullmann's Encyclopedia of Industrial Chemistry*. Weinheim, Germany: Wiley-VCH Verlag GmbH & Co. KGaA, 2000. ISBN: 3527306730. DOI: 10.1002/14356007.a16_465.pub3.

[151]
S.-T. BAI; G. DE SMET; Y. LIAO; R. SUN; C. ZHOU; M. BELLER; B. U. W. MAES; B. F. SELS: *Homogeneous and heterogeneous catalysts for hydrogenation of CO2 to methanol under mild conditions*. Chem. Soc. Rev. 50.7 (2021), pp. 4259–4298. DOI: 10.1039/d0cs01331e.

[152]
A. KUMAR; P. DAW; D. MILSTEIN: *Homogeneous Catalysis for Sustainable Energy: Hydrogen and Methanol Economies, Fuels from Biomass, and Related Topics*. Chem. Rev. 122.1 (2022), pp. 385–441. DOI: 10.1021/acs.chemrev.1c00412.

[153]
K. SORDAKIS; C. TANG; L. K. VOGT; H. JUNGE; P. J. DYSON; M. BELLER; G. LAURENCZY: *Homogeneous Catalysis for Sustainable Hydrogen Storage in Formic Acid and Alcohols*. Chem. Rev. 118.2 (2018), pp. 372–433. DOI: 10.1021/acs.chemrev.7b00182.

[154]
B. G. SCHIEWECK; P. JÜRLING-WILL; J. KLANKERMAYER: *Structurally Versatile Ligand System for the Ruthenium Catalyzed One-Pot Hydrogenation of CO2 to Methanol*. ACS Catal. 10.6 (2020), pp. 3890–3894. DOI: 10.1021/acscatal.9b04977.

[155]
G. ZANG; P. SUN; A. ELGOWAINY; M. WANG: *Technoeconomic and Life Cycle Analysis of Synthetic Methanol Production from Hydrogen and Industrial Byproduct CO2*. Environ. Sci. Technol. 55.8 (2021), pp. 5248–5257. DOI: 10.1021/acs.est.0c08237.

[156]
M. MOHAMMADI; H. YOUNESI; G. NAJAFPOUR; A. R. MOHAMED: *Sustainable ethanol fermentation from synthesis gas by Clostridium ljungdahlii in a continuous stirred tank bioreactor*. J. Chem. Technol. Biotechnol. 87.6 (2012), pp. 837–843. DOI: 10.1002/jctb.3712.

[157]
C. PEINADO; D. LIUZZI; A. SANCHÍS; L. PASCUAL; M. A. PEÑA; J. BOON; S. ROJAS: *In Situ Conditioning of CO2-Rich Syngas during the Synthesis of Methanol*. Catalysts 11.5 (2021), p. 534. DOI: 10.3390/catal11050534.

[158]
S. WILD; S. POLIERER; T. A. ZEVACO; D. GUSE; M. KIND; S. PITTER; K. HERRERA DELGADO; J. SAUER: *Direct DME synthesis on CZZ/H-FER from variable CO2/CO syngas feeds*. RSC advances 11.5 (2021), pp. 2556–2564. DOI: 10.1039/d0ra09754c.

[159]
B. LACERDA DE OLIVEIRA CAMPOS; K. HERRERA DELGADO; S. WILD; F. STUDT; S. PITTER; J. SAUER: *Surface reaction kinetics of the methanol synthesis and the water gas shift reaction on Cu/ZnO/Al2O3*. React. Chem. Eng. 6.5 (2021), pp. 868–887. DOI: 10.1039/D1RE00040C.

[160]
Y. SLOTBOOM; M. J. BOS; J. PIEPER; V. VRIESWIJK; B. LIKOZAR; S. KERSTEN; D. BRILMAN: *Critical assessment of steady-state kinetic models for the synthesis of methanol over an industrial Cu/ZnO/Al2O3 catalyst*. Chem. Eng. J. 389 (2020), p. 124181. DOI: 10.1016/j.cej.2020.124181.

[161]
B. ACHARYA; A. DUTTA; P. BASU: *Ethanol production by syngas fermentation in a continuous stirred tank bioreactor using Clostridium ljungdahlii*. Biofuels 10.2 (2019), pp. 221–237. ISSN: 1759-7269. DOI: 10.1080/17597269.2017.1316143.

[162]
L. PERRET; B. LACERDA DE OLIVEIRA CAMPOS; K. HERRERA DELGADO; T. A. ZEVACO; A. NEUMANN; J. SAUER: *COx Fixation to Elementary Building Blocks: Anaerobic Syngas Fermentation vs. Chemical Catalysis*. Chem. Ing. Tech. 94.11 (2022), pp. 1667–1687. DOI: 10.1002/cite.202200153.

[163]
F. LIEW; A. M. HENSTRA; M. KOEPKE; K. WINZER; S. D. SIMPSON; N. P. MINTON: *Metabolic engineering of Clostridium autoethanogenum for selective alcohol production*. Metab. Eng. 40 (2017), pp. 104–114. DOI: 10.1016/j.ymben.2017.01.007.

[164]
G. BOZZANO; F. MANENTI: *Efficient methanol synthesis: Perspectives, technologies and optimization strategies*. Prog. Energy Combust. Sci. 56 (2016), pp. 71–105. DOI: 10.1016/j.pecs.2016.06.001.

[165]
L. P. TRAN; S. D. SIMPSON: "A fermentation process". EP Patent 2 753 700 B1. 2020.

[166]
J.-P. LANGE: *Methanol synthesis: a short review of technology improvements*. Catal. Today 64.1-2 (2001), pp. 3–8. DOI: 10.1016/S0920-5861(00)00503-4.

[167]
Q.-Z. LI; X.-L. JIANG; X.-J. FENG; J.-M. WANG; C. SUN; H.-B. ZHANG; M. XIAN; H.-Z. LIU: *Recovery Processes of Organic Acids from Fermentation Broths in the Biomass-Based Industry*. J. Microbiol. Biotechnol. 26.1 (2016), pp. 1–8. DOI: 10.4014/jmb.1505.05049.

[168]
R. M. HANDLER; D. R. SHONNARD; E. M. GRIFFING; A. LAI; I. PALOU-RIVERA: *Life Cycle Assessments of Ethanol Production via Gas Fermentation: Anticipated Greenhouse Gas Emissions for Cellulosic and Waste Gas Feedstocks*. Ind. Eng. Chem. Res. 55.12 (2016), pp. 3253–3261. DOI: 10.1021/acs.iecr.5b03215.

[169]
X. CHEN; Y. CHEN; C. SONG; P. JI; N. WANG; W. WANG; L. CUI: *Recent Advances in Supported Metal Catalysts and Oxide Catalysts for the Reverse Water-Gas Shift Reaction*. Front. Chem. 8 (2020), p. 709. DOI: 10.3389/fchem.2020.00709.

[170]
M. AGHAZADEH: *Enhancing Bioethanol Fermentation through Removal of Acetic Acid Using Liquid-Liquid Extraction*. Dissertation. Indiana: Purdue University, 2016.

[171]
L. HANDOJO; A. K. WARDANI; D. REGINA; C. BELLA; M. T. A. P. KRESNOWATI; I. G. WENTEN: *Electro-membrane processes for organic acid recovery*. RSC Adv. 9.14 (2019), pp. 7854–7869. DOI: 10.1039/c8ra09227c.

[172]
P. HU; S. CHAKRABORTY; A. KUMAR; B. WOOLSTON; H. LIU; D. EMERSON; G. STEPHANOPOULOS: *Integrated bioprocess for conversion of gaseous substrates to liquids*. Proc. Natl. Acad. Sci. U. S. A. 113.14 (2016), pp. 3773–3778. DOI: 10.1073/pnas.1516867113.

[173]
B. LAGOA-COSTA; H. N. ABUBACKAR; M. FERNÁNDEZ-ROMASANTA; C. KENNES; M. C. VEIGA: *Integrated bioconversion of syngas into bioethanol and biopolymers*. Bioresour. Technol. 239 (2017), pp. 244–249. DOI: 10.1016/j.biortech.2017.05.019.

[174]
L. MENIN; V. BENEDETTI; F. PATUZZI; M. BARATIERI: *Techno-economic modeling of an integrated biomethane-biomethanol production process via biomass gasification, electrolysis, biomethanation, and catalytic methanol synthesis*. Biomass Conv. Bioref. 166 (2020), p. 276. DOI: 10.1007/s13399-020-01178-y.

[175]
F. PONTZEN; W. LIEBNER; V. GRONEMANN; M. ROTHAEMEL; B. AHLERS: *CO2-based methanol and DME – Efficient technologies for industrial scale production*. Catal. Today 171.1 (2011), pp. 242–250. DOI: 10.1016/j.cattod.2011.04.049.

[176]
I. K. STOLL; N. BOUKIS; A. NEUMANN; K. OCHSENREITHER; T. A. ZEVACO; J. SAUER: *The Complex Way to Sustainability: Petroleum-Based Processes versus Biosynthetic Pathways in the Formation of C4 Chemicals from Syngas*. Ind. Eng. Chem. Res. 58.35 (2019), pp. 15863–15871. DOI: 10.1021/acs.iecr.9b01123.

[177]
F. OSWALD: *Upgrading the toolbox for fermentation of crude syngas: Process characterization for complete carbon usage, cyanide adaption and production of C4 components*. Dissertation. Karlsruhe: Karlsruhe Institute of Technology, 2019. DOI: 10.5445/IR/1000089485.

[178]
S. J. ROUTLEDGE: *Beyond de-foaming: the effects of antifoams on bioprocess productivity*. Comput. Struct. Biotechnol. J. 3 (2012), pp. 1–7. DOI: 10.5936/csbj.201210014.

[179]
L. PERRET; N. BOUKIS; J. SAUER: *Raw measurement data on the influence of pH and H2 partial pressure on syngas fermentation with Clostridium ljungdahlii*. Mendeley Data V2 (2023). DOI: 10.17632/nnx6brc9hj.2.

[180]
L. PERRET; N. BOUKIS; J. SAUER: *Raw measurement data on the influence of increased cell densities on product ratio and productivity in syngas fermentation with Clostridium ljungdahlii*. Mendeley Data V1 (2023). DOI: 10.17632/8gtc54zykn.1.

[181]
A. INFANTES-LÓPEZ: *Advancing towards biomass-derived syngas fermentation - Evaluation of process parameters and gas composition effects*. Dissertation. Karlsruhe: Karlsruhe Institute of Technology, 2020. DOI: 10.5445/IR/1000124785.

[182]

J.-H. KIM; M. LEE; H. JEONG; S. KO; S.-H. MOON; I. S. CHANG: *Recycling of minerals with acetate separation in biological syngas fermentation with an electrodialysis system*. Chem. Eng. J. 459 (2023), p. 141555. DOI: 10.1016/j.cej.2023.141555.

[183]

N. WAN; A. SATHISH; LE YOU; Y. J. TANG; Z. WEN: *Deciphering Clostridium metabolism and its responses to bioreactor mass transfer during syngas fermentation*. Sci. Rep. 7.1 (2017), p. 10090. DOI: 10.1038/s41598-017-10312-2.

[184]

J. R. PHILLIPS; H. K. ATIYEH; R. S. TANNER; J. R. TORRES; J. SAXENA; M. R. WILKINS; R. L. HUHNKE: *Butanol and hexanol production in Clostridium carboxidivorans syngas fermentation: Medium development and culture techniques*. Bioresour. Technol. 190 (2015), pp. 114–121. DOI: 10.1016/j.biortech.2015.04.043.

[185]

K. VALGEPEA; R. DE SOUZA PINTO LEMGRUBER; K. MEAGHAN; R. W. PALFREYMAN; T. ABDALLA; B. D. HEIJSTRA; J. B. BEHRENDORFF; R. TAPPEL; M. KÖPKE; S. D. SIMPSON; L. K. NIELSEN; E. MARCELLIN: *Maintenance of ATP Homeostasis Triggers Metabolic Shifts in Gas-Fermenting Acetogens*. Cell Syst. 4.5 (2017), pp. 505–515. DOI: 10.1016/j.cels.2017.04.008.

[186]

J. MOCK; Y. ZHENG; A. P. MUELLER; S. LY; L. TRAN; S. SEGOVIA; S. NAGARAJU; M. KÖPKE; P. DÜRRE; R. K. THAUER: *Energy Conservation Associated with Ethanol Formation from H2 and CO2 in Clostridium autoethanogenum Involving Electron Bifurcation*. J. Bacteriol. 197.18 (2015), pp. 2965–2980. DOI: 10.1128/JB.00399-15.

[187]

S. RAMIÓ-PUJOL; R. GANIGUÉ; L. BAÑERAS; J. COLPRIM: *Effect of ethanol and butanol on autotrophic growth of model homoacetogens*. FEMS Microbiol. Lett. 365.10 (2018), pp. 1–4. DOI: 10.1093/femsle/fny084.

[188]

J. BERTSCH; V. MÜLLER: *CO Metabolism in the Acetogen Acetobacterium woodii*. Appl. Environ. Microbiol. 81.17 (2015), pp. 5949–5956. DOI: 10.1128/AEM.01772-15.

[189]

J. M. PEREZ; H. RICHTER; S. E. LOFTUS; L. T. ANGENENT: *Biocatalytic reduction of short-chain carboxylic acids into their corresponding alcohols with syngas fermentation*. Biotechnol. Bioeng. 110.4 (2013), pp. 1066–1077. DOI: 10.1002/bit.24786.

[190]

H. PORTZ: *Brand- und Explosionsschutz von A - Z: Begriffserläuterungen und brandschutztechnische Kennwerte*. 1. Aufl. Vieweg Praxis. Wiesbaden: Vieweg, 2005. ISBN: 3-528-01755-4.

[191]

K.-H. GROTE; B. BENDER; D. GÖHLICH: *Dubbel*. Berlin, Heidelberg: Springer Berlin Heidelberg, 2018. ISBN: 978-3-662-54804-2. DOI: 10.1007/978-3-662-54805-9.

[192]

M. KÖPKE; S. D. SIMPSON: *Pollution to products: recycling of 'above ground' carbon by gas fermentation*. Curr. Opin. Biotechnol. 65 (2020), pp. 180–189. DOI: 10.1016/j.copbio.2020.02.017.

[193]

S. KARMANN; S. PANKE; M. ZINN: *Fed-Batch Cultivations of Rhodospirillum rubrum Under Multiple Nutrient-Limited Growth Conditions on Syngas as a Novel Option to Produce Poly(3-Hydroxybutyrate) (PHB)*. Front. Bioeng. Biotechnol. 7 (2019), p. 59. DOI: 10.3389/fbioe.2019.00059.

[194]

J. VILLADSEN; J. NIELSEN; G. LIDÉN: *Bioreaction engineering principles*. 3. ed. New York, NY and Heidelberg: Springer, 2011. ISBN: 978-1-4419-9688-6.

[195]

E. B. G. HÄUSLER; L. A. M. VAN DER WIELEN; A. J. J. STRAATHOF: *Evaluation of gas supply configurations for microbial product formation involving multiple gaseous substrates*. Bioresour. Bioprocess. 3.1 (2016), p. 868. DOI: 10.1186/s40643-016-0095-7.

[196]

F. OSWALD; I. K. STOLL; M. ZWICK; S. HERBIG; J. SAUER; N. BOUKIS; A. NEUMANN: *Formic Acid Formation by Clostridium ljungdahlii at Elevated Pressures of Carbon Dioxide and Hydrogen*. Front. Bioeng. Biotechnol. 6 (2018), p. 6. DOI: 10.3389/fbioe.2018.00006.

[197]

C.-M. KLASK; N. KLIEM-KUSTER; B. MOLITOR; L. T. ANGENENT: *Nitrate Feed Improves Growth and Ethanol Production of Clostridium ljungdahlii With CO2 and H2, but Results in Stochastic Inhibition Events*. Front. Microbiol. 11 (2020), p. 724. DOI: 10.3389/fmicb.2020.00724.

[198]
S. SCHULZ; B. MOLITOR; L. T. ANGENENT: *Acetate augmentation boosts the ethanol production rate and specificity by Clostridium ljungdahlii during gas fermentation with pure carbon monoxide*. Bioresour. Technol. 369 (2023), p. 128387. DOI: 10.1016/j.biortech.2022.128387.

[199]
H. N. ABUBACKAR; M. C. VEIGA; C. KENNES: *Carbon monoxide fermentation to ethanol by Clostridium autoethanogenum in a bioreactor with no accumulation of acetic acid*. Bioresour. Technol. 186 (2015), pp. 122–127. DOI: 10.1016/j.biortech.2015.02.113.

[200]
H. N. ABUBACKAR; Á. FERNÁNDEZ-NAVEIRA; M. C. VEIGA; C. KENNES: *Impact of cyclic pH shifts on carbon monoxide fermentation to ethanol by Clostridium autoethanogenum*. Fuel 178 (2016), pp. 56–62. ISSN: 00162361. DOI: 10.1016/j.fuel.2016.03.048.

[201]
J. L. COTTER; M. S. CHINN; A. M. GRUNDEN: *Ethanol and acetate production by Clostridium ljungdahlii and Clostridium autoethanogenum using resting cells*. Bioprocess. Biosyst. Eng. 32.3 (2009), pp. 369–380. DOI: 10.1007/s00449-008-0256-y.

[202]
P. D. COTTER; C. HILL: *Surviving the acid test: responses of gram-positive bacteria to low pH*. Microbiol. Mol. Biol. Rev. 67.3 (2003), pp. 429–453. DOI: 10.1128/MMBR.67.3.429-453.2003.

[203]
S. J. KWON; J. LEE; H. S. LEE: *Acetate-assisted carbon monoxide fermentation of Clostridium sp. AWRP*. Process Biochem. 113 (2022), pp. 47–54. DOI: 10.1016/j.procbio.2021.12.015.

[204]
K. HANISCH: *Einfluss von pH und CO2/CO-Verhältnis bei der Gasfermentation im CSTR mit Biomasserückhalt*. Master's Thesis. Karlsruhe: Karlsruhe Institute of Technology, 2022.

[205]
LEGIERUNGSZUSCHLAG.INFO: *Legierungszuschlag für Werkstoff 1.4301*. Ed. by NORDER BAND AG. 2022. URL: https://legierungszuschlag.info/wkst/4301 (visited on 06/29/2022).

[206]
M. VOSS: *1.4301 (X5CrNi18-10) Datenblatt*. Ed. by STAHLHANDEL GRÖDITZ GMBH. 2022. URL: https://www.stahlportal.com/lagervorrat/14301-x5crni18-10/ (visited on 06/29/2022).